Forschungszentrum Karlsruhe
Technik und Umwelt

Wissenschaftliche Berichte
FZKA 6345

Contributions of the Institut für Kernphysik to the 26th Int. Cosmic Ray Conference Salt Lake City 1999

K.-H. Kampert (Editor)

Institut für Kernphysik

August 1999

Forschungszentrum Karlsruhe

Technik und Umwelt

Wissenschaftliche Berichte

FZKA 6345

Contributions of the Institut für Kernphysik to the 26th Int. Cosmic Ray Conference Salt Lake City 1999

edited by
Karl-Heinz Kampert

Institut für Kernphysik

Forschungszentrum Karlsruhe GmbH, Karlsruhe
1999

Als Manuskript gedruckt

Forschungszentrum Karlsruhe GmbH
Postfach 3640, 76021 Karlsruhe

Mitglied der Hermann von Helmholtz-Gemeinschaft
Deutscher Forschungszentren (HGF)

ISSN 0947-8620

Contributions of the Institut für Kernphysik to the 26th Int. Cosmic Ray Conference Salt Lake City, 1999

Summary

The cosmic-ray research activities of the Institut für Kernphysik are focussed on the two experiments **KASCADE** and **AUGER**.

The **KASCADE experiment** has started continuos data taking on the site of Forschungszentrums Karlsruhe in 1996. KASCADE comprises an extended 200 × 200 m^2 array of detector stations for measuring electrons and muons, a compact 16 × 20 m^2 central detector system for precise investigations of the hadronic shower core, and a 50 m long tunnel enabling muon tracking over a size of 150 m^2. The major goals of the experiment are the determination of the primary energy spectrum and elemental composition of cosmic rays in the energy range of the *knee* (10^{14} eV ≤ E ≤ 10^{17} eV). The experimental data, presented in several contributions below, allow for distinctive tests of high-energy hadronic interaction models. Furthermore, detailed analyses of the primary energy spectrum have been performed. Preliminary data of the chemical composition point to an increasingly heavier composition above the *knee*. However, subtle differences are identified in quantitative comparisons between hadronic and electromagnetic observables, with a preference to a heavier composition by hadronic observables. This effect is largely attributed to deficiencies in the modeling of high-energy hadronic interactions, such as are implemented in CORSIKA to simulate the development of extensive air showers. We report also about recent additions and improvements of the CORSIKA simulation package.

The highest energy cosmic rays (E ≥ 10^{19} eV) will be measured over an effective area of 3000 km^2 with the international **Pierre-Auger-Observatory.** Origin, sources, and type of these particles are still unknown and subject to intense discussions in the literature. A demonstration hybrid observatory will commence operation in Argentina's Mendoza Province next year (2000). The experiment will utilize a hybrid set-up of 1600 water Cherenkov detectors and of 4 air fluorescence eyes. Besides performing air-shower simulations with the CORSIKA package, the Karlsruhe group will contribute significantly to the development and construction of the fluorescence cameras and their electronics. We report on the design of the system and on the status of development.

The two major activities are complemented by a number of individual contributions reporting about related work.

Beiträge des Instituts für Kernphysik zur 26. Int. Cosmic Ray Conference Salt Lake City, 1999

Zusammenfassung

Die wissenschaftlichen Aktivitäten des Instituts für Kernphysik konzentrieren sich im Bereich der kosmischen Strahlung auf die Experiment **KASCADE** und **AUGER**.

Das **KASCADE Experiment** hat 1996 seinen Betrieb auf dem Gelände des Forschungszentrums Karlsruhe aufgenommen und nimmt seither kontinuierlich Daten. Es besteht aus einem ausgedehnten 200×200 m^2 Array von Detektorstationen zum Nachweis von Elektronen und Myonen, einem kompakten 16×20 m^2 Zentraldetektorsystem zur präzisen Vermessung des hadronischen Schauerkerns, sowie einem 50 m langen Tunnel zum Nachweis von Myonspuren. Die wichtigsten Forschungsziele von KASCADE sind die Bestimmung des Energiespektrums und der Elementzusammensetzung der kosmischen Strahlung im Bereich des Knie's (10^{14} eV $\leq E \leq$ 10^{17} eV). Die in den folgenden Beiträgen präsentierten Daten ermöglichen erstmals eine präzise Überprüfung hadronischer Wechselwirkungsmodelle bei hohen Energien und geben detaillierte Aufschlüsse über den Verlauf des Primärenergiespektrums. Die zum Teil noch vorläufigen Analysen verschiedener Observablen deuten insgesamt auf eine zunehmend schwerer werdende Massenzusammensetzung oberhalb des Knie's hin. Quantitative Unterschiede zeigen aber auch, daß die zur Luftschauersimulation verwendeten Wechselwirkungsmodelle noch weitere Verbesserungen erfordern. Die Simulationen erfolgen mit dem Programmpaket CORSIKA, über dessen Aktualisierungen berichtet wird.

Die höchstenergetische kosmische Strahlung ($E \geq 10^{19}$ eV) soll mit dem internationalen **Pierre-Auger-Observatory** auf einer Fläche von 3000 km^2 untersucht werden. Quellen, Herkunft und Art dieser Teilchen gelten bislang als völlig unverstanden. Der Nachweis der Teilchen wird über eine Hybridanordnung aus 1600 Wasser-Cherenkov-Tanks und 4 entfernten Fluoreszenzdetektoren geschehen. Die Karlsruher Gruppe beteiligt sich neben den genannten Luftschauersimulationen maßgeblich an der Entwicklung und am Aufbau der Fluoreszenz-Kameras. Eine Proptyp-Hybridanordnung soll ab 2000 in Argentinien (Mendoza) den Betrieb aufnehmen. Das geplante Design wird vorgestellt und über den Stand der Entwicklungsarbeiten berichtet.

Beide Arbeitsschwerpunkte werden schließlich durch verschiedene Einzelbeiträge ergänzt, welche tangierend zu den laufenden Arbeiten entstanden sind.

Contents

OG.1.2.11

The KASCADE Air Shower Experiment: Composition Analyses and Energy Spectrum

K.-H. Kampert[1,2,*], T. Antoni[2], W.D. Apel[2], F. Badea[3], K. Bekk[2], K. Bernlöhr[2], E. Bollmann[2], H. Bozdog[3], I.M. Brancus[3], A. Chilingarian[4], K. Daumiller[1], P. Doll[2], J. Engler[2], F. Feßler[2], H.J. Gils[2], R. Glasstetter[1], R. Haeusler[2], W. Hafemann[2], A. Haungs[2], D. Heck[2], J.R. Hörandel[1†], T. Holst[2], J. Kempa[5], H.O. Klages[2], J. Knapp[1‡], H.J. Mathes[2], H.J. Mayer[2], J. Milke[2], D. Mühlenberg[2], J. Oehlschläger[2], M. Petcu[3], H. Rebel[2], M. Risse[2], M. Roth[2], G. Schatz[2], F.K. Schmidt[1], T. Thouw[2], H. Ulrich[2], A. Vardanyan[4], B. Vulpescu[3], J.H. Weber[1], J. Wentz[2], T. Wibig[5], T. Wiegert[2], D. Wochele[2], J. Wochele[2], J. Zabierowski[6],

[1]*Institut für Experimentelle Kernphysik, University of Karlsruhe, D-76021 Karlsruhe, Germany*
[2]*Institut für Kernphysik, Forschungszentrum Karlsruhe, D-76021 Karlsruhe, Germany*
[3]*National Institute of Physics and Nuclear Engineering, RO-7690 Bucharest, Romania*
[4]*Cosmic Ray Division, Yerevan Physics Institute, Yerevan 36, Armenia*
[5]*Department of Experimental Physics, University of Lodz, PL-90950 Lodz, Poland*
[6]*Soltan Institute for Nuclear Studies, PL-90950 Lodz, Poland*

Abstract

Since its start-up early 1996 KASCADE has collected more than 200 Mio. events with an energy threshold of approx. 10^{14} eV. A unique feature of KASCADE is the simultaneous measurement of electrons, muons, and hadrons at high quality. The large body of data can consistently be described only, if an increasingly heavier composition is assumed above the knee. Quantitatively, subtle differences are identified between hadronic and electromagnetic measurements, with the former pointing to an overall heavier composition. The *knee* in the primary energy spectrum is observed at E_k = 4-5 PeV with a change of the spectral index from $\gamma \simeq 2.7$ to 3.1. We critically discuss the preliminary results and point out possible future improvements, particularly in the modeling of EAS.

1 Introduction:

Detailed measurements of the primary cosmic ray (CR) energy spectrum and chemical composition can provide very powerful means of tracing both their origins and mechanisms of acceleration. Much progress has been made particularly in the energy range where direct measurements on high-flying balloons and satellites are possible (see e.g. Drury, Meyer, Ellison 1999). However, because of the rapidly falling energy spectrum, such measurements are restricted to energies $E \lesssim 5 \cdot 10^{14}$ eV. With only marginal overlap in primary energy, ground based extensive air shower (EAS) experiments take over and they presently allow measurements up to about 10^{20} eV. Ironically, a break in the primary energy spectrum, the so called "knee" is observed at $E \simeq 4 \cdot 10^{15}$ eV, i.e. at an energy not accessible to direct measurements. Measuring the chemical composition as function of primary energy across the knee, again, would provide the key to an understanding of this remarkable phenomenon.

It is hoped, that EAS experiments can provide such data. The measurements are relatively difficult and the interpretation of the ground level observations in terms of the characteristics of the primary flux requires the use of model calculations to simulate the propagation of the particles through the atmosphere. EAS simulations in turn depend on extrapolations applied to data of high-energy particle interactions studied at particle accelerators. Consequently, a wide spread of values about the primary composition have been reported, covering almost the entire range between a pure proton or pure iron distribution (see recent reviews by Watson 1997; Erlykin & Wolfendale 1998).

*corresponding author; e-mail: kampert@ik1.fzk.de
†present address: University of Chicago, Enrico Fermi Institute, Chicago, IL 60637
‡now at: University of Leeds, Leeds LS2 9JT, U.K.

The goal of the KASCADE experiment (Doll et al., 1990) is to determine the primary CR spectrum and composition in the knee region by simultaneously measuring a large number of EAS observables on an event-by-event basis and with high quality. This 'redundancy', as shall be demonstrated, uncovers systematic biases in the interpretation of the data, thereby enabling also tests of the high-energy hadronic interaction models plugged into EAS simulations. Related to this, various interaction models have been implemented into the CORSIKA simulation package (Heck et al., *HE 2.5.28* and refs. therein) and were compared to measured data (Hörandel et al., *HE 1.3.01*). The most consistent results of the different observables are obtained using the VENUS and QGSJET model. The agreement on the primary energy spectrum is fairly satisfactory, however, reconstructions of the chemical composition still seem to require improved versions of hadronic interaction models. The available data already provide the means to contribute to the improvements of such models.

2 Experimental Status

Data taking in a correlated mode with most components in operation has been started in April 1996 (Klages et al., 1997). At present, trigger thresholds are adjusted to limit the total trigger rate to $\sim$ 4 Hz, corresponding to an effective energy threshold in the array of $\sim 10^{14}$ eV for protons and $\sim 3 \cdot 10^{14}$ eV for iron. Most of the 200 Mio. raw data events have been processed with all detector calibrations and error checks. Parallel to data taking, installations still continue, most notably the streamer tube tracking detectors sketched as muon tunnel in Fig. 1. The installations will be finished in fall 1999 and preliminary data taken for a subsystem look very encouraging. The system will enlarge the area for muon measurements by 150 m^2 and will allow to reconstruct the mean muon production height on event-by-event basis for primary energies above the knee. This will add another important observable to determine the primary composition and to perform systematic studies relevant for tests of interaction models.

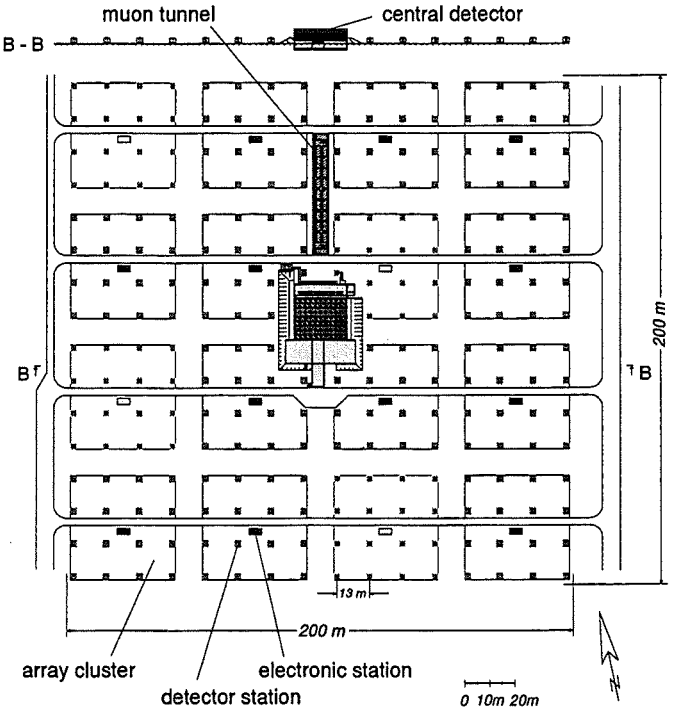

Figure 1: Schematic layout of the KASCADE experiment.

The central detector is presently being upgraded by adding detectors at the very top and bottom. A top layer of TMP ionization chambers is added to improve the acceptance particularly for the electromagnetic component of low-energy air showers. This will improve the position reconstruction of the hadronic shower core and complement the muonic and hadronic measurements. Studying the balance of electromagnetic, muonic, and hadronic energy will put even stronger constraints on interaction models as is achieved presently (Risse et al., *HE 1.3.02*). Muon measurements beneath the multi-wire proportional chambers are being improved by adding a plane of 300 m^2 streamer tubes with pad read-out. The pad-size of 8 $\times$ 16 cm^2 will enable muon density measurements in the center of shower cores without suffering from saturation effects. Again, such measurements are important for a reliable reconstruction of the CR composition.

3 Composition Analyses

An important prerequisite in any study of the chemical composition is the availability of reliable hadronic interaction models. Usually, such models are tuned to describe data measured in the central rapidity region at high-energy particle accelerators. Their application to EAS simulations at the knee requires extrapolations to

the very forward region which has not been measured in sufficient detail. Consequently, large variations are observed in the predictions of various models with observable differences identified also in EAS parameters, most dominantly in hadronic observables of the shower core. In KASCADE, such data have successfully been used for detailed comparisons. The QGSJET model was found to provide the best overall description of the experimental data in the energy range up to the knee, similarly to the results by Erlykin and Wolfendale (1998). However, at energies of 10 PeV, also QGSJET fails to describe the hadron data, i.e. primary masses significantly heavier than iron are required for consistency with the data. This is generally considered an 'unphysical' solution, and doubts about the reliability of the model are raised. A comment to such approaches seems appropriate: Already at energies below 10 PeV QGSJET (and other models) require an iron dominated flux to be conform to high-energy hadron data. This should not be considered evidence that the model predictions are still reliable but only, there is no obvious reason to reject the model. Consequently, the chemical composition extracted from hadronic data, thus will tend to be rather heavy. In fact, this is observed by KASCADE as well as in Chacaltaya data (Fig. 2). Following general practice, we plot the mean logarithmic mass $\langle \ln A \rangle$ as a function of primary energy, bearing in mind its ambiguity for different elemental compositions. The grey band at energies up to $3 \cdot 10^{14}$ eV indicates the uncertainty of direct measurements. The composition indicated by the hadron data (Engler et al., *HE 2.2.44*) follows the general trend of increasing masses and reaches $\langle \ln A \rangle \simeq 3$ at energies of 10 PeV.

Another important approach of extracting the composition is given by the electron and muon sizes. Because of significantly smaller shower and experimental sampling fluctuations, their ratio can be calculated on an event-by-event basis, so that fluctuations caused by the height of first interaction in the atmosphere cancel out to some extend. Comparisons to simulations are remarkable, because they proof that no single mass component can describe the experimental data. Furthermore, protons are found to be the lightest and iron the heaviest particles needed for a description of the data (Weber et al., *HE 2.2.42*). Again, an increasingly heavier composition above the knee is required to describe the data. However, as can be seen from Fig. 2, the overall composition appears to be significantly lighter. The sensitivity of this result to the interaction model is moderately weak, e.g. differences predicted by QGSJET and VENUS are within the error bars. A related analysis has been presented by Glasstetter et al. (*HE 2.2.03*). Here, the composition is inferred from the absolute fluxes and spectral shapes of the muon and electron size distributions. The result is well in line with those discussed above. Finally, pattern analyses with high-energy muons and penetrating hadrons observed in the MWPC below the calorimeter (Haungs et al., *HE 2.2.39*) and multivariate approaches using several experimental observables (Roth et al., *HE 2.2.40*) have been performed. The results, also included in Fig. 2, are intermediate between those discussed above. For the latter one, this may be expected because of 'averaging' over several experimental observables.

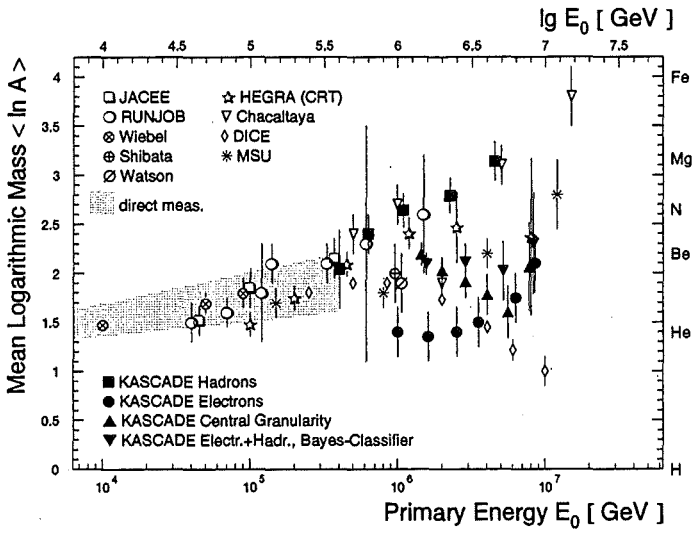

Figure 2: Compilation of preliminary KASCADE and other data on $\langle \ln A \rangle$ as a function of primary energy.

4 Primary Energy Spectrum

Reconstructing the primary energy spectrum from EAS size distributions requires knowledge of the primary mass composition and of the relationship between shower size parameters and primary energy. Also, stochastic fluctuations in the shower development need to be corrected for. Results have been presented at this conference

using the information from electrons and muons, and of hadrons. To be consistent, the energy spectrum extracted from the electron and muon size spectra is based on the composition extracted by these observables, while that of the hadrons, it is based on the composition preferred by the hadronic data (Hörandel et al., *HE 2.2.41*). The agreement between different observables or interaction models is very good, as can be seen from Fig. 3. The result of the deconvolution into 'light' and 'heavy' based on the electron and muon size spectra is represented by the lines (dashed lines are extrapolations of the present data), while the hadronic data are given by the black squares. Interestingly, the knee seems to be caused by protons, i.e. light primaries only.

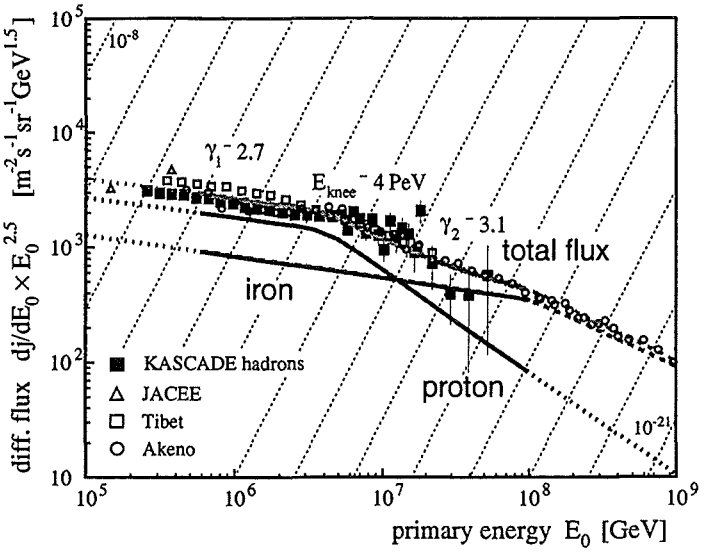

Figure 3: Primary CR energy spectrum from KASCADE and other experiments (see text for details).

Within the fit range no indication of a knee is observed for the iron (heavy) component. However, to be consistent with Akeno and other data also at energies above 10^{17} eV, a knee in the heavy component would be expected in that energy range, i.e. at the same rigidity as for protons. More data are still needed to verify this interesting observation. The position of the knee in the total flux spectrum is reconstructed at $E_k \simeq$ 4-5 PeV and the indices are $\gamma_1 = (2.7 \pm 0.05)$ and $\gamma_2 = (3.1 \pm 0.07)$. The sharpness of the knee in the primary energy spectrum appears moderately mild. The average flux above the knee as deduced from hadrons, muons, and electrons, respectively, is $J(> E_k) \simeq (9.5 \pm 1.5) \cdot 10^{-8}$ m^{-2} s sr^{-1}.

5 Concluding Remarks

In summary, already after about 3 years of operation KASCADE has provided a variety of important results. These include stringent tests of hadronic interaction models and of EAS simulations, detailed investigations of the electron, muon, and hadron shower size distributions, of the related primary energy spectrum, as well as preliminary estimates of the chemical composition of primary CRs. The 'redundancy' of the measurements turns out to be of vital importance in revealing systematic uncertainties. Reasonable agreement is found for the reconstructed primary energy spectrum, but firm conclusions about the mass composition - besides the overall trend of increasing masses above the knee - still have to await improved versions of interaction models. Sensitive parameters in the interaction models are inelastic cross-sections, as well as the 'inelasticity' of an interaction. Further improvements towards a more consistent description of EAS parameters are expected from more abundant electromagnetic processes and neutral particle production in the first (i.e. high-energy) interactions. Such investigations are of very general interest for any EAS experiment and are pursued in close collaboration with the authors of the models. In parallel, the experimental techniques are getting more advanced, with new observables waiting to be included. We are confident, that this approach will lead to a more consistent interpretation of EAS parameters needed to solve the puzzles of the knee.

References

O'C Drury, L., Meyer, J.P., Ellison, D.C., 1999, astro-ph/9905008
Watson, A., Proc. 25th ICRC (Durban, 1997), Vol. 8, p257
Erlykin, A.D., Wolfendale, A.W., 1998, Astrop. Phys. 9, 213
Doll, P. et al., KASCADE Collaboration, Kernforschungszentrum Karlsruhe, Report KfK 4648 (1990)
Klages, H.O., et al., KASCADE Collaboration, Nucl. Phys. B (Proc. Suppl.) 52B (1997) 92

HE 1.3.01

Test of High–Energy Hadronic Interaction Models using EAS Data

J.R. Hörandel[2,7] T. Antoni[1], W.D. Apel[1], F. Badea[3],K. Bekk[1], K. Bernlöhr[1], E. Bollmann[1], H. Bozdog[3], I.M. Brancus[3], A. Chilingarian[4], K. Daumiller[2], P. Doll[1], J. Engler[1], F. Feßler[1], H.J. Gils[1], R. Glasstetter[2],R. Haeusler[1], W. Hafemann[1], A. Haungs[1], D. Heck[1], T. Holst[1], K.H. Kampert[1,2], H. Keim[1], J. Kempa[5], H.O. Klages[1], J. Knapp[2,8], H.J. Mathes[1], H.J. Mayer[1], J. Milke[1], D. Mühlenberg[1], J. Oehlschläger[1], M. Petcu[3], H. Rebel[1], M. Risse[1], M. Roth[1], G. Schatz[1], F.K. Schmidt[2], T. Thouw[2], H. Ulrich[2], A. Vardanyan[3], B. Vulpescu [3], J.H. Weber[2], J. Wentz[1], T. Wibig[6], T. Wiegert[1], D. Wochele[1], J. Wochele[1], J. Zabierowski[6]

[1] *Institut für Kernphysik, Forschungszentrum Karlsruhe, D-76021 Karlsruhe, Germany*

[2] *Institut für Experimentelle Kernphysik, University of Karlsruhe, D-76128 Karlsruhe, Germany*

[3] *Institute of Physics and Nuclear Engineering, RO-7690 Bucharest, Romania*

[4] *Cosmic Ray Division, Yerevan Physics Institute, Yerevan 36, Armenia*

[5] *Department of Experimental Physics, University of Lodz, PL-90950 Lodz, Poland*

[6] *Soltan Institute for Nuclear Studies, PL-90950 Lodz, Poland*

Abstract

The analysis of extensive air shower (EAS) data depends strongly on simulations of the air shower development in the atmosphere. The most critical point are the hadronic interaction models used in shower simulation codes for energies far above collider energies. The investigation of the hadronic component of EAS allows a detailed study of interaction models. Using several observables of this air shower component as observed with the KASCADE hadron calorimeter a comparison between measurements and simulations is presented. The program CORSIKA with the hadronic models QGSJET, VENUS, and SIBYLL has been used for the shower simulation. It turns out that QGSJET describes the measurements best followed by the model VENUS.

1 Proem:

To investigate cosmic rays in the PeV region and above one is forced to observe extensive air showers induced in the atmosphere. To interpret the secondary particles at ground level the measured data are compared with results from Monte Carlo calculations, describing the development of the EAS in the atmosphere and the individual detectors.

The interactions of the secondary particles in the detectors at ground level are well known from collider experiments. More complex is the description of the high energy hadronic interactions of the primary particles with the air nuclei and the production of secondary particles at energies above today's collider energies.

Many phenomenological models have been developed to reproduce the experimental results. Extrapolations to higher energies, to small angles, and to nucleus–nucleus collisions have been performed under different theoretical assumptions. Many EAS experiments have used specific models to determine the primary energy and to extract information about the primary mass composition leading to partly contradictory results. Experience shows that different models can lead to different results when applied to the same data.

Therefore, it is of crucial importance to verify the individual models experimentally as thoroughly as possible. The KASCADE experiment (Klages et al. 1997) allows the detailed study of different EAS observables of the hadronic, electromagnetic, and muonic component. By comparison of measured results with data obtained from Monte Carlo calculations of the EAS development in the atmosphere using the program CORSIKA (Heck et al. 1998), different models implemented in the latter can be tested.

[7]corresponding author, present address: The University of Chicago, Enrico Fermi Institute, 933 East 56^{th} Street, Chicago, IL 60637, USA; http://ik1au1.fzk.de/~joerg

[8]now at: The University of Leeds, Leeds LS2 9JT, U.K.

2 Experimental Set up:

The fine–segmented hadron calorimeter of the KASCADE experiment allows to measure individual hadrons in the core of an EAS. The 300 m^2 iron–sampling–calorimeter is equipped with 10 000 liquid ionisation chambers in eight layers (Engler et al. 1999). A layer of plastic scintillators on top of the calorimeter and a second one below the third iron layer act as trigger for the ionisation chambers. The electromagnetic and muonic component are measured by a 200 × 200 m^2 array of 252 detector stations equipped with scintillation counters. More details are given in these proceedings (Hörandel et al. 1999).

3 Measurements and simulations:

About 10^8 events were recorded from October 1996 to August 1998. In 6×10^6 events, at least one hadron was reconstructed. Events accepted for the present analysis have to fulfil the following requirements: More than two hadrons are reconstructed, the zenith angle of the shower is less than 30° and the core, as determined by the scintillator array, hits the calorimeter or lies within 1.5 m distance outside its boundary. For showers with a primary energy of more than 1 PeV the core can be measured in addition using the first calorimeter layer by the electromagnetic punch-through. The fine sampling of the ionisation chambers yields 0.5 m spatial resolution for the core position. For events with such a precise core position it has to lie within the calorimeter at least 1 m distance from its boundary. After all cuts 40 000 events were left for the final analysis.

EAS simulations are performed using the CORSIKA versions 5.2 and 5.62 as described in (Heck et al. 1998). The interaction models chosen in the tests are VENUS 4.12 (Werner 1993), QGSJET (Kalmykov et al. 1993), and SIBYLL 1.6 (Fletcher et al. 1994). A sample of 2000 proton and iron–induced showers were simulated with SIBYLL and 7000 p and Fe events with QGSJET. With VENUS 2000 showers were generated, each for p, He, O, Si, and Fe primaries. The showers were distributed in the energy range from 0.1 PeV up to 31.6 PeV according to a power law with a differential index of -2.7 and within an zenith angle intervall from 15° to 20°. In addition the changing of the spectral index to -3.1 at the knee position was taken into account in a second set of calculations. The shower axes were spread uniformly over the calorimeter surface extended by 2 m beyond its boundary.

In order to determine the signals in the individual detectors, all secondary particles at ground level are passed through a detector simulation program using the GEANT package. By these means, the instrumental response is taken into account and the simulated events are analysed in the same way as the experimental data, an important aspect to avoid systematic biases by reconstruction algorithms.

4 Results:

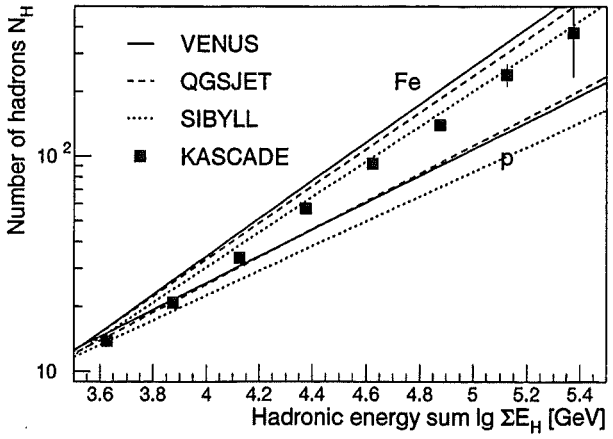

Figure 1: Number of hadrons as a function of the hadronic energy sum.

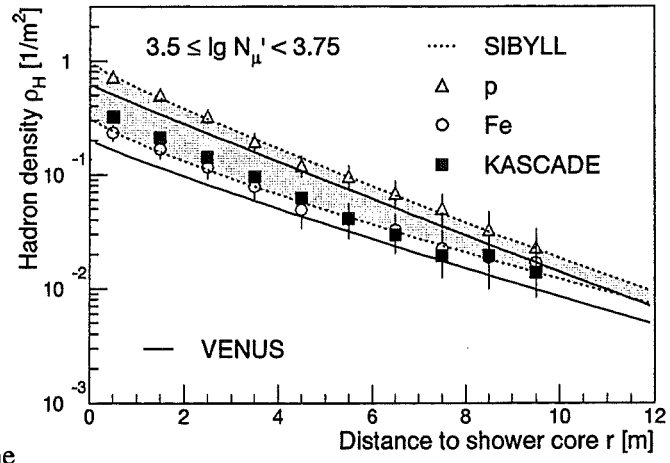

Figure 2: Lateral distribution of hadrons.

The cosmic ray mass composition is poorly known above 0.5 PeV. Therefore, the interaction models can

be tested only by comparing their predictions for the extreme primary masses, namely protons and iron nuclei. If the measured observable lies in between these predictions, the corresponding model is compatible with the data, otherwise we have to exclude it.

When comparing measurements and simulations, it is necessary to divide the data into intervals of fixed shower size. For our investigations we use shower size parameters of all three components, i.e. the number of electrons and muons as well as the hadronic energy sum. For the muonic shower size a muon number obtained by integration of the muon lateral distribution in the range from 40 to 200 m is used. Several hadronic observables have been investigated (Hörandel 1998), some of them are discussed in the following.

A first example of the investigations is presented in Figure 1. The number of hadrons in each shower is plotted versus the hadronic energy sum. Results from EAS simulations with CORSIKA for primary protons and iron nuclei using different interaction models are compared with measurements. Since only hadronic observables are involved in this plot, the self consistent description of the hadronic component within the models can be tested. The abscissa covers an energy range of approximately 0.5 PeV to 15 PeV. Almost the same results are obtained by the models VENUS and QGSJET. The measurements lie well in between the proton and iron predictions, exhibiting an increase of the mean mass with rising energy. SIBYLL generates lower hadron numbers relative to the two other models. Comparison of these predictions to the measurements leads to an incredibly high and energy independent iron content of cosmic rays.

The lateral distribution of hadrons is shown in Figure 2 for a muonic shower size interval corresponding to an energy of about 1.2 PeV. VENUS and SIBYLL predictions are compared with measured results. The measurements are compatible with the VENUS calculations leaving the elemental composition to be somewhere between pure proton or pure iron primaries. QGSJET produces almost the same results and is therefore not shown. In contradiction to that, the measurements follow the lower boundary of the SIBYLL calculations, suggesting, that all primaries are iron nuclei, at this energy obviously an improbable result. The lateral distribution demonstrates, and other observables in a simular manner as reported previously (Antoni et al. 1999), that the SIBYLL code generates

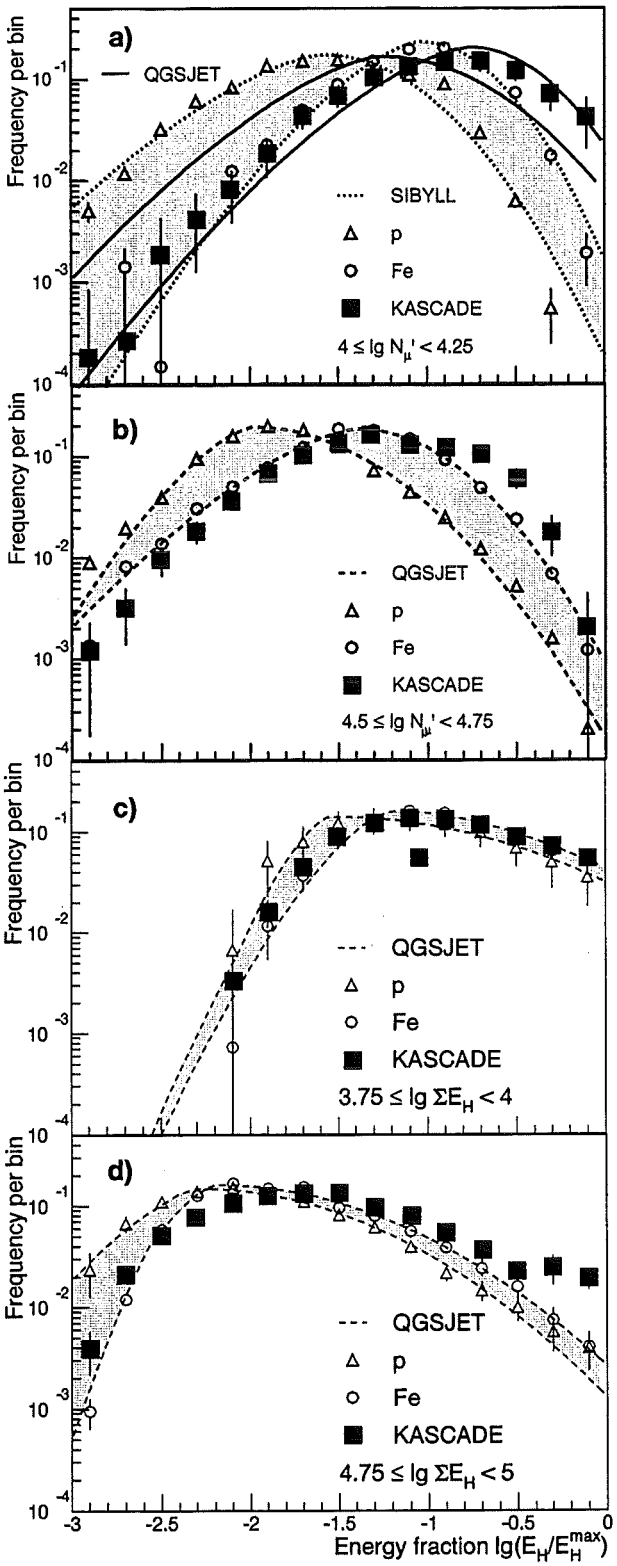

Figure 3: Frequency distribution of energy fraction for different interaction models and energy ranges.

too low muon numbers leading to a heavier elemental composition of cosmic rays. As demonstrated in Figure 1 this behaviour is not limited to muonic shower size bins, the same effect can be observed also in hadronic shower size intervals. In general VENUS produces mostly similar results as QGSJET but exhibits some deviations when the results are classified in electromagnetic shower size bins (Hörandel 1998).

A further observable is the frequency distribution of the fraction of the energy of each hadron normalised to the maximum hadron energy in a particular shower as shown in Figure 3. CORSIKA predictions for pure proton and iron nuclei using the models QGSJET and SIBYLL are compared with measured results for different energy ranges for muonic and hadronic shower size intervals. The first interval (Fig. 3a) corresponds to an energy of approximately 2 PeV, just below the knee position. The data are compatible to the QGSJET predictions, exhibiting a composition somewhere in between protons and iron nuclei. The picture shows one more example that SIBYLL is not able to describe the measurements satisfactorily. An example for a hadronic shower size bin is given in Figure 3c, the interval corresponds to about 1 PeV. It is remarkable that all investigated models predict almost the same energy fraction distributions when the data are classified in hadronic energy sum intervals, even SIBYLL is then able to describe the data. In addition shower size bins above the knee are shown in the Figures 3b and d, corresponding to 12 PeV and 8 PeV, respectively. QGSJET describes the measurements well below the knee, but above, even this models exhibits some discrepancies relative to the measurements as demonstrated for muonic and hadronic shower size bins. This behaviour is visible in other observables too (Hörandel et al. 1998).

5 Conclusion:

Three interaction models have been tested by examining the hadronic cores of large EAS. Several observables have been investigated: The lateral distribution, the lateral energy density, the differential energy spectrum, the distance distribution, the number of hadrons and their energy sum, the maximum hadron energy as well as the fraction of the energy of each hadron to the maximum hadron energy in each shower. All observables are investigated for five different thresholds of hadron energy from 50 GeV up to 1 TeV and the showers are divided into shower size intervals of all components, the number of electrons and muons as well as the hadronic energy sum. It turned out that QGSJET reproduces the measured data best, but at large shower sizes, i.e. energies above the knee even this model fails to reproduce certain observables. VENUS describes the data well, but there are deviations when binning the data in intervals of the electron number. SIBYLL has most problems to describe the data. To sum up, it can be concluded, that the results are described by the models VENUS and QGSJET reasonably well, at least up to energies of about 5 PeV.

References

Antoni, T. et al. (KASCADE Collaboration) 1999, "Test of high–energy interaction models using the hadronic core of EAS", submitted to J. Phys. G (see also astro-ph/9904287)
Engler J. et al. 1999, "A warm–liquid calorimeter for cosmic–ray hadrons", to be publ. in Nucl. Instr. Meth.
Fletcher, R.S. et al. 1994, Phys. Rev. D50, 5710
Heck D. et al. 1998, Report FZKA 6019, Forschungszentrum Karlsruhe
Hörandel, J.R. 1998, Report FZKA 6015, Forschungszentrum Karlsruhe
Hörandel, J.R. et al. (KASCADE Collaboration) 1998, "Test of high–energy hadronic interaction models using the hadronic shower core measured with the KASCADE calorimeter", Proc. 10^{th} ISVHECRI, Gran Sasso
Hörandel, J.R. et al. (KASCADE Collaboration) 1999, Proc. 26^{th} ICRC (Salt Lake City), HE 2.2.41
Kalmykov, N.N., Ostapchenko, S.S. 1993, Yad. Fiz. 56, 105; Phys. At. Nucl. 56, 346
Klages, H.O. et al. (KASCADE Collaboration) 1997, Nucl. Phys. B (Proc. Suppl.) 52B, 92
Werner K. 1993, Phys. Rep. 232, 87

HE 1.3.02

Precision Test of Hadronic Interaction Models with KASCADE Data

M. Risse[1]*, T. Antoni[1], W.D. Apel[1], F. Badea[2], K. Bekk[1], K. Bernlöhr[1], E. Bollmann[1], H. Bozdog[2], I.M. Brancus[2], A. Chilingarian[3], K. Daumiller[4], P. Doll[1], J. Engler[1], F. Feßler[1], H.J. Gils[1], R. Glasstetter[4], R. Haeusler[1], W. Hafemann[1], A. Haungs[1], D. Heck[1], J.R. Hörandel[4‡], T. Holst[1], K.-H. Kampert[1,4], H. Keim[1], J. Kempa[5], H.O. Klages[1], J. Knapp[4§], H.J. Mathes[1], H.J. Mayer[1], J. Milke[1], D. Mühlenberg[1], J. Oehlschläger[1], M. Petcu[2], H. Rebel[1], M. Roth[1], G. Schatz[1], F.K. Schmidt[4], T. Thouw[1], H. Ulrich[1], A. Vardanyan[3], B. Vulpescu[2], J.H. Weber[4], J. Wentz[1], T. Wibig[5], T. Wiegert[1], D. Wochele[1], J. Wochele[1], J. Zabierowski[6]

[1]*Institut für Kernphysik, Forschungszentrum Karlsruhe, D-76021 Karlsruhe, Germany*

[2]*Institute of Physics and Nuclear Engineering, RO-7690 Bucharest, Romania*

[3]*Cosmic Ray Division, Yerevan Physics Institute, Yerevan 36, Armenia*

[4]*Institut für Experimentelle Kernphysik, University of Karlsruhe, D-76021 Karlsruhe, Germany*

[5]*Department of Experimental Physics, University of Lodz, PL-90950 Lodz, Poland*

[6]*Soltan Institute for Nuclear Studies, PL-90950 Lodz, Poland*

Abstract

Extrapolations of hadronic interaction models into kinematical and energy regions beyond the limit of accelerator data may heavily influence the interpretation of EAS data, especially the estimation of primary energy spectra and mass composition. In order to test and possibly improve the model predictions, the muon trigger and hadron rate observed with the KASCADE central detector are analysed and compared to CORSIKA simulations. The hadrons detected result from primary particles in the energy range of 0.1 to 500 TeV. Taking the measured particle fluxes from direct observations, we find fewer hadrons than predicted. Adopting a slightly larger total cross-section for pp interactions, such as suggested by findings of the CDF experiment at Fermilab, a noticeable improvement but still unsatisfactory description is obtained. Investigations to further improve the predictions are under way; the physical implications of the results are discussed.

1 Introduction

For cosmic-ray research, the test of hadronic interaction models is interesting in terms of particle physics and necessary in terms of astrophysics. The particle physics interest, on the one hand, results from the fact that the very forward region of high-energy collisions, which determines the development of an extensive air shower, is unexplored by current (and planned) laboratory measurements. At the highest energies of $\sqrt{s} = 0.9$ TeV, the UA5 experiment detected only about 30% of the total energy, and the CDF experiment at $\sqrt{s} = 1.8$ TeV even only about 5%. Thus, the study of EAS, especially by comparing the predictions of different models with data, might provide new insights in the region beyond the kinematical and energetic limits of colliders. The astrophysical necessity, on the other hand, emerges when trying to deduce energy spectra and mass composition from EAS measurements. The interpretation is decisively influenced by using different models. A well-known example is the mass composition concluded from the depth of shower maximum. The composition varies from mixed to pure iron, depending on the model assumed (see e.g. Watson, 1997). Therefore, a reliable test of simulation models is desirable. The idea of the test described in the following is to check with the calorimeter, how many hadrons, propagated through the atmosphere, arrive at observation level, and this in an energy range where the primary flux is reasonably well known from direct observations, viz. 0.1 to 500 TeV. We trigger on the muon content of such low-energy EAS, which have developed somewhere in the atmosphere, ask for the hadrons at observation level, and compare with simulations.

*corresponding author; e-mail: risse@ik1.fzk.de

‡present address: University of Chicago, Enrico Fermi Institute, Chicago, IL 60637

§now at: University of Leeds, Leeds LS2 9JT, U.K.

2 Observables

The main part of the KASCADE central detector is the hadron calorimeter, for experimental details see (Klages et al., 1997). Utilizing 40000 electronic channels of liquid ionization chambers in 8 sampling layers (with an area of $16 \cdot 20$ m^2), it allows to measure position, angle of incidence, and energy of individual hadrons with $\approx$ 100% efficiency above 100 GeV. Embedded is a layer of 456 plastic scintillation counters, used as a fast trigger. A muon trigger is given, if a minimum number of detectors (e.g. 9) have coincidently above 1/3 of a m.i.p.'s signal. After a successful muon trigger, it is looked for at least one hadron with more than 100 GeV in the calorimeter. The frequency of such events defines the muon trigger rate and the (muon selected) hadron rate. This approach of selecting the events in the muonic shower component and of comparing in the 'critical' hadronic one, which combines two components with different longitudinal shower developments, puts high demands on the models and therefore is an excellent testing instrument.

3 Measurement & Simulation

The measured rates show long-term stability on the percent level after being corrected for dead time and air pressure effects (each $\leq$ 10%). For a description of the calorimeter performance see also (Engler et al., 1999). The simulations are performed using the CORSIKA air shower program (Heck et al., 1999, and references therein), and the detector response is calculated with the GEANT package (GEANT, 1993). The five primary particle classes p, He, O, Mg, and Fe are simulated in accordance with the spectra given by direct measurements (e.g. Wiebel, 1994); for extrapolations to higher energies ($>$ 1 PeV), the individual spectral indices are assumed to be constant. The simulation covers the complete acceptance in terms of primary energy, zenith angle, and distance of shower core to the central detector. The hadronic interaction models VENUS (Werner, 1993), SIBYLL (Fletcher et al., 1994) and QGSJET (Kalmykov & Ostapchenko, 1993), as given in CORSIKA version 5.62, have been analysed. As a consequence, modifications in QGSJET have been implemented ($\Rightarrow$ CORSIKA 5.63) and examined, see section 4.

Figure 1 displays for QGSJET (5.63) the contribution of the primary energies to the rates. One observes

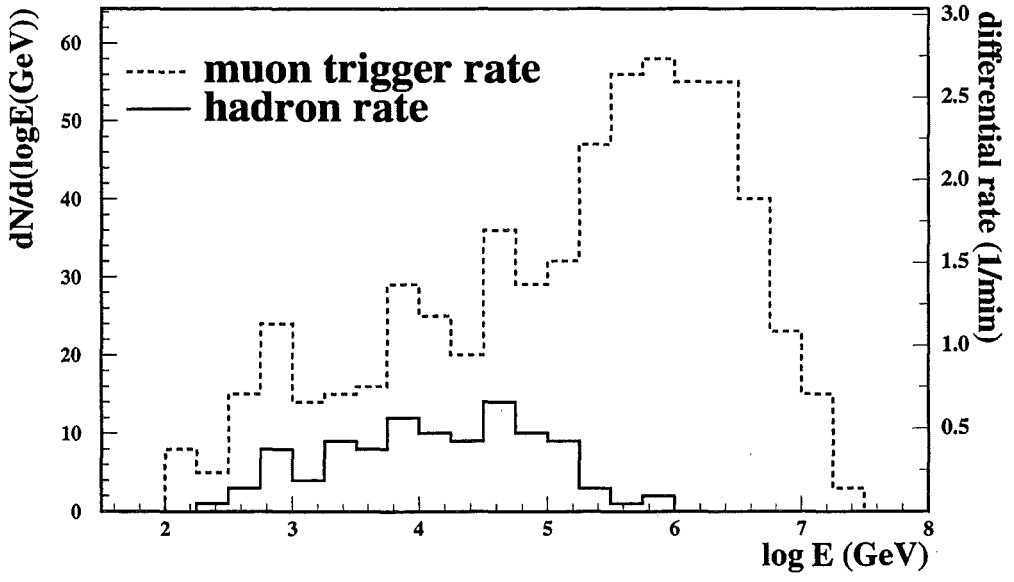

Figure 1: The contribution of primary particle energies to the muon trigger and hadron rate, in terms of absolute rates (right axis) and number of events in the simulation (left axis) for QGSJET (CORSIKA version 5.63, see text).

that the hadron rate originates from energies for which the flux is well determined by direct measurements: Thus, this observable does not suffer from the uncertainties in composition and absolute fluxes at high energies – an important aspect when trying to perform a precision test.

4 Results

The resulting integral rates are compiled in Figure 2, showing the muon trigger rates versus the hadron rates obtained by the simulations and compared with measured values. The error bars represent the statistical uncertainties of the simulations. It should be emphasized, however, that in the simulations an additional systematical error should be born in mind which results from the systematical uncertainties in the direct measurements. It can be estimated to $\pm(10...20)\%$. For the muon trigger rate, an additional error of roughly the same amount has to be considered because of contributions of higher primary energies. However, when regarding the ratio of the rates, the uncertainties in the absolute flux cancel out to first approximation.

From the figure it can be seen that the three interaction models (open symbols) predict fairly well the muon trigger rate but generate a too large hadron rate by more than a factor of 2 when compared to the measured

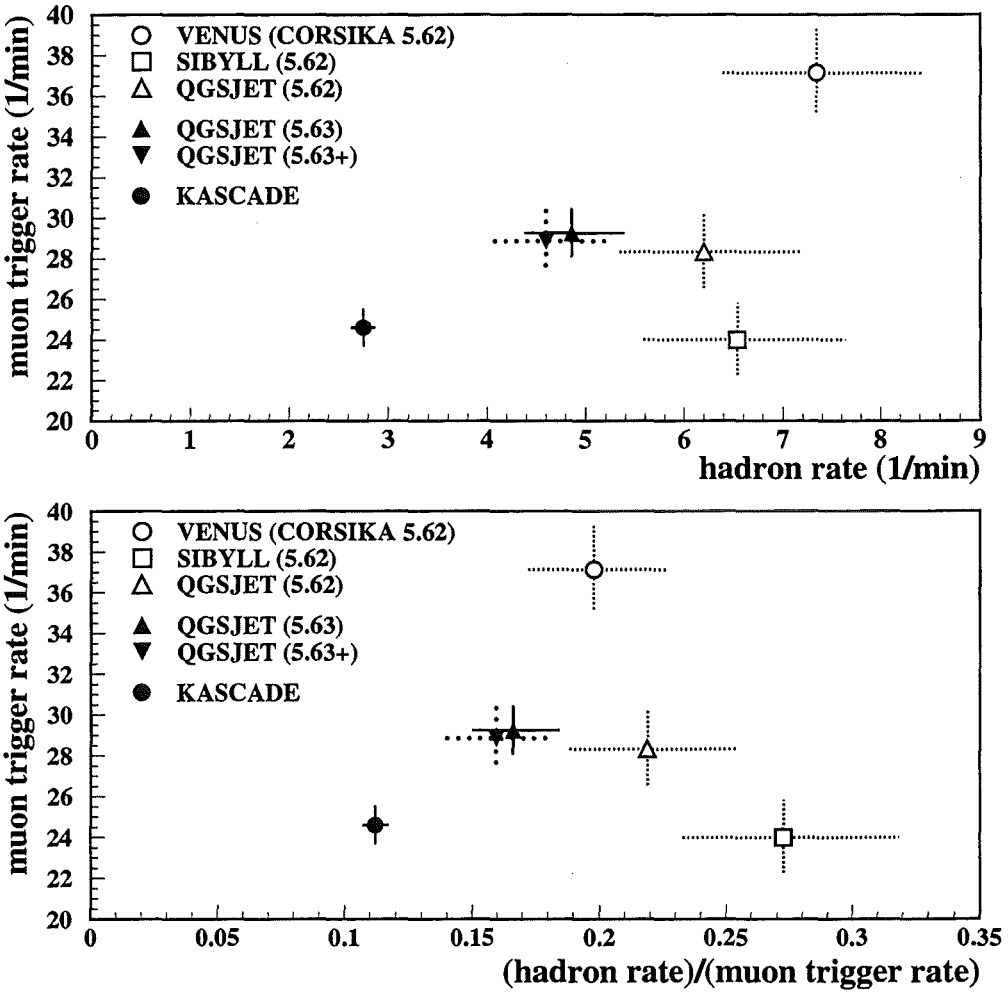

Figure 2: The integral muon trigger and hadron rates, resp. their ratio.

KASCADE value. All models propagate the showers too deeply into the atmosphere. In reality, hadronic cascades develop much faster than the models predict. VENUS also produces significantly more muons, which is consistent with findings of (Knapp, 1997). SIBYLL generates the highest ratio of hadrons to muons as seen in the lower part of Figure 2, mostly as a result of its relative low muon number. Other investigations have revealed the SIBYLL muon number being too low at high energies (see for instance Hörandel et al., 1999; Antoni et al., 1999). The data are explained better by QGSJET, but still not well enough. Several attempts have been undertaken by the authors of this model to improve the agreement (Ostapchenko, 1998). In CORSIKA version 5.63, the total inelastic cross-section has been increased by about 5%, which is justified by the new nucleon-nucleon inelastic cross-section of 80 mb obtained by the CDF Collaboration at an energy of $\sqrt{s} = 1.8$ TeV (Abe et al., 1994), corresponding to 1.6 PeV laboratory momentum. The inelastic cross-sections of mesons and of nuclei have been changed accordingly. Indeed, the simulated hadron rate is reduced without a noticeable effect on the muon trigger rate as shown in Figure 2: The decrease amounts to about 22% and reflects the sensitivity of this EAS observable on changes in basic model parameters.

A further modification of the authors concerns the restriction of diffractive collisions. A previous upper limit in the QGSJET model to diffractive masses $m_D < 5$ GeV has been omitted. However, as can be seen in Figure 2 (QGSJET 5.63+), this does not influence the shower development much; a minor improvement can be stated, nevertheless.

5 Conclusion

A precision test of air shower simulation models, especially sensitive to the hadronic part, has been developed by analysing the muon trigger and hadron rates of the KASCADE experiment. All hadronic interaction models examined so far predict a significantly larger hadron rate than observed. An improvement has been achieved in the QGSJET model by adopting higher inelastic cross-sections. Further improvements in the interaction model and extensions to the testing procedure are under way. On top of the calorimeter a complete layer of ionization chambers will be installed; with 100% coverage it will allow to check also the electromagnetic part of low-energy showers. In conclusion, EAS experiments reveal new insights in particle physics and hopefully might generate reliable models as a basis for solid astrophysical interpretations.

Acknowledgments

We are very grateful to S.S. Ostapchenko for illuminating discussions and appreciate the preparation of the modifications in QGSJET.

References

Abe, F., et al., CDF Collaboration, 1994, Phys. Rev. D 50, 5550
Antoni, T., et al., KASCADE Collaboration, 1999, J. Phys. G, submitted
Engler, J., et al., 1999, Nucl. Instr. Meth., to be published
Fletcher, R.S., Gaisser, T.K., Lipari, P., Stanev, T., 1994, Phys. Rev. D 50, 5710
GEANT, 1993, CERN Program Library Long Writeup W5013, CERN, Genf
Heck, D., et al., 1999, Proc. 26th ICRC (Salt Lake City, 1999) HE 2.5.28
Hörandel, J.R., et al., 1999, Proc. 26th ICRC (Salt Lake City, 1999) HE 1.3.01
Kalmykov, K.K., & Ostapchenko, S.S., 1993, Yad. Fiz. 56, 105
Klages, H.O., et al., KASCADE Collaboration, 1997, Proc. 25th ICRC (Durban, 1997), Vol. 8, 297
Knapp, J., 1997, Report FZKA 5970, Forschungszentrum Karlsruhe
Ostapchenko, S.S., 1998, private communication
Watson, A.A., 1997, Proc. 25th ICRC (Durban, 1997), Vol. 8, Fig. 10
Werner, K., 1993, Phys. Rep. 232, 87
Wiebel, B., 1994, WUB 94-08, Bergische Universität-Gesamthochschule Wuppertal

HE 2.2.02

Cosmic Ray Energy Spectrum around the Knee by Muon Density Measurements at KASCADE

A. Haungs[1]*, T. Antoni[1], W.D. Apel[1], A.F. Badea[2], K. Bekk[1], K. Bernlöhr[1], E. Bollmann[1], H. Bozdog[2], I.M. Brancus[2], A. Chilingarian[3], K. Daumiller[4], P. Doll[1], J. Engler[1], F. Feßler[1], H.J. Gils[1], R. Glasstetter[4], R. Haeusler[1], W. Hafemann[1], D. Heck[1], J.R. Hörandel[4] †, T. Holst[1], K.-H. Kampert[1,4], H. Keim[1], J. Kempa[5], H.O. Klages[1], J. Knapp[4‡], K.U. Köhler[1], H.J. Mathes[1], H.J. Mayer[1], J. Milke[1], D. Mühlenberg[1], J. Oehlschläger[1], M. Petcu[2], H. Rebel[1], M. Risse[1], M. Roth[1], G. Schatz[1], F.K. Schmidt[4], T. Thouw[1], H. Ulrich[1], A. Vardanyan[3], B. Vulpescu[2], J.H. Weber[4], J. Wentz[1], T. Wibig[5], T. Wiegert[1], D. Wochele[1], J. Wochele[1], J. Zabierowski[6], S. Zagromski[1],

[1]*Forschungszentrum Karlsruhe, Institut für Kernphysik, D-76021 Karlsruhe, Germany*

[2]*National Institute of Physics and Nuclear Engineering, RO-7690 Bucharest, Romania*

[3]*Cosmic Ray Division, Yerevan Physics Institute, Yerevan 36, Armenia*

[4] *Institut für Experimentelle Kernphysik, University of Karlsruhe, D-76021 Karlsruhe, Germany*

[5]*Department of Experimental Physics, University of Lodz, PL-90950 Lodz, Poland*§

[6] *Soltan Institute for Nuclear Studies, PL-90950 Lodz, Poland*§

Abstract

A system of large-area position sensitive multiwire proportional chambers (MWPC), installed below the hadron calorimeter of the KASCADE (KArlsruhe Shower Core and Array DEtector) central detector is able to measure the muon density spectra at fixed distances from the core of EAS in the knee region. Comparisons of these muon density spectra with Monte Carlo simulations for different primaries and various high-energy interaction models lead to an estimation of the slopes before and after the knee and its position. In contrast to many other knee determinations this method does not invoke the integration of sampled lateral particle distributions, and the muon density spectrum is a directly measurable observable with reduced systematic uncertainties.

1 Introduction:

Since forty years a conspicuous change of the spectral index from ca. -2.7 to -3.1 of the power law description of the primary cosmic ray spectrum around 3 PeV is known. In spite of a lot of experimental efforts, there remain many open questions, in particular about the detailed position and the shape of the knee region, about the variation of the primary mass composition, in addition to the question of the astrophysical origin of the observed features at all. There is a number of theoretical conjectures about the mass composition, predicting a variation from dominantly light nuclei to a composition of heavier nuclei.

Local muon density spectra at fixed distances from the shower axis have been measured and display conspicuous kinks at certain values of the local muon density. The analysis of this observation by use of extensive Monte Carlo EAS simulation calculations relates the observed kinks to the knee of the primary cosmic ray energy spectrum and implies new a methodical approach of EAS investigations.

2 Apparatus:

KASCADE is a multidetector setup (Klages et al. 1997) built in Karlsruhe, Germany for measurements of EAS especially in the primary energy range of the knee region. The KASCADE detector array has an area of $200 \times 200\,m^2$ and 252 detector stations (positioned on rectangular grids with 13 m spacing) consisting of liquid scintillators for measuring the electromagnetic and of plastic scintillators for measuring the muonic component

*corresponding author; e-mail: haungs@ik3.fzk.de

†present address: University of Chicago, Enrico Fermi Inst., IL 60637; ‡now at: University of Leeds, Leeds LS2 9JT, U.K.

§partly supported by the Polish State Committee for Scientific Research (Grant No.2P03B16012)

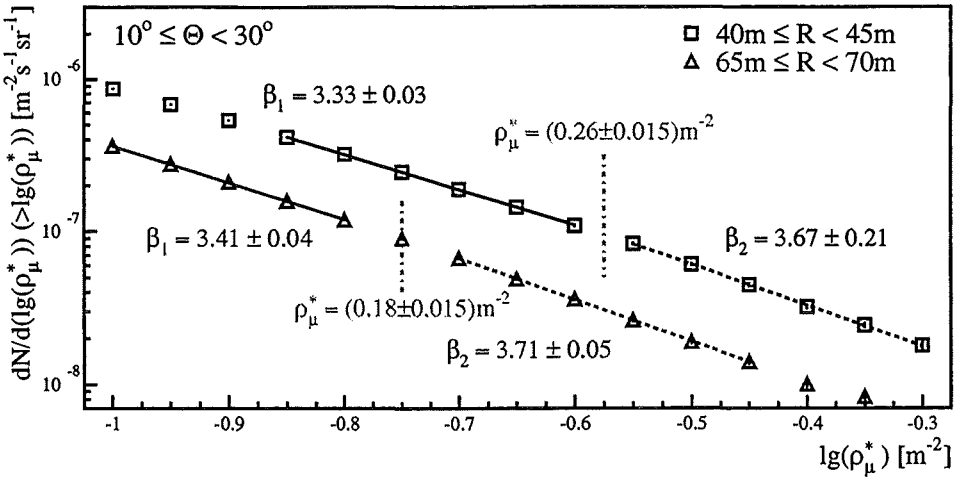

Figure 1: Integral muon density spectra measured by the MWPC for showers with two different core distances. The vertical lines assign the position of the knee in the muon density spectra. The β represent the indices of the fitted power law functions.

of EAS. This array provides the data necessary for the reconstruction of the basic EAS characteristics like the size N_e, muon size N_μ^{tr}, core location, and angle of incidence of each single air shower. The present measurements of the muon densities use a setup of 32 multiwire proportional chambers (MWPC) of the central detector. It consists of 16 stacks (5 m^2-9 m^2) of two chambers one upon another. Each chamber consists of three layers of crossed anode wires and cathode stripes. The crossing angle of the cathodes to the anode wires is $\pm 34°$ at each of the three different size types of the chambers. The MWPC allows a accurate determination of the position and angle of single muons with a spatial resolution of around 1 cm. The total sensitive area of the MWPC setup is $2 \times 129\ m^2$. The absorber of the calorimeter effects an energy threshold of 2 GeV for vertical muons. For each single shower the local muon density ρ_μ^* can be estimated with help of the number of reconstructed muons in the MWPC setup and its sensitive area as a function of the angle of incidence of the EAS (Haungs et al. 1999).

3 Muon Density Spectra:

The spectrum of ρ_μ^* of the EAS observed in a certain distance from the shower core and for a certain range of the angle of shower incidence is the quantity of the present investigation. Figure 1 display integral muon density spectra measured with the MWPC system ($E_\mu > 2$ GeV) for two particular core distances and for the zenith angle range $10° \leq \Theta \leq 30°$ measured in c. 5000 hours. The spectra follow a power law form $dN/d\rho_\mu^* \propto (\rho_\mu^*)^{-\beta}$. Both spectra show a kink, expressed by the change of the spectral index β. The spectral indices and the positions of the estimated knees are included in Figure 1. The quoted errors represent the statistical uncertainties. Due to the reduced efficiency of the trigger threshold for small sized showers the first data points of the spectrum of the smaller core distance have not been included in the fit procedure. With increasing distance from the shower core the position of the kink shifts to lower muon densities as a consequence of the lateral distributions of the EAS muons of decreasing muon densities with increasing R. This explains also the steeper slopes of the density spectra at larger R.

In order to analyze these results and to relate the local muon densities to the energy and nature of the primaries detailed Monte Carlo calculations simulating the EAS development have been performed. Using the CORSIKA v 5.62 code (Heck et al. 1998) samples of proton and iron induced EAS of the energy range of $5 \cdot 10^{14}$ eV

	δ (QGSJet)		δ (VENUS)	
	proton	iron	proton	iron
40 m$\leq R \leq$ 45 m	0.718 ± 0.015	0.807 ± 0.009	0.776 ± 0.016	0.784 ± 0.010
65 m$\leq R \leq$ 70 m	0.727 ± 0.017	0.809 ± 0.012	0.811 ± 0.015	0.763 ± 0.012

Table 1: Exponents of the power law function $\rho_\mu^* \propto E^\delta$ for different core distances, primaries and high-energy interaction models.

	proton	iron
	QGSJet	
γ_1	$2.71 \pm 0.01_{stat} \pm 0.38_{sys}$	$2.92 \pm 0.01_{stat} \pm 0.27_{sys}$
γ_2	$2.95 \pm 0.04_{stat} \pm 0.46_{sys}$	$3.18 \pm 0.04_{stat} \pm 0.34_{sys}$
E_{knee}	$(7.27 \pm 0.43_{stat} \pm 2.33_{sys}) \cdot 10^{15}$ eV	$(4.56 \pm 0.10_{stat} \pm 1.10_{sys}) \cdot 10^{15}$ eV
	VENUS	
γ_1	$2.88 \pm 0.01_{stat} \pm 0.27_{sys}$	$2.83 \pm 0.01_{stat} \pm 0.25_{sys}$
γ_2	$3.14 \pm 0.04_{stat} \pm 0.35_{sys}$	$3.08 \pm 0.05_{stat} \pm 0.32_{sys}$
E_{knee}	$(5.34 \pm 0.24_{stat} \pm 1.36_{sys}) \cdot 10^{15}$ eV	$(4.60 \pm 0.21_{stat} \pm 0.99_{sys}) \cdot 10^{15}$ eV

Table 2: Spectral indices γ_i of the primary energy spectrum, obtained with different high-energy interaction models and primary particles by combining both core distance spectra. Additionally the estimated position of the knee is given. The main sources of the systematic errors are the evaluation of the position of the kink in the measured muon density spectra and the uncertainty of δ due to the multiple use of single showers in the detector simulation.

to $1 \cdot 10^{16}$ eV, distributed along a primary energy spectrum $\propto E^{-2.7}$ are generated with two different interaction models (QGSJet and VENUS). The detector efficiency has been included in the simulations, using each simulated EAS ten times in the considered ranges of the core distance. Figure 2 displays the relations between the average muon density ρ_μ^* and the primary energy, described by a power law $\rho_\mu^* \propto E^\delta$ as an example for one interaction model and one core distance. The values of all δ resulting from a fitting procedure are listed in Table 1. The quoted uncertainties are due to the limited statistics of the simulated showers. On basis of these results the position of the knee in the muon density spectra and the spectral indices β are related to the knee position and the index γ of the energy spectrum $dN/dE = dN/d\rho_\mu^* \cdot d\rho_\mu^*/dE$ leading to $\gamma = \delta \cdot (\beta - 1) + 1$. The results of this procedure are given in Table 2.

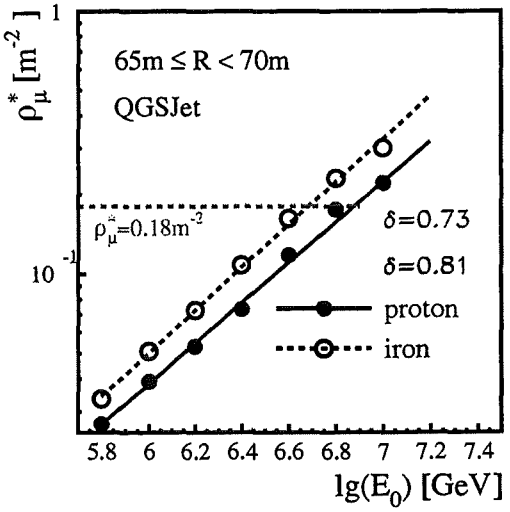

Figure 2: Example of the dependence of the local muon density on the primary energy for different primaries (CORSIKA simulations with full detector simulation included).

With the help of the estimated shower sizes N_e and N_μ^{tr} (Glasstetter et al. 1999) by the KASCADE field detectors a global distinction between showers induced by light and heavy primaries is realized. The relevant parameter for the EAS separation is the muon number - electron number ratio $lg(N_\mu^{tr})/lg(N_e)$ with N_μ^{tr} and N_e corrected to the zenithal incidence with the measured attenu-

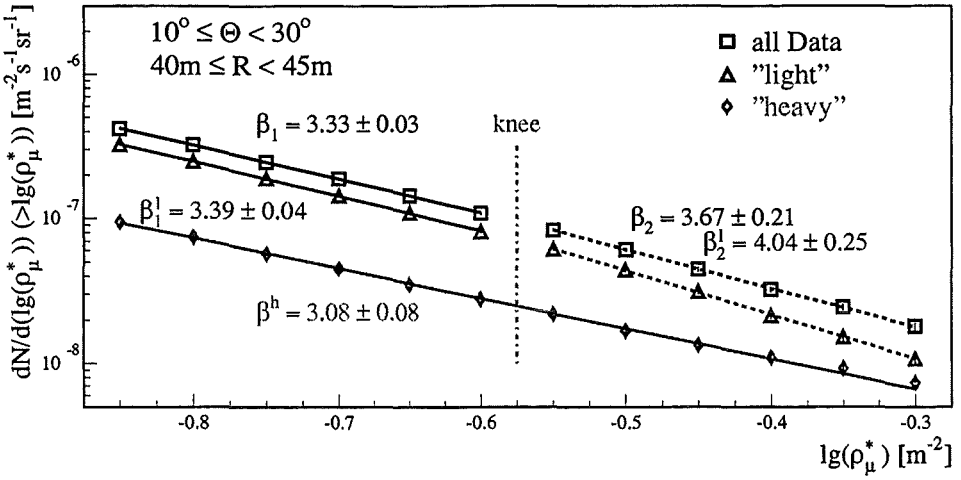

Figure 3: Integral muon density spectra measured by the MWPC for all showers for enhanced "light" and for enhanced "heavy" showers. The vertical line assigns the position of the knee in the muon density spectra estimated for "all" EAS.

ation lengths λ_μ and λ_e by the KASCADE group. Figure 3 shows for one range of the shower core distance the obtained spectra for all, "light" and "heavy" induced EAS. The kink in the spectrum of the light induced showers is clearly rising. With the above described procedure, combining both ranges of core distance the indices of the primary energy spectrum for both samples are calculated using the interaction model QGSJet (VENUS). While the spectra of the light induced EAS with $\gamma_l^1 = 2.76(2.94)$ and $\gamma_l^2 = 3.20(3.42)$ show a clear knee, the spectra of the heavy induced EAS have a passing slope of $\gamma_h = 2.76(2.62)$ without any kink between 10^{15} eV and 10^{16} eV. The results has small statistical errors, and an estimated systematic error of ≈ 0.3 is mainly due to the limited statistic in the Monte Carlo simulations.

4 Concluding Remarks:

A result of considerable interest is the first observation of kinks in muon density spectra measured at fixed distances from the shower core. Adopting a particular mass composition and invoking Monte Carlo simulations (by CORSIKA), the kinks and slopes of the density spectra can be related to the knee position and spectral indices of the primary energy spectrum. The resulting indices for the all-particle energy spectrum are about -2.8 before and about -3.1 after the knee position of about $5 \cdot 10^{15}$ eV. Thus we may summarize that after the evidence for the existence of the knee discontinuity in the N_e spectrum by many experiments, lateron in the spectrum of the EAS muon content and recently in the hadron number by the KASCADE group (Hörandel et al. 1999), also the muon density is shown to reveal consistently the phenomenon. The present analysis give first hints that the knee appearance at ca. $5 \cdot 10^{15}$ eV is strongly dominated by the light component of the charged cosmic rays.

References

Glasstetter, R. et al. 1999, Proc. 26th ICRC (Salt Lake City, 1999), HE 2.2.03
Haungs, A. et al. 1999, FZKA-Report 6263, Forschungszentrum Karlsruhe, Germany
Heck, D. et al. 1998, FZKA-Report 6019, Forschungszentrum Karlsruhe, Germany
Hörandel, J.R. et al. 1999, Proc. 26th ICRC (Salt Lake City, 1999), HE 2.2.41
Klages, H.O. et al. 1997, Proc. 25th ICRC (Durban, 1997), Vol 8, 297

HE.2.2.03

Analysis of Electron and Muon Size Spectra of EAS

R. Glasstetter[1]*, T. Antoni[2], W.D. Apel[2], F. Badea[3], K. Bekk[2], K. Bernlöhr[2], E. Bollmann[2], H. Bozdog[3], I.M. Brancus[3], A. Chilingarian[4], K. Daumiller[1], P. Doll[2], J. Engler[2], F. Feßler[2], H.J. Gils[2], R. Haeusler[2], W. Hafemann[2], A. Haungs[2], D. Heck[2], J.R. Hörandel[1†], T. Holst[2], K.-H. Kampert[1,2], J. Kempa[5], H.O. Klages[2], J. Knapp[1‡], H.J. Mathes[2], H.J. Mayer[2], J. Milke[2], D. Mühlenberg[2], J. Oehlschläger[2], M. Petcu[3], H. Rebel[2], M. Risse[2], M. Roth[2], G. Schatz[2], F.K. Schmidt[1], H. Schieler[2], T. Thouw[2], H. Ulrich[2], A. Vardanyan[4], B. Vulpescu[3], J.H. Weber[1], J. Wentz[2], T. Wibig[5], T. Wiegert[2], D. Wochele[2], J. Wochele[2], J. Zabierowski[6],

[1]*Institut für Experimentelle Kernphysik, University of Karlsruhe, D-76021 Karlsruhe, Germany*

[2]*Institut für Kernphysik, Forschungszentrum Karlsruhe, D-76021 Karlsruhe, Germany*

[3]*National Institute of Physics and Nuclear Engineering, RO-7690 Bucharest, Romania*

[4]*Cosmic Ray Division, Yerevan Physics Institute, Yerevan 36, Armenia*

[5]*Department of Experimental Physics, University of Lodz, PL-90950 Lodz, Poland*

[6]*Soltan Institute for Nuclear Studies, PL-90950 Lodz, Poland*

Abstract

The electron and muon numbers of extensive air showers in the energy region around the knee are measured by the detectors of the KASCADE array. To understand the resulting size spectra one has to take into account the fluctuations of the shower development in the atmosphere as well as the uncertainties of the applied reconstruction methods. A consistent interpretation of both spectra allows to derive a primary energy spectrum and a mass composition.

1 Introduction:

The KASCADE–Experiment (Klages et al., 1997) at the *Forschungszentrum Karlsruhe* (110m a.s.l., Germany) was designed to determine the different particle numbers and distributions in an extensive air shower (EAS) in quite a number of ways in the energy region around the so-called *knee* (10^{14}-10^{17}eV). Therefore, it consists of a 200×200m^2 scintillator array with 252 detector stations for the detection of the extensive electron and muon component and a 16×20m^2 central sampling calorimeter for the measurement of individual hadrons. Additionally, there are multiwire proportional chambers and streamer tubes for muon tracking. The various types of particle detection minimize ambiguities which arise from the large fluctuations in the shower development. They enable us to derive the energy and mass of the primary particle on an event-by-event basis via multiparameter analysis methods.

A different approach, which is used in this analysis, is to look at the spectra of electron and muon numbers as they are measured by the KASCADE–array and derive the primary energy spectrum from these. This is possible since the energy spectra of different primary particles transform differently to the size spectra; the muon number of an EAS is increasing with primary mass, whereas the electron number is decreasing.

However, in any analysis the shower development fluctuations as well as the reconstruction errors have to be known quantitatively to account for systematical errors, especially if dealing with steep power law spectra.

The spectra used for this analysis are based on a data set measured from Oct. 1996-Nov. 1998 with over 12 Mio. reconstructed events in a zenith angle interval from 18° to 25°. The so-called *truncated* muon number $N_{\mu,tr}$ used in the following denotes the integrated number of muons in the region from 40m to 200m around the core, whereas the electron number N_e is reconstructed over all radial distances.

*corresponding author; e-mail: ralph@ik1.fzk.de

†present address: University of Chicago, Enrico Fermi Institute, Chicago, IL 60637

‡now at: University of Leeds, Leeds LS2 9JT, U.K.

2 Mathematics:

The influence of any type of fluctuations on a certain distribution of observables or even just the transformation of one observable to another is described by a *Fredholm integral equation of 1st kind*:

$$\frac{dJ_i}{d\lg N_j} = \int_{-\infty}^{\infty} \frac{dJ_i}{d\lg E}\, p_i(\lg E \to \lg N_j)\, d\lg E \quad \text{with } i = p, ..., fe \text{ and } j = e, \mu \tag{1}$$

The lefthand side represents the evaluated size spectra for various primaries i, and the so-called *kernel* function p_i is the probability for a primary of the given energy E that an air shower is reconstructed with a certain shower size N_j.

Actually it is helpful to factorize the kernel function to reflect the stages of shower development, detector sampling and reconstruction:

$$p(\lg E \to \lg N_j) = \int_{-\infty}^{\infty} p_{dev}(\lg E \to \lg N'_j)\, p_{eff}(\lg N'_j)\, p_{rec}(\lg N'_j \to \lg N_j)\, d\lg N'_j \tag{2}$$

with the probability p_{dev}, that a shower arrives at the observation level with given size N', the trigger efficiency p_{eff}, which depends mainly on the number of detected particles and the probability p_{rec}, taking into account the statistical and systematical reconstruction errors.

To solve equation (1) for the primary spectrum dJ_i/dE an appropriate parameterization of the primary spectrum is done and the spectral parameters are estimated by fitting the theoretical distribution (1) to the measured size spectra. This method allows us to use the additional information that the primary spectrum obeys a power law. In the following analysis the primary energy spectrum is parameterized as a function of five parameters. The spectral indices $\gamma_{1,2}$ below and above the knee, the position of the knee E_k, the flux at the knee dJ/dE_{knee} and the width of the knee ΔE, which describes the region around the knee, where the spectral index is changing from γ_1 to γ_2.

3 Fluctuations:

To determine the above kernel functions one needs detailed information about the dependence of fluctuations on primary energy resp. showers size for the various primary particles. The shower simulation code CORSIKA (Heck et al., 1998) was used with the interaction model OGSJET to obtain the necessary data. To minimize the amount of simulations the MC data set was limited to proton and iron primaries with a zenith angle of 22°. For the study of the shower development fluctuations and the average dependence of shower size upon primary energy the *thinning* option of CORSIKA was used which allowed the generation of an appropriate large number of individual showers from 3×10^{13}eV up to 10^{17}eV. A different data set of full simulated showers from 10^{14}eV to 10^{16}eV was used to get the detector responses from a detailed detector monte carlo. These responses where analyzed in the same way as the experi-

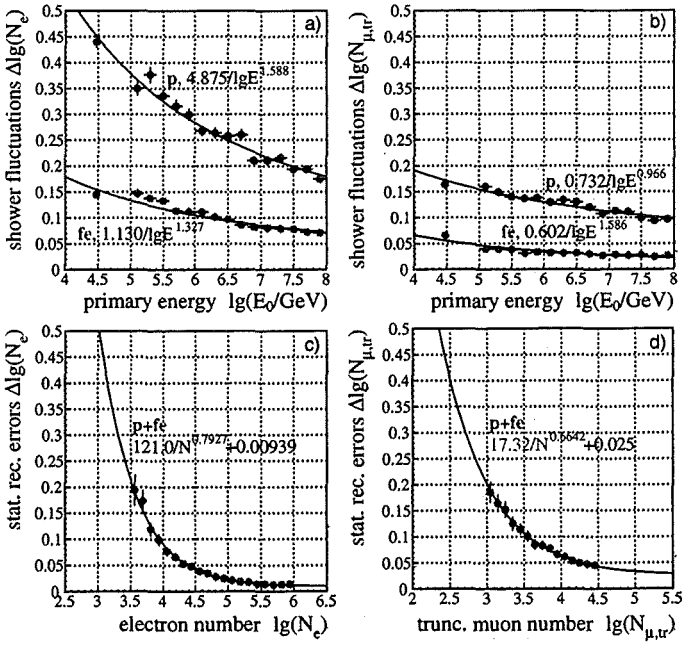

Figure 1: Shower development fluctuations and statistical reconstruction errors of shower sizes.

mental data by the KASCADE reconstruction code to get the statistical and systematical errors of the reconstruction as well as the efficiencies.

Figure 1 shows the parameterized standard deviations resulting from this analysis. Both kind of fluctuations are well described by a normal distribution on a logarithmic scale. Since the statistical errors do not depend significantly on the type of the primary, only one function is used for the parameterization. It can be seen that for protons the shower fluctuations always are dominating, whereas for iron induced showers those are reduced by a factor of about 3. Therefore the statistical errors become important, especially for the muon component of small showers.

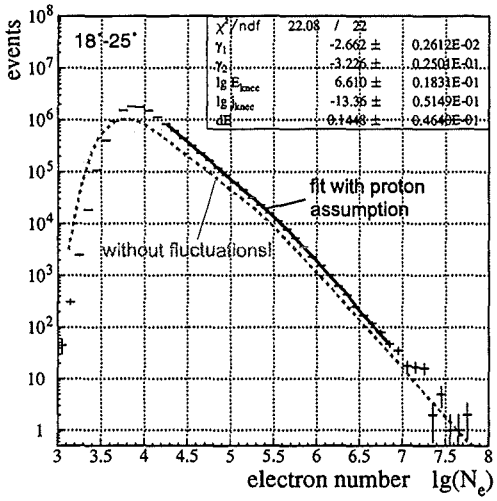

Figure 2: Fit of shower size spectrum including proton fluctuations.

To illustrate the effect of the fluctuations in Fig. 2, the fit of the electron size spectrum using the proton kernel function and the resulting energy spectrum parameters are plotted. The data are as well described as in former analyses (Glasstetter et al., 1998) where the size spectra directly were parameterized by two power law functions. Now the fluctuations have been taken into account and the values of the parameters have changed significantly. The dashed line shows the hypothetical spectrum that would have been measured with the quoted primary parameters and fluctuations *switched off*.

In Table 1 the results of direct fits are listed together with the actual ones, which are obtained by separate fits to the electron and truncated muon spectra assuming a pure proton or iron composition. Fit errors are not given because the systematical errors by assuming the wrong composition are at least a factor of 10 larger than the statistical ones. As one can see the primary spectral indices have become smaller by 0.1-0.2. The knee positions are also at smaller values, hence, the primary fluxes at the knee have become larger. Nevertheless, the fluxes and spectral indices above the knee, derived separately from the electron and muon spectra with these assumed pure compositions, are still inconsistent even with fluctuations taken into account.

		PROTON				IRON			
		γ_1	γ_2	E_{knee}	dJ_{knee}/dE	γ_1	γ_2	E_{knee}	dJ_{knee}/dE
no fluct.	N_e	-2.83	-3.42	5.6	$2.5{\cdot}10^{-14}$	-2.85	-3.44	11.	$1.3{\cdot}10^{-14}$
	$N_{\mu,tr}$	-2.88	-3.04	4.7	$5.2{\cdot}10^{-14}$	-2.88	-3.04	3.7	$6.6{\cdot}10^{-14}$
incl. fluct.	N_e	-2.66	-3.22	4.0	$4.7{\cdot}10^{-14}$	-2.84	-3.31	9.0	$2.1{\cdot}10^{-14}$
	$N_{\mu,tr}$	-2.58	-2.99	3.0	$16.{\cdot}10^{-14}$	-2.69	-3.02	3.5	$7.1{\cdot}10^{-14}$

Table 1: Comparison of primary energy spectra fit parameters derived independently from electron and muon spectra assuming pure compositions (E_{knee} in PeV and dJ_{knee}/dE in $\mathrm{m^{-2}s^{-1}sr^{-1}GeV^{-1}}$).

4 Spectra and Composition:

The above analyses have shown that it is obviously impossible to describe the observed size spectra by any pure composition in a consistent way. On the other hand, using the presented fitting procedure there is no reason anymore to fit the size spectra separately. Therefore, a combined χ^2-minimization has been chosen to fit both size spectra simultaneously:

$$\chi^2 = \sum_{j=e}^{\mu} \sum_{k=n_{min,j}}^{n_{max,j}} \left(\frac{dJ/d\lg N_j \cdot \Delta \lg N_j - J_{j,k}}{\sqrt{J_{j,k}}}\right)^2 \qquad (3)$$

The $J_{j,k}$ represent the number of events in the bin k with width $\Delta \lg N_j$ and the theoretical functions $dJ/d\lg N_j$ are now the sum over the Fredholm integrals (1) for the two extreme primary particles (p and Fe), which should be taken as representatives for a light and heavy group of primary particles.

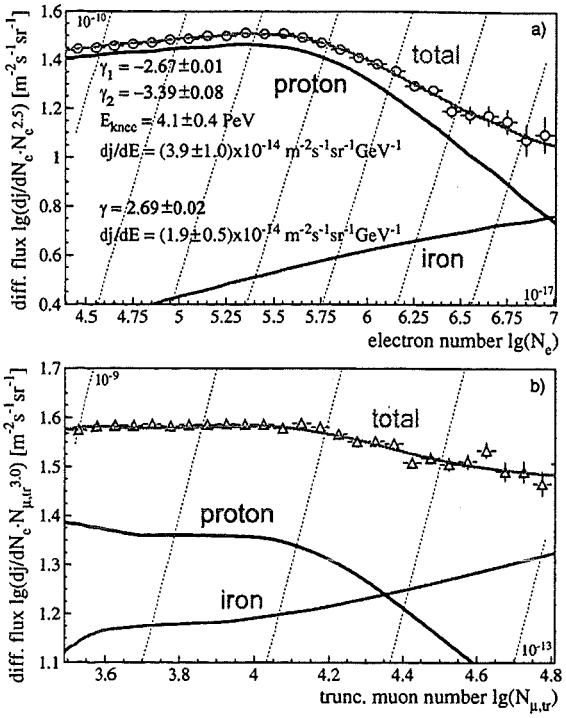

Figure 3: Electron and trunc. muon size spectra fitted simultaneously with a two-component composition ($\vartheta = 18° - 25°$).

ranges in Fig. 3, the lines outside are extrapolated. Below the knee at approx. 4PeV there is a nearly constant composition with 30% heavy contributions. This changes above the knee at 10^{16}eV to 50% and at 10^{17}eV even to 80%. The total flux in that region coincides well with values of other experiments and the generally accepted values for the spectral indices.

If the heavy component would proceed with that behavior, then the all-particle spectrum above 10^{17}eV should become flatter as the extrapolated straight line indicates. This would be in disagreement with most experiments performed in that region, whereas a rigidity like cut-off of the iron component due to the escape of the particles from the galaxy at around $26 \times E_{k,proton}$ with an index of 3.1 (dashed line) fits the data.

To reduce the number of free parameters, the width of the knee was fixed to $\Delta E = \pm 0.15$, which resulted from the single spectra fits. There are 8 free parameters: the spectral indices, the knee position and the flux at the knee for each primary. An first attempt has shown that the spectral index of the iron component above the knee with respect to the fit error is nearly identical to the index below the knee with an very large error on the *knee position.* Therefore, the final fit was performed with a six parameter function, describing the iron component as a single power law without any bend in slope within the fitted region.

The resulting primary parameters with statistical errors are plotted in Figure 3 together with the underlying size spectra. The dotted lines represent lines of constant flux, with the maximum and minimum values plotted in the corners. Despite our simplifications both spectra are described very well over the whole range (χ^2/ndf=1.14). The electron size spectrum (a) is dominated by the proton component, which is responsible for the steep slope above the knee, whereas the trunc. muon number spectrum (b) reflects more the behavior of the total energy spectrum.

Figure 4 shows the parameterized primary energy spectra. The grey shaded regions correspond to the fitted

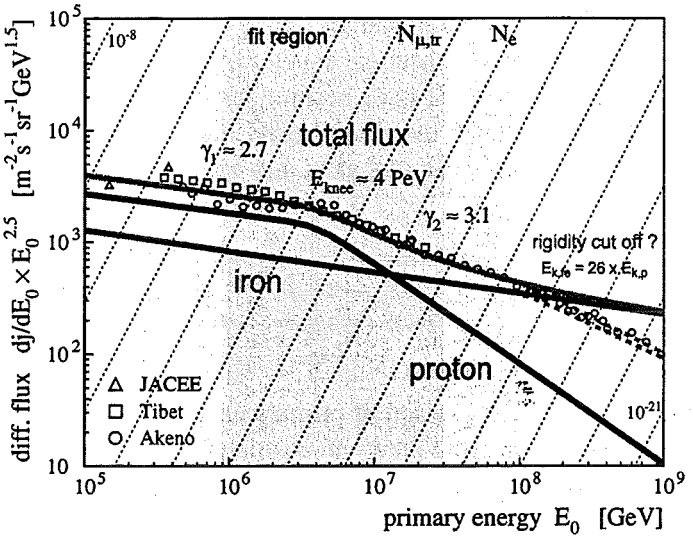

Figure 4: Energy spectra resulting from the simultaneous fit of electron and trunc. muon spectra.

References

Glasstetter, R., Hörandel, J.R. et al., 1998, Proc. 16^{th} ECRS, Alcalá, 559
Heck, D. et al., 1998, FZKA 6019, Forschungszentrum Karlsruhe
Klages, H.O. et al., 1997, Nucl. Phys. B (Proc. Suppl.), 52B 92

HE 2.2.04

Estimation of the Energy Spectrum in the Knee Region by the KASCADE-Experiment

A.A. Chilingarian[1*], T. Antoni[2], W.D. Apel[2], F. Badea[4], K. Bekk[2], K. Bernlöhr[2], E. Bollmann[2], H. Bozdog[4], I.M. Brancus[4], K. Daumiller[2], P. Doll[2], J. Engler[2], F. Feßler[2], H.J. Gils[2], R. Glasstetter[2], R. Haeusler[2], W. Hafemann[2], A. Haungs[2], D. Heck[2], J.R. Hörandel[2 †], T. Holst[2], K.-H. Kampert[2], J. Kempa[3], H.O. Klages[2], J. Knapp[2 ‡], H.J. Mathes[2], H.J. Mayer[2], J. Milke[2], D. Mühlenberg[2], J. Oehlschläger[2], M. Petcu[4], H. Rebel[2], M. Risse[2], M. Roth[2], G. Schatz[2], F.K. Schmidt[2], T. Thouw[2], H. Ulrich[2], A. Vardanyan[1], B. Vulpescu[4], J.H. Weber[2], J. Wentz[2], T. Wibig[3], T. Wiegert[2], D. Wochele[2], J. Wochele[2], J. Zabierowski[3]

[1]*Yerevan Physics Institute, Cosmic Ray Division, Armenia*[§]

[2]*Institut für Kernphysik and Institut für Experimentelle Kernphysik, Forschungszentrum and Universität Karlsruhe P.O. Box 3640, D–76021 Karlsruhe, Germany*

[3]*Institute for Nuclear Studies and Dept. of Experimental Physics, University of Lodz, PL–90950 Lodz, Poland*

[4]*National Institute of Physics and Nuclear Engineering, RO–7690 Bucharest, Romania*

Abstract

The KASCADE experiment measuring a larger number of EAS observables with an improved sampling of the electron-photon, hadron, and muon components than previous experiments, provides data accurate enough for an event-by-event analysis of the energy dependence of the primary cosmic ray flux in the energy range of $10^{14} - 10^{16}$ eV. Multivariate statistical analysis approaches enable to estimate the primary cosmic ray flux and the elemental composition. The major feature in the observed PeV energy region, the so called *knee* is reproduced, spectral indices and the knee energy are determined.

1 Introduction:

The knowledge of the energy spectra of primary cosmic rays in the knee region is of great importance for testing alternative hypotheses of the cosmic ray (CR) origin, acceleration, and propagation. The manifold interpretations of CR experiments have their causal connection in the inadequate knowledge about the characteristics of hadronic interactions above accelerator energies. Moreover uncertainties in the CR composition, caused by strong fluctuations of the shower parameters give rise to this ambiguities. The different detector types of the KASCADE experiment (Klages, 1997) measure simultaneously the three charged shower components. This allows not only to take the whole valuable information of EAS showers into account, but to make cross checks in estimating the energy and mass of individual events by different observables. Systematic effects by using various observables e.g. for energy estimation can be studied.

2 EAS Reconstruction:

2.1 The detector setup: The basic concept of the KASCADE experiment is to measure a large number of observables for each individual event with good accuracy and high degree of sampling. For this reason 252 detector stations forming a detector array of 200×200 m^2 containing liquid scintillation detectors for detecting the electromagnetic component on the top of a lead/iron absorber plate as well as plastic scintillators below the shielding. A detector coverage of more than 1% for the electromagnetic and about 2% for the muonic component EAS is achieved. In combination with a precise measurement of the hadrons using a large iron sampling calorimeter the shower core can be investigated in great detail. So the main part of the central detector

*corresponding author: e-mail: chili@ik3.fzk.de

†now at: University of Chicago, Enrico Fermi Institute, Chicago, IL 60637

‡now at: University of Leeds, Leeds LS2 9JT, U.K.

§The work has been partly supported by a research grant (No.94964) of the Armenian Government and by the ISTC project A116.

system is a large hadron calorimeter. It consists of an 20×16 m^2 iron stack with eight horizontal gaps. 10,000 ionisation chambers are used in six gaps and below the iron stack for the measurement of hadronic energy in a total of 40,000 electronic channels. The third gap is equipped with 456 scintillation detectors for triggering and timing purposes. Below the iron stack two layers of multiwire proportional chambers (MWPCs) are mounted for the measurement of muon tracks and studies of structures in the muon lateral distribution in EAS cores.

2.2 Relevant Observables: The presented detailed analysis of EAS benefits from the simultaneous measurement of a large number of quantities for each individual event. This enables multidimensional analyses for the reconstruction of the energy and the mass of the primary. Specific EAS parameters measurable by the experiment KASCADE are used, like the number of electrons N_e, the truncated number of muons N_μ^{tr} (Glasstetter, 1997; Weber, 1997), the number of reconstructed hadrons N_h^{100GeV} with an energy larger than 100 GeV, the sum of the energy of this hadrons $\sum E_h$, the energy of the mostenergetic hadron $\max E_h$ (Hörandel, 1997) and the number of muons $N_\mu^\star$ with an energy threshold of $E_\mu \geq 2$ GeV measured below the central calorimeter by the MWPCs (Haungs, 1996).

Two sets of data are used. "Selection I" uses the information from the array of field stations on electrons and muons. It permits to analyse the data with good statistical accuracy but has no information from the central detector. "Selection II" uses in addition many observables measured in the central detector but has the disadvantage of a reduced data sample (Roth, 1999).

Therefore 720,000 events with an energy larger than $E \approx 5 \cdot 10^{14}$ eV and a maximal core distance to the centre of the field array of 91 m are selected (set "selection I"). Approximately 8000 high-energetic ($E > 10^{15}$ eV), central showers are collected by cuts of N_μ^{tr} ($> 10^{3.6}$), the core location ($R_{core} < 5$ m from the centre of the central detector system), at least one hadron with an energy above 100 GeV and 10 muons in the MWPCs (set "selection II").

2.3 Simulations: Simulations have been performed with the models VENUS and QGSJet in the energy range $10^{14} - 3.16 \cdot 10^{16}$ eV using the CORSIKA code (Heck, 1998).

For each primary (p, He, O, Si, and Fe) approximately 2000 EAS events have been simulated, distributed in the energy range with an decreasing particle flux. The core of the EAS lies within a 5 m radius away from the centre of the central detector. The response of all detector components is taken into account in great detail using the GEANT code. Afterwards the simulated events are treated like measured ones, therefore measured and simulated data are stored and furthermore reconstructed with the same procedures.

3 Energy Estimation:

The techniques presented by Chilingarian (Chilingarian, 1998) on the basis of nonparametric multivariate methods (neural networks, Bayesian decision making) are developed and applied to infer the energy and/or the mass of primary particles on an event-by-event analysis.

The best summary of accumulated knowledge in simulation trials are the nonparametric multidimensional

	QGSJet	VENUS
γ_1	$2.72 \pm 0.003 \pm 0.03$	$2.87 \pm 0.003 \pm 0.04$
γ_2	$3.22 \pm 0.05 \pm 0.06$	$3.25 \pm 0.04 \pm 0.06$
E_{knee} [10^6 GeV]	$6.39 \pm 0.14 \pm 0.7$	$6.22 \pm 0.27 \pm 0.8$
ϵ	$14.10 \pm 5.58 \pm 5.$	$11.61 \pm 4.04 \pm 6.$
χ^2/dof	3.90	3.68

Table 1: Spectral indices and different other parameters as a result of the fitting procedure (including statistical and systematical errors).

probability density functions as well as a set of weights of "trained" neural networks. Due to the stochastic nature of the cascade development in the atmosphere it can't be expected that analytic probability distributions will describe any measurable EAS parameter. Moreover, very long (usually unregular) tails of the parameter distributions require considerable large amount of simulations to map all possible misclassifications and errors.

The Feed-Forward Neural Network (FFNN) provides the mapping of a complicated input signal to the regressand value (energy) in the estimation case (and to the class assignments in the classification case) (Chilingarian, 1994, 1997). The network training is performed by minimising a special quality function Q. The figure of merit to be minimised is simply the discrepancy of apparent and target outputs over all training samples M_k of all primaries $k \in \{p, O, Fe\}$.

The network has typically a $2 \times 5 \times 3 \times 1$ topology using N_e, N_μ^{tr} as input and the energy as output parameters.

The fitting function to the energy response function (output) is

$$f(E) = c \cdot E^{-\gamma_1} \left(1 + \left(\frac{E}{E_{knee}}\right)^{\epsilon}\right)^{\frac{\gamma_1 - \gamma_2}{\epsilon}}.$$

Table 1 displays the results of the fitting procedure. The parameter ϵ describes the curvature of the knee feature. A small one (e.g. $\epsilon = 1$) gives a sharp and a large one (e.g. $\epsilon = 40$) a smooth knee.

The all-particle energy spectrum resulting from different networks shows strong model dependence ($\gamma_{QGSJet} = 2.72$ and $\gamma_{VENUS} = 2.87$; see figure 1). The slope difference 0.16 between the models below the knee is even larger than the methodical errors of 0.04.

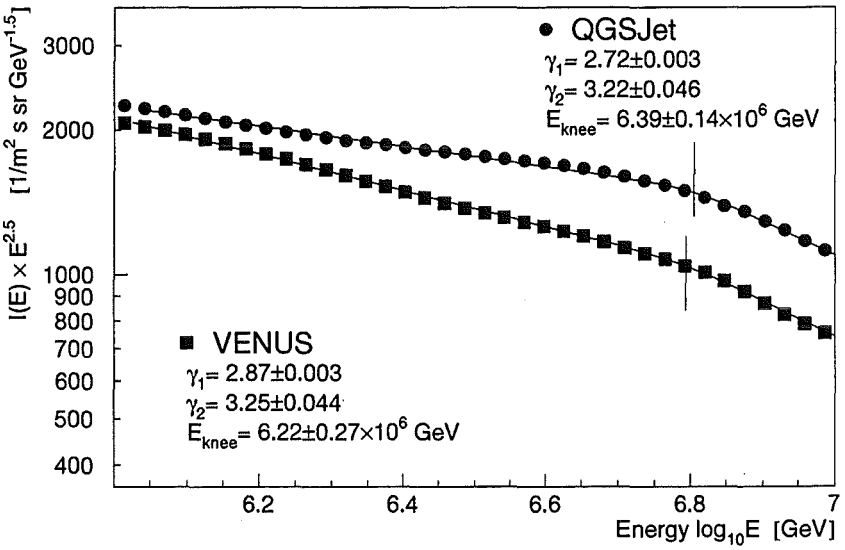

Figure 1: All particle energy spectrum of "selection I" data (see text for explanation) as a result of a neural net analysis (QGSJet and VENUS data trained networks were used).

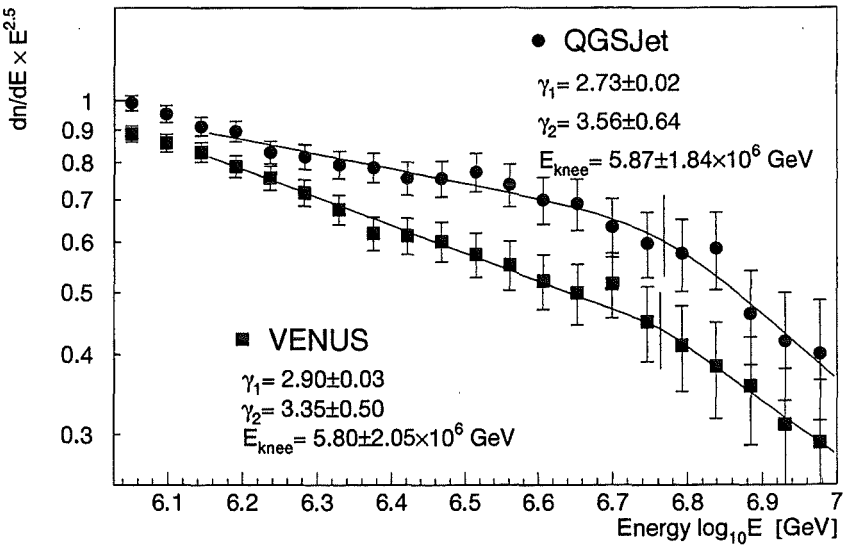

Figure 2: All-particle energy spectrum of "selection II" data with ordinate units (see text for explanation) as a result of a neural net analysis (QGSJet and VENUS data trained networks were used).

To proof the possibility of selecting different data sets without introducing systematic errors, the same trained network (N_e, N_μ^{tr}, s) was applied to estimate the energy of the "selection II" events. The resulting energy spectrum is given in figure 2. Within the statistical errors

the spectral indices (QGSJet and VENUS) below the knee are the same as in figure 1. There aren't enough measured events above the knee to reconstruct a reasonable index with small statistical errors. These events provide nevertheless the opportunity to estimate the spectral index below the knee by using different sets of observables in neural net analyses. The good agreement of the resulting indices is shown in case of QGSJet trained networks in table 2.

	Spectral Index	Observables	
	$2.72 \pm 0.003 \pm 0.02$	selection I N_e, N_μ^{tr}, s	
	$2.73 \pm 0.03 \pm 0.05$	selection II N_e, N_μ^{tr}, s	*
	$2.70 \pm 0.05 \pm 0.05$	selection II N_μ^{tr}, $N_\mu^{\star}$	*
	$2.74 \pm 0.05 \pm 0.05$	selection II N_μ^{tr}, $N_h^{E>100\,\mathrm{GeV}}$	*
	$2.74 \pm 0.05 \pm 0.05$	selection II $N_\mu^{\star}$, $N_h^{E>100\,\mathrm{GeV}}$	*
	$2.71 \pm 0.04 \pm 0.05$	selection II $N_\mu^{\star}$, $\sum E_h$	*
	$2.75 \pm 0.05 \pm 0.09$	selection II $N_\mu^{\star}$, $\max E_h$	*
	2.73 ± 0.05	all (*) averaged	

Table 2: Spectral index γ_1 below the knee (QGSJet simulations) as a result of the neural net analysis. (The systematic errors are estimated by different types of network topologies.)

The results of the presented analyses on the energy dependence of the all-particle spectrum have preliminary character due to the insufficient amount of simulated events and also the lag of central detected showers to determine spectral indices above the knee. Nevertheless the major feature of the observed energy region (the abrupt change of the spectrum) is reproduced. Taking different sets of observables the resulting spectral indices remain the same within the statistical errors. The results show the necessity of investigating the model dependence in detail in order to overcome artifical features of specific models and to get reliable information for understanding origin, acceleration, and propagation of cosmic rays.

References

Chilingarian, A. et al., Proc. 16th ECRS (Madrid, 1998), 571
Chilingarian, A.A. 1994, *Neurocomputing* 6, 497
Chilingarian, A.A. et al. 1997, *Nuclear. Phys. B (Proc. Suppl.)* 52B, 237
Glasstetter, R. et al., Proc. 25th ICRC (Durban, 1997) Vol 6, 157
Haungs, A. et al. 1996, *Nucl. Instr. Meth.* A372, 515
Heck, D. et al. 1998, FZKA-Report 6019, Forschungszentrum Karlsruhe, Germany
Hörandel, J.R. et al., Proc. 25th ICRC (Durban, 1997) Vol 6, 93
Klages, H.O. et al. 1997, *Nucl. Phys. B (Proc. Suppl.)*, 52B, 92
Roth, M. 1999, FZKA-Report 6262, Forschungszentrum Karlsruhe, Germany
Weber, J.H. et al., Proc. 25th ICRC (Durban, 1997) Vol 6, 153

HE 2.2.37

A Model Independent Method for Determination of Muon Density Fluctuations in EAS

M. Giller[5] T. Antoni[1], W.D. Apel[1], A.F. Badea[2], K. Bekk[1], K. Bernlöhr[1], E. Bollmann[1], H. Bozdog[2], I.M. Brancus[2], A. Chilingarian[3], K. Daumiller[4], P. Doll[1], J. Engler[1], F. Feßler[1], H.J. Gils[1], R. Glasstetter[4], R. Haeusler[1], W. Hafemann[1], A. Haungs[1] D. Heck[1], T. Holst[1], J.R. Hörandel[4], K.-H. Kampert[1,4], H. Keim[1], J. Kempa[5], H.O. Klages[1], J. Knapp[4], H.J. Mathes[1], H.J. Mayer[1], J. Milke[1], D. Mühlenberg[1], J. Oehlschläger[1], M. Petcu[2], T. Pytlos[5], H. Rebel[1], M. Risse[1], M. Roth[1], G. Schatz[1], F.K. Schmidt[4], T. Thouw[1], H. Ulrich[1], A. Vardanyan[3], B. Vulpescu[2], J.H Weber[4], J. Wentz[1], T. Wibig[5], T. Wiegert[1], D. Wochele[1], J. Wochele[1], J. Zabierowski[6], S. Zagromski[1],

[1]*Forschungszentrum Karlsruhe, Institut für Kernphysik, Karlsruhe, Germany*

[2]*Institute of Physics and Nuclear Engineering, Bucharest, Romania*

[3]*Cosmic Ray Division, Yerevan Physics Institute, Yerevan, Armenia*

[4] *Institut für Experimentelle Kernphysik, University of Karlsruhe, Germany*

[5] *Division of Experimental Physics, University of Lodz, Łódź, Poland*

[6] *Soltan Institute for Nuclear Studies, Łódź, Poland*

Abstract

It is shown how to determine fluctuations of the muon density in EAS at a given distance from the core, for showers with a fixed size. The method does not make use of any pre-assumed lateral muon distribution and uses only information whether muon detector has been hit by at least one muon.

1 Introduction:

The KASCADE experiment gives a unique opportunity to study in detail some shower characteristics due to a large number of detectors. In particular it is suitable to determine fluctuations of the muon densities in showers using the information from the Array of 192 muon detectors (3.24 m^2 each). In this paper we present how to determine the muon density probability distribution at a given core distance R for showers with fixed shower size N_e. In our method the muon density ρ_μ at a given R, is not being determined for each individual shower as that would need an a priori assumption about its lateral distribution. We prefer to avoid this and the fluctuations of $\rho_\mu(R)$ have been reconstructed from a sample of showers with fixed N_e.

2 The idea:

The shower sample used in this analysis has been obtained from a sample of the KASCADE data. We have chosen only almost vertical showers (zenith angle $< 18^o$). Our sample has been further divided into rather narrow bins of shower size $\Delta \log N_e = 0.1$. Our aim is to determine probability density distribution f(N) of the number of muons N falling on a fixed distance ring, for a sample of showers from a fixed N_e bin. The core distance has been divided into bins of $\Delta R = 10$ m. We shall use here the information from the muon Array detectors, with $E_{th} > 0.3$ GeV. Fluctuations of N are caused by fluctuations in shower development in the atmosphere and by the distribution of the primary particle mass.

Let us first choose the showers with a fixed number of muon detectors m at a given distance ring. If their number is $n(m)$ then the average number of showers $\langle \mathrm{F}(k;m) \rangle$ with k (out of m) muon detectors being hit by at least one muon, should be

$$\langle \mathrm{F}(k;m) \rangle = n(m) \int_0^\infty \binom{m}{k} \left(1 - e^{-\alpha N}\right)^k e^{-\alpha N(m-k)} \cdot \mathrm{f}(N) dN \qquad (1)$$

where $\alpha = S_{det}/S_{ring}$ (ratio of the area of a muon detector to that of the whole distance ring). In (1) we have assumed that showers have radial symmetry and that the N muons fall on the whole ring $(R, R + \Delta R)$

independently and randomly. To determine $\mathrm{F}(k;m)$ experimentally we need a criterion for a muon detector to be hit by at least one muon. First, we make our analysis only for distances $R > 40$ m, where the punch through effect can be almost neglected (at least for smaller showers). Next, after looking at distributions of the energy deposit for single muons from many muon detectors, we have chosen $E > 3.5$ MeV as our condition that a detector has been hit by muon(s). We would like to underline here that for our purpose we do not have to worry about how many muons have hit a detector (which is not always possible with a good accuracy).

The actually observed number of showers $\mathrm{F}(k;m)$ with k hit detectors fluctuates with the Poissonian distribution around its expected value, given by (1) and is of course the better representation of its mean $\langle \mathrm{F}(k;m) \rangle$, the bigger is the number of showers $n(m)$. The KASCADE experiment has a big advantage of having many muon detectors (192 in the Array), allowing the number m of available detectors in a given ring to reach values even above twenty (being around 10 most frequently).

Thus, in principle we can measure many values $\mathrm{F}(k;m)$ as $0 \leq k \leq m$, and for many m as well. Our sample, however, was not big enough for all experimental $\mathrm{F}(k;m)$ to represent their expected values $\langle \mathrm{F}(k;m) \rangle$ with a good accuracy. So, to determine $\mathrm{f}(N)$ (for any N_e and R bin) we have summed our $\mathrm{F}(k;m)$ histograms over all m (over all positions of the shower core), obtaining histograms $\mathrm{F}(k) = \Sigma_m \mathrm{F}(k;m)$. By summing up over m we lose some information contained in the k distributions for each individual m. We gain however, by getting smaller statistical relative uncertainties of $\mathrm{F}(k)$ and by simplifying evaluation of $\mathrm{f}(N)$.

3 Factorial moments of the distribution of k and a check of the Array:

From (1) are can easily calculate moments of the probability distribution of k: $\langle k \rangle$, $\langle k^2 \rangle$ and so on. It turns out, however, that in this case it is the factorial moments of k which are in a simpler way related to the muon number distribution $\mathrm{f}(N)$:

$$\langle k(k-1)\dots(k-i+1) \rangle = m(m-1)\dots(m-i+1) \cdot \int_0^\infty \left(1 - e^{-\alpha N}\right)^i \mathrm{f}(N) dN \qquad (2)$$

for $i = 1, 2, \dots$. As $1 - e^{-\alpha N} = p$, where p is the probability of hitting a detector once N muons have fallen on the ring, we see that the integrals in the right-hand sides of (2) represent the successive moments of the distribution of p. Thus, in principle, having all moments one could obtain the probability distribution of p, $\mathrm{g}(p)$, and then $\mathrm{f}(N) = \mathrm{g}[p(N)]$. We notice, however, that the higher is the order of the factorial moment of k, the smaller is the part of the k distribution on which it depends. Thus, as the number of showers with higher k finally decreases, one would need very big statistics in order to determine higher order moments of k (and p) with a reasonable accuracy. So, in our analysis we shall not use formulae (2) to determine muon fluctuations $\mathrm{f}(N)$. We shall use them, however, to check the homogeneity of the detection conditions of the Array. From (2) it follows that neither $\langle k \rangle / m$ nor $\langle k(k-1) \rangle / m(m-1)$ should on average, depend on m, that is, on the position of the shower core. Fig.1 represents the experimentally obtained ratios, as a function of m, for fixed N_e and different R. It can be seen that, within the statistical errors, the ratios do remain independent of m for almost any case, confirming the homogeneity of the Array.

4 Methods of determining muon density fluctuations $\mathrm{f}(N)$:

As we have already explained, the basis for determining $\mathrm{f}(N)$ (for any fixed N_e and R bin) is a set of equations (1) summed over m, for $k = 0, 1..., m_{max}$. To find $\mathrm{f}(N)$, we have applied the three following methods:

4.1 Numerical fit: The integral in the right-hand side of (1) summed over m was approximated by a sum of 10 values of the integrated function at 10 values of N. The ten unknowns $\mathrm{f}(N_i)$ were then found by a maximum likelihood method allowing for the statistical fluctuations of $\mathrm{F}(k)$. The CERN program MINUIT was used to find these best fitting values $\mathrm{f}(N_i)$ on condition that $\mathrm{f}(N_i) \geq 0$.

4.2 Method using three moments of N distribution: It can be applied if $\alpha N \ll 1$. After expanding $e^{-\alpha N}$ in (2), keeping only first three terms and averaging over m we can express the three experimentally de-

termined factorial ratios: $\langle k \rangle \,/\, \langle m \rangle$, $\langle k(k-1) \rangle \,/\, \langle m(m-1) \rangle$ and $\langle k(k-1)(k-2) \rangle \,/\, \langle m(m-1)(m-2) \rangle$ as linear combinations of $\overline{N}$, $\overline{N^2}$, and $\overline{N^3}$. The latter moments can be easily found. Next we assume that $\mathrm{f}(N)$ has a shape of a gamma function: $\mathrm{f}(N) \sim N^{p-1} e^{-qN}$, and calculate p and q from $\overline{N}$, and $\overline{N^2}$.

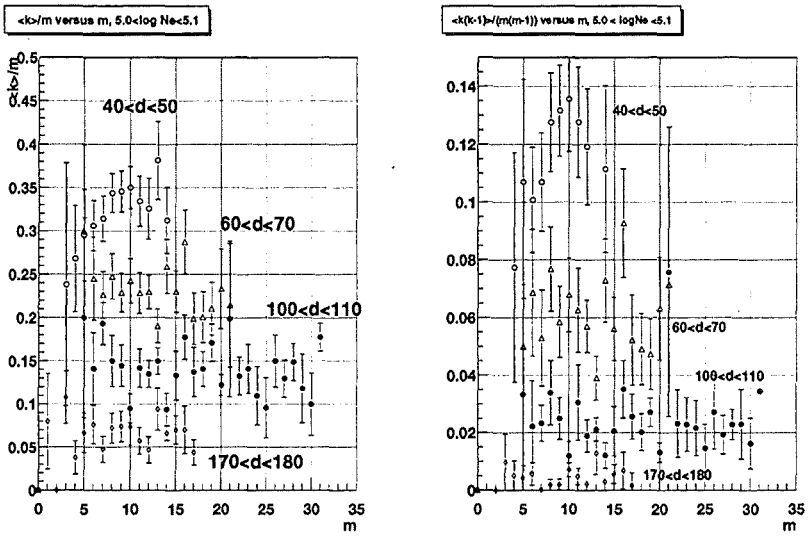

Figure 1: Ratios of the first (left) and second (right) factorial moments, $\langle k \rangle / m$ and $\langle k(k-1) \rangle / m(m-1)$ for $5 < \log N_e < 5.1$ and several $R(m)$.

4.3 Method adopting $\mathrm{f}(N)$ as a gamma function: Here, we assume from the very beginning that $\mathrm{f}(N)$ can be described by a gamma function. Inserting it into equations (2a) and (2b) and averaging over m we can express the first two factorial ratios (as in the previous case) as function of p and q. The parameters p and q can be found numerically. This method does not require small muon densities, as in the case 4.2.

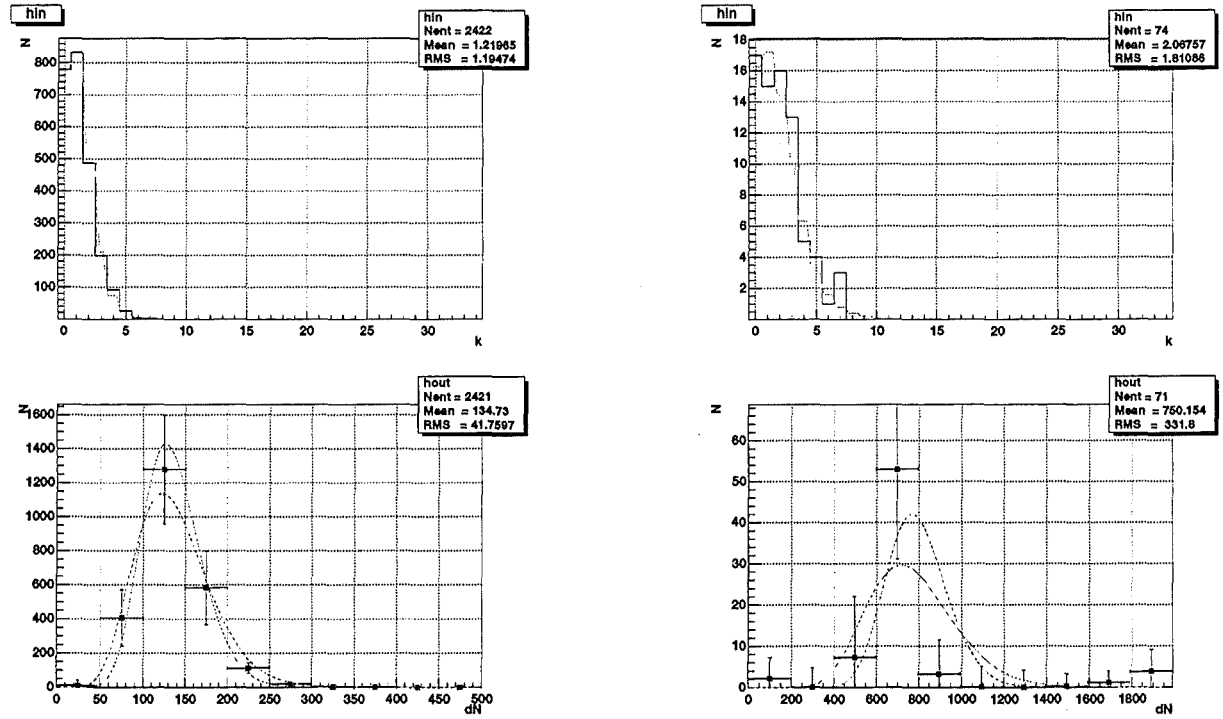

Figure 2: Distribution of the number of hit muon detectors (N_e, R fixed) – upper histograms. Corresponding calculated distributions of N – number of muons in the distance ring – lower graphs. Left graphs: $4.5 < \log N_e < 4.6$ and $60 < R < 70$m; right graphs: $5.5 < \log N_e < 5.6$ and $160 < R < 170$m. Points – method 4.1; dashed line – method 4.2; dotted line – method 4.3. The dotted histograms (upper graphs) are calculated $\langle \mathrm{F}(k) \rangle$ for $\mathrm{f}(N)$ found by method 4.1 (MINUIT).

5 Results:

Fig.2 illustrates the results of our analysis. The upper histograms are the observed distributions $\mathrm{F}(k)$, chosen for some particular values of N_e and R. The lower graphs represent the corresponding distributions $\mathrm{f}(N) \cdot \Delta N$ (multiplied by the total number of events for each case), obtained by the three methods. It can be seen that $\mathrm{f}(N)$ obtained by the three different methods give similar results. For example for $5.0 < \log N_e < 5.1$ the differences of $\overline{N}$ calculated by the three methods are typically below 5%. The muon lateral distributions $\rho_\mu(R)$ obtained in this paper agree reasonably well with the results of another analysis of the KASCADE data (Leibrock et al., 1998), as it is shown in Fig.3. The dispersions of the distribution $\mathrm{f}(N)$ obtained by the three methods differ more significantly, sometimes even by factor of two. The first method, based on MINUIT, gives usually the biggest value. As it fits ten values of $\mathrm{f}(N)$, instead of two parameters of an analytic (gamma) function, as in the other two methods, we think that it gives a better description of reality (although it probably is more sensitive to fluctuations of $\mathrm{F}(k)$. The dispersions σ_ρ relative to $\overline{\rho_\mu}$ determined by the first method, are presented in Fig. 4. We can see that typical values are 30 - 40%. For rather small N_e, where our statistics were the best, a trend of increasing relative fluctuations with the core distance R can be observed, although its statistical significance is not big. The fluctuations of ρ_μ for fixed N_e should be sensitive to the primary composition. Shower simulations are needed to show how big this effect is for the low energy muons considered here. With big statistics, available from the KASCADE experiment, it would be possible to obtain more detailed determination of the shapes of the N (*i.e.* ρ_μ) distributions.

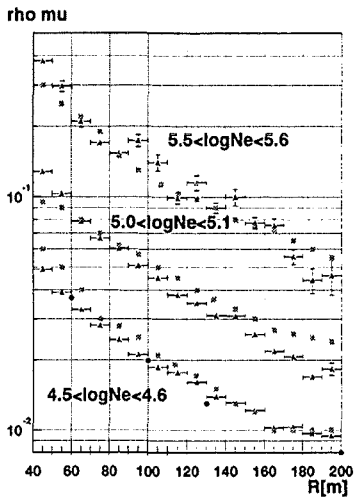

Figure 3: Comparison of the average lateral distributions of muons (ρ_μ in m^{-2}) obtained in this work (triangles) for three bins in N_e, with Leibrock et al. (squares). Circles show values obtained by EAS–TOP (Aglietta et al.) for $E_\mu > 1$ GeV.

This work has been partly supported by the Polish Committee for Scientific Research (KBN), grant no. 2PO3B16012.

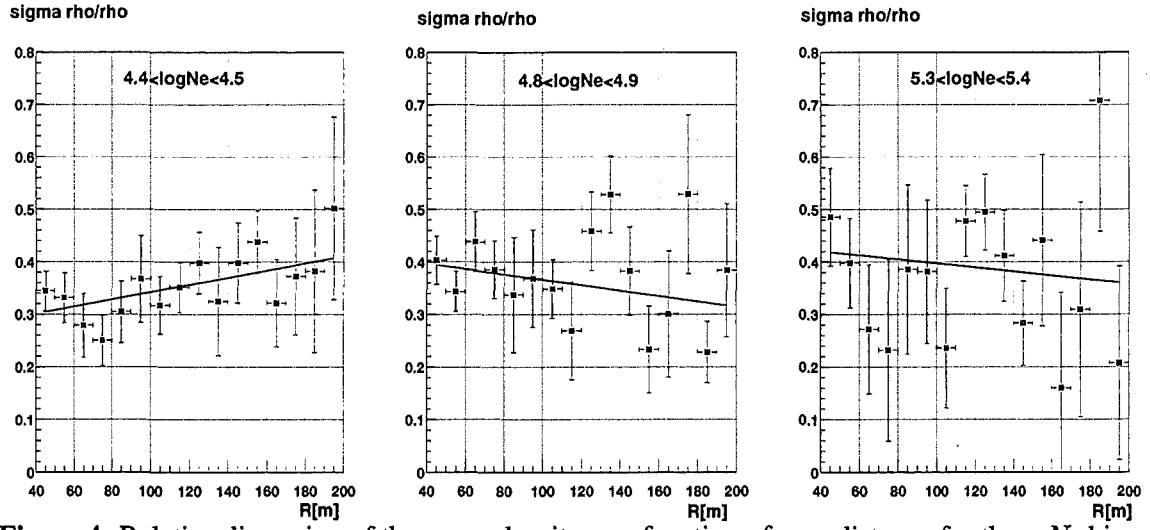

Figure 4: Relative dispersion of the muon density as a function of core distance for three N_e bins.

References

Aglietta, M., et al., (EAS-TOP Coll.), 1995, Proc 24th ICRC, **2**, 664

Leibrock, H., Haungs, A., Rebel, H., 1998, Interner Bericht (51.02.03-F145.0003-98-02), FZ Karlssruhe

HE 2.2.38

Studies of the relative arrival time distributions of the electromagnetic and the muon EAS component in the KASCADE Experiment

R. Haeusler[1], T. Antoni[1], W.D. Apel[1], A.F. Badea[2], K. Bekk[1], K. Bernlöhr[1], E. Bollmann[1], H. Bozdog[2], I.M. Brancus[2], A. Chilingarian[3], K. Daumiller[4], P. Doll[1], J. Engler[1], F. Feßler[1], M. Föller[1] H.J. Gils[1], R. Glasstetter[4], W. Hafemann[1]*, A. Haungs[1], D. Heck[1], T. Holst[1], J.R. Hörandel[1] K.-H. Kampert[1,4], H. Keim[1], J. Kempa[5], H.O. Klages[1], J. Knapp[4] H.J. Mathes[1], H.J. Mayer[1], J. Milke[1], D. Mühlenberg[1], J. Oehlschläger[1], M. Petcu[2], U. Raidt[1] H. Rebel[1], M. Risse[1], M. Roth[1], G. Schatz[1] F.K. Schmidt[4], T. Thouw[1], H. Ulrich[1], A. Vardanyan[3], B. Vulpescu[2], J. Weber[4], J. Wentz[1], T. Wibig[5], T. Wiegert[1], D. Wochele[1], J. Wochele[1], J. Zabierowski[6], S. Zagromski[1],

[1]*Forschungszentrum Karlsruhe, Institut für Kernphysik, D-76021 Karlsruhe, Germany*

[2]*Institute of Physics and Nuclear Engineering, Bucharest, Romania*

[3]*Cosmic Ray Division, Yerevan Physics Institute, Yerevan, Armenia*

[4] *Institut für Experimentelle Kernphysik, University of Karlsruhe, Germany*

[5]*University of Lodz, Institute of Physics, Lodz, Poland*

[6] *Soltan Institute for Nuclear Studies, Lodz, Poland*

Abstract

Arrival time distributions of EAS muons and their differences from the arrival times of the electronmagnetic component, has been measured with the timing facilities of the central detector of the KASCADE experiment. The results have been analysed in terms of CORSIKA Monte-Carlo simulations of the EAS development, based on the QGSJET model.

1 Introductions:

Arrival time distributions of EAS particles reflect the longitudinal EAS development and provide information about the interactions driving the shower cascade. In particular, the muon component has been studied under these aspects. EAS Monte-Carlo simulations by use of the CORSIKA program (Heck et al., 1998) predict differences of the arrival time distributions of the electromagnetic and muon components, specifically showing, that the muon component arrives earlier with respect to the arrival time τ_{cor} of the shower core. Fig. 1 displays the time profile: the mean of the arrival times vs. the distance from the shower axis of the electromagnetic and muon component :

$$\langle \tau_{e,\mu} \rangle = \frac{1}{N} \cdot \sum_{i=1}^{N} \tau_{e,\mu}^{i} - \tau_{cor}^{i} \qquad (1)$$

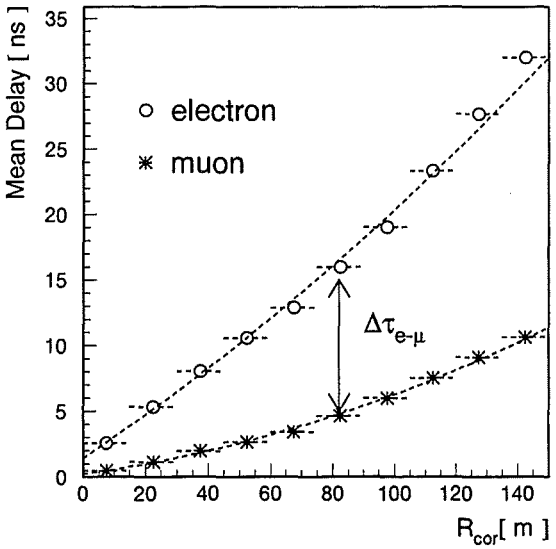

Figure 1: Mean arrival times of the electromagnetic and muon component for simulated EAS

The figure reproduces also the known feature (Ambrosio et al.; 1997, Brancus et al., 1998) that the time profile of the electromagnetic component varies by a steeper increase with the core distance, since the electrons

*corresponding author; e-mail: hafemann@ik3.fzk.de

arriving at the observation level are generally produced in deeper layers of the atmosphere than the observed muons. This fact leads also to the larger delay in the arrival of the electromagnetic component. Though there are practical difficulties to determine the arrival time of the shower core with sufficient accuracy, the difference $\Delta\tau_{e-\mu} = \langle\tau_e\rangle - \langle\tau_\mu\rangle$ is an experimentally accessible quantity. In the present contribution we report about measurements of the relative time profile $\Delta\tau_{e-\mu}(R_{cor})$ for two different energy thresholds of the detected muons. The results are compared with predictions of Monte-Carlo simulations.

2 Experimental setup and general procedures:

For the measurements the timing and particle detection facilities of the KASCADE central detector (Klages et al., 1997) are used: the so called topcluster, which is an array of 50 scintillation detectors placed on top of the central KASCADE detector (active area: 22.8 m^2 which correspond to an active area of 7.5%), the trigger plane, which is the third active layer of the calorimeter, an eye of 456 scintillation detectors (active area: 208 m^2 which correspond to an active area of 65%) and finally a setup of position sensitive multiwire proportional chambers (MWPC) installed below the calorimeter. The energy detection threshold for muons observed with the trigger plane is 0.4 GeV, while with the MWPC muons with $E_\mu > 2.0$ GeV can be filtered out.

The arrival times measured with the topcluster and the triggerlayer have to be corrected due to two experimental effects of the timing detectors:
(i) the timing signals are affected by the actual energy deposit due to the light production and the discriminator threshold (energy deposit effect),
(ii) the timing signal depends from the number of particles simultaneously hitting the scintillator detectors (multiplicity effect).

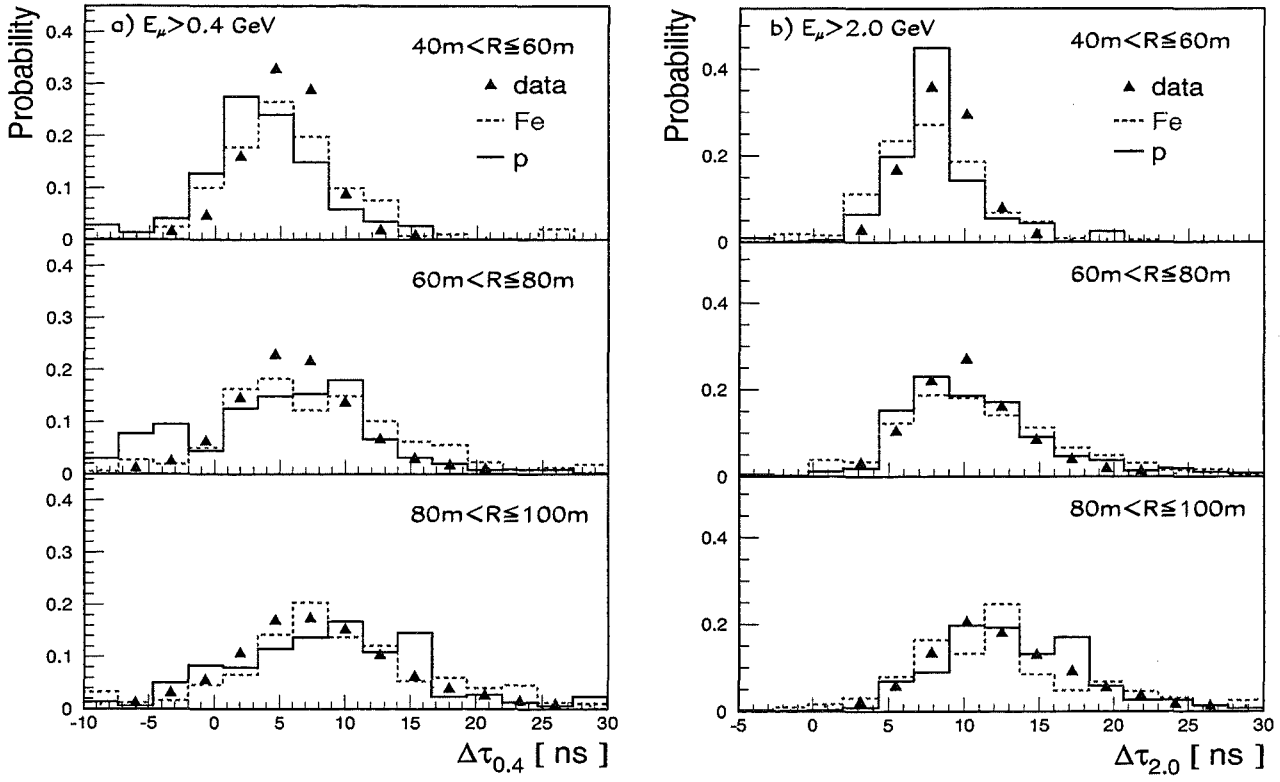

Figure 2: Distributions of relative arrival times of the electromagnetic and muon components (of two different muon detection thresholds) as compared with EAS simulation predictions

Therefore these effects have to be corrected by procedures based on realistic detector simulations. This is particularly nescessary for the topcluster detectors. For defining the electron component, as detected with the topcluster, the absence of a coincidence with events in the triggerlayer or MWPC is required. Detector simulations show that with this condition 70% of muon events in the topcluster are removed. This rate corresponds to the limit given by the active area of the trigger plane.

3 Comparison with predictions of Monte-Carlo EAS simulations:

The experimental data, accumulated in a period of 10 months comprise c. 200.000 EAS events with the requirement that at least 3 timing detectors must have fired and with the reconstructed zenith angle of EAS incidence of $15° < \theta \leq 20°$. Results of the measurements are shown in Figs. 2 and 3 and compared to simulation results in different ranges of the energy indicative muon number N_μ^{tr}. It has been shown that for the KASCADE case the number of muons N_μ^{tr} summed up between 40 and 200 m from the shower center is an energy identifier, nearly independent from the mass of the primary. The actual simulation calculations (based on QGSJET model) cover an energy range of $5 \cdot 10^{14} - 1 \cdot 10^{16}$ eV (divided in 5 overlapping energy bins for three mass groups: H = protons, O = CNO group, Fe = heavy group) for an energy distribution of a spectral index of -2.7. They comprise a set of 2000 showers for each case. The response of the KASCADE detector system and the timing qualities have been simulated using the CRES programm, dedicately developed by the KASCADE group on basis of the GEANT code.

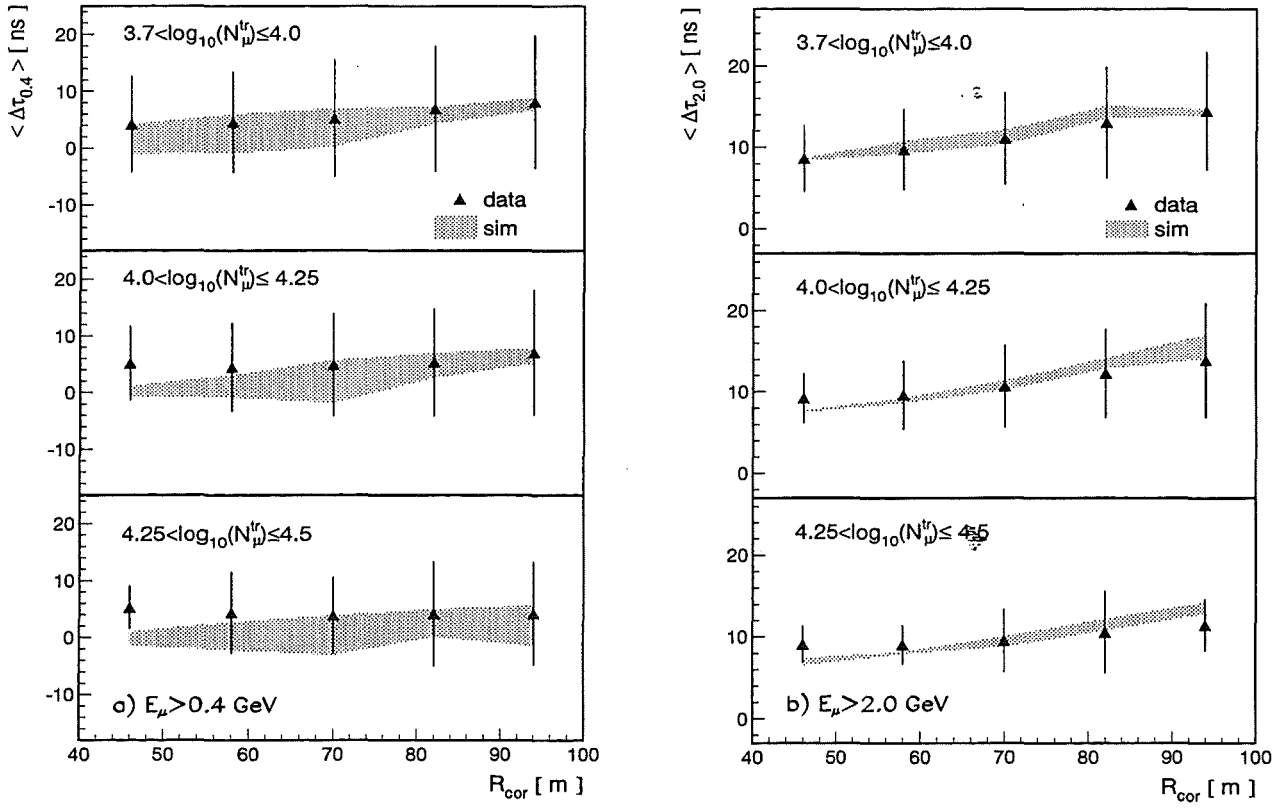

Figure 3: Comparison of the profiles of relativ arrival times of the electromagnetic and muon component with the predictions for simulated showers.

Fig. 2 displays such distributions of $\Delta\tau_{0.4}$ and of $\Delta\tau_{2.0}$, for $\log_{10} N_\mu^{tr} > 3.7$ (corresponding to a primary energy of about $E_{prim} > 2 \cdot 10^{15}$ eV) and for different distances from the EAS core. We notice the good agreement of the experimental data with the simulations, but significant differences between the different primaries in the relative arrival time distributions are not observed.

Fig. 3 presents the relative time profiles of $\Delta\tau_{0.4}$ and of $\Delta\tau_{2.0}$ for different $\log_{10} N_\mu^{tr}$ ranges. The data are compared with simulation results (which cover the range of proton and iron induced showers). For the low energy muon case there appears some slight disagreement. This might be an indication that at small distances, where the particle density is large, some problems with the corrections do remain.

4 Concluding remarks:

The present experimental studies of the relative arrival times of the EAS muon and electromagnetic component, give evidence for the different time profiles of the two EAS components and confirm former theoretical conjectures. The exploratory comparisons of the data with Monte-Carlo simulations exhibit a remarkably good agreement, but with insignificant discrimination power for the mass of the cosmic ray primary.

5 Acknowledgements:

The work has been partly supported by a grant of the Romanian National Agency for Science, Research and Technology as well as by a research grant (No.94964) of the Armenian Government and by the ISTC project A116. The collaborating group of the Cosmic Ray Division of the Soltan Institute of Nuclear Studies in Lodz and of the University of Lodz is supported by the Polish State Committee for Scientific Research (Grant No. 2 P03B 160 12). The KASCADE collaboration work is embedded in the frame of scientific-technical cooperation (WTZ) projects between Germany and Romania (No.RUM-014-97), Armenia (No. 002-98) and Poland (No.92-94).

References

Ambrosio, M. et al., 1997, Astropart. Phys., 7, 329
Brancus, I.M. et al., 1998, FZKA-Report 6151, (Forschungszentrum Karlsruhe)
Heck, D. et al., 1998, FZKA-Report 6019, (Forschungszentrum Karlsruhe)
Klages, H.O. et al., 1997, Nucl. Phys. B (Proc.Suppl.), 52B, 92

HE 2.2.39

Estimate of the Cosmic Ray Composition by a Pattern Analysis of the Core of PeV EAS

A. Haungs[1]*, T. Antoni[1], W.D. Apel[1], A.F. Badea[2], K. Bekk[1], K. Bernlöhr[1], E. Bollmann[1], H. Bozdog[2], I.M. Brancus[2], A. Chilingarian[3], K. Daumiller[4], P. Doll[1], J. Engler[1], F. Feßler[1], H.J. Gils[1], R. Glasstetter[4], R. Haeusler[1], W. Hafemann[1], D. Heck[1], J.R. Hörandel[4] †, T. Holst[1], K.-H. Kampert[1,4], H. Keim[1], J. Kempa[5], H.O. Klages[1], J. Knapp[4‡], H.J. Mathes[1], H.J. Mayer[1], J. Milke[1], D. Mühlenberg[1], J. Oehlschläger[1], M. Petcu[2], H. Rebel[1], M. Risse[1], M. Roth[1], G. Schatz[1], F.K. Schmidt[4], T. Thouw[1], H. Ulrich[1], A. Vardanyan[3], B. Vulpescu[2], J.H. Weber[4], J. Wentz[1], T. Wibig[5], T. Wiegert[1], D. Wochele[1], J. Wochele[1], J. Zabierowski[6], S. Zagromski[1],

[1]*Forschungszentrum Karlsruhe, Institut für Kernphysik, D-76021 Karlsruhe, Germany*

[2]*National Institute of Physics and Nuclear Engineering, RO-7690 Bucharest, Romania*

[3]*Cosmic Ray Division, Yerevan Physics Institute, Yerevan 36, Armenia*

[4] *Institut für Experimentelle Kernphysik, University of Karlsruhe, D-76021 Karlsruhe, Germany*

[5]*Department of Experimental Physics, University of Lodz, PL-90950 Lodz, Poland*

[6] *Soltan Institute for Nuclear Studies, PL-90950 Lodz, Poland*

Abstract

A system of large-area position sensitive multiwire proportional chambers (MWPC), installed below the hadron calorimeter of the KASCADE (KArlsruhe Shower Core and Array DEtector) central detector is able to observe the density distributions of the high energy muons and hadrons penetrating the calorimeter. By use of a classification in terms of multifractal moments, a mass sensitive parametrisation of the density distributions is given. In combination with additional measured parameters, i.e. number of reconstructed muons in the core and the shower size an artificial neural net analysis leads to an estimation of the relative abundances of the different primary components in cosmic rays in the energy region around the "knee".

1 Introduction:

The KASCADE (KArlsruhe Shower Core and Array DEtector) experiment (Klages et al. 1997) aims at the determination of the chemical composition of cosmic rays in the energy region around the so-called "knee" by extensive air shower (EAS) observations. The multi detector arrangement of KASCADE allows to measure simultaneously observables in all three charged particle components of the air shower and, especially for EAS with the core inside the 300 m^2 central detector, a measurement of structures of the particle density distributions in the center by a pattern analysis with multifractal moments. With an eligible choose of a set of such observables an event by event classification of the EAS with respect to the primary mass can be performed. The resulting relative abundances of groups of equal primary masses and with the measured primary energy spectrum could help to discriminate between different theories of the source, acceleration and transport of the charged cosmic rays in the Galaxy.

2 Reconstruction of a Mass Parameter per single EAS:

2.1 The KASCADE Detector: The KASCADE detector array consists of a detector field having an area of 200 × 200 m^2 and 252 detector stations positioned on rectangular grids with 13 m spacing. Each station contains liquid scintillators in stainless steel containers of 100 cm diameter with a photomultiplier on the top for the electron-photon detection. The 12 clusters in the outer (inner) region of the field contain two of such electron-photon detectors, positioned in the diagonal of each station, while the stations of the inner four clusters contain four of such detectors. The outer 12 clusters are additionally equipped with muon detectors.

*corresponding author; e-mail: haungs@ik3.fzk.de

†present address: University of Chicago, Enrico Fermi Inst., IL 60637; ‡now at: University of Leeds, Leeds LS2 9JT, U.K.

These are four plastic scintillators ($90 \cdot 90 \cdot 3\,cm^3$ each) placed under absorber material of 10 cm lead and 4 cm iron. The array provides the general EAS trigger and the data necessary for the reconstruction of the basic EAS characteristics like electron and muon number, core location and angle of incidence.
Apart from an iron sampling calorimeter the KASCADE central detector consists of a setup of two layers multiwire proportional chambers (MWPC), installed in the basement of the central detector. Each muon chamber consists of three layers of crossed wires and stripes in a 16 mm thick argon-methane volume which allow a reconstruction of the crossing point of hit particles. The particles observed with the MWPCs are mainly muons with $E_\mu \geq 2\,GeV$, but also the "punch-through" of tails of hadron cascades in the shower core, penetrating the iron absorber (c.1000 g/cm^2) above. Due to the good spatial resolution (c.8 mm) of the MWPCs and in total a sensitive area of 122 m^2 covering more than 60 percent of a central area with $R < 8\,m$, the hit pattern in the shower core and, by tracking, the number of muons in the shower core can be measured accurately, enabling a reasonable analysis of signatures for the mass of the EAS primary (Haungs et al. 1996).

2.2 Observables: For this analysis the relevant parameters reconstructed for each registered shower from the data of the field array are: the core location, the arrival direction of the shower, the shower size N_e (total number of electrons), and the so-called truncated muon number N_μ^{tr}. The latter is the content of muons with $E_\mu > 250\,MeV$ in the limited range of the lateral distribution in the distance of 40 m - 200 m from the shower center. The reconstruction of the data from the MWPC system provides the tracks of muons above a threshold of 2 GeV ($N_\mu^\star$) and a hit pattern: number and spatial distribution of muons and of produced secondaries (Figure 1). The analysis of this hit pattern in terms of multifractal moments leads to two generalized multifractal dimensions D_6 and D_{-6} (Haungs et al. 1996, Haungs et al. 1998), which characterizes the positions and sizes (number of secondaries in the MWPC) of the high-energy (punch-through) hadrons, the lateral distributions of muons and secondaries and the degree of fluctuations in the pattern, i.e. in the shower core. High-energy ($E_{prim} > 10^{15}\,eV$) and central ($R_{core} < 5\,m$ from the center of the MWPC system) showers are enriched by cuts of N_μ^{tr} and of the estimated core location; around 2500 measured showers are available for the analysis of the structure of the shower core.

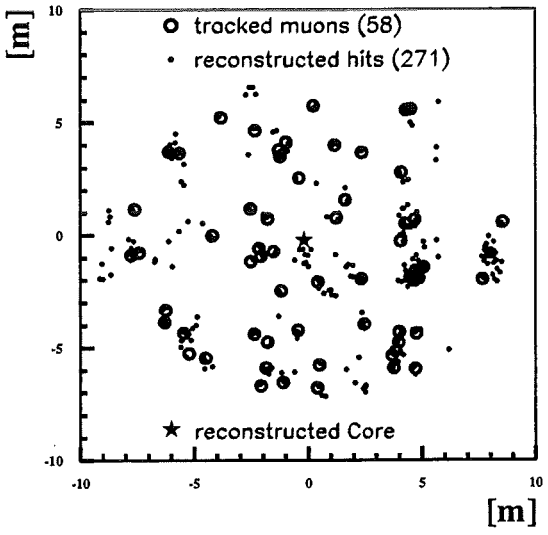

Figure 1: Example of a typical hit density distribution measured by the MWPC system. Additionally the positions of tracked muons are included.

2.3 Simulations: For detailed studies first a set of EAS, simulated for the KASCADE observation level (110 m a.s.l.), has been prepared using the Monte Carlo air shower simulation program CORSIKA (Heck et al. 1998), which includes different packages of high-energy interaction models like VENUS and QGSJET. The simulation calculations cover the energy range of $10^{14}\,eV$ - $10^{16}\,eV$ for five different mass groups with isotropic incidence. Showers of different primary masses have different longitudinal developments in the atmosphere leading to different lateral distributions in the shower core (Figure 2). Detector effects and fluctuations smear out this signal, but still the different structure remains in the data of the MWPC system. The response of all KASCADE detector systems to the EAS components has been determined by simulations using the GEANT code. The output of the simulations is stored in the same way as the measured data, therefore measured and simulated data can be reconstructed with the same procedures.

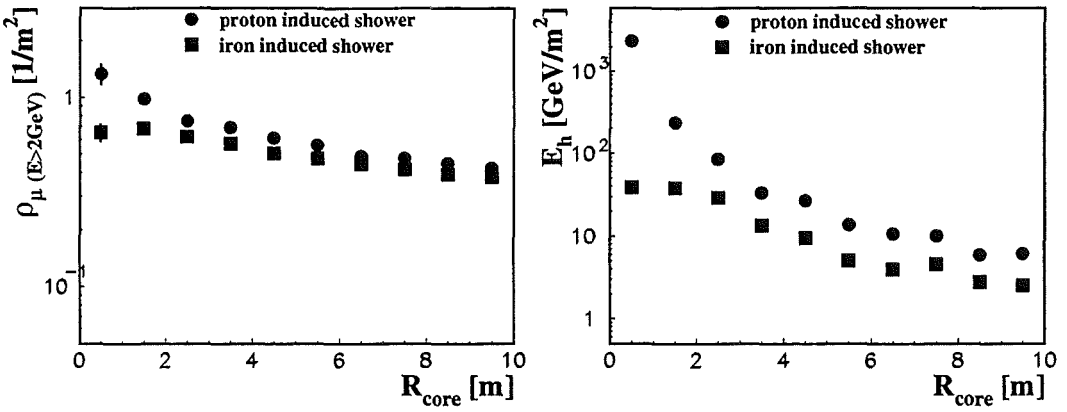

Figure 2: Average muon density and hadronic energy density of proton and iron induced showers in the inner region: CORSIKA (QGSJet) simulations taking into account the energy spectrum above 1 PeV with an isotropic shower incidence.

2.4 Classification: Using five experimentally determined mass sensitive observables for each shower (shower size N_e, number of tracked muons in the MWPC system $N_\mu^\star$, generalized multifractal dimensions D_6 and D_{-6}, and the zenith angle of the shower direction Θ) as input parameters, a simple artificial neural network is constructed. The net reduces the five parameters to one parameter, representing probability of the primary mass. The net is trained by simulated proton, oxygen and iron showers, which are generated on the basis of the QGSJet model, fulfilling the selection cuts and following a flattened power law spectrum and an isotropical distribution of the arrival directions up to 40°. After the training independent samples of simulated and measured showers are classified according to this mass parameter.

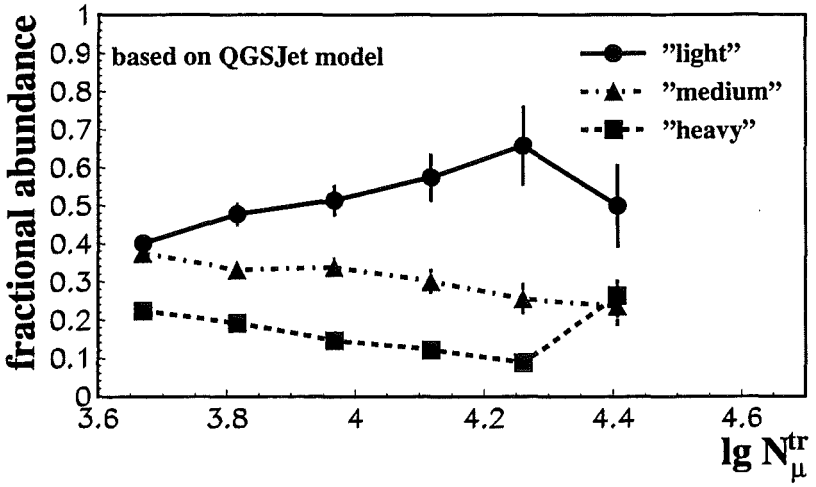

Figure 3: Relative abundances of different mass groups of primary cosmic rays in the energy region around the knee ($lgN_\mu^{tr} \approx 4.1$), analyzed on the basis of the interaction model QGSJet. The error bars contain the statistics of both, data and simulations.

3 The Chemical Composition:

For exploring the variation of the mass composition, the mass parameter distributions have been specified by different ranges of the truncated muon number. Using the simulated distributions a misclassification matrix hgas been calculated and the relative abundances of the three mass groups (light, medium and heavy) have been reconstructed for each N_μ^{tr}-range (Figure 3). Simulations have been shown, that primary Helium and Silicon nuclei in the present analysis are be representated by the light and heavy group, respec-

tively. For transforming the variation from the muon number into the primary energy of the particles, the linear dependence of lgN_μ^{tr} from lgE_0 above the selection threshold of $lgN_\mu^{tr} > 3.5$ is adopted (Figure 4). The fair independence of such a relation from the primary mass reduces the systematic error of such a simple transformation. Figure 5 shows the mean logarithmic mass of the primary cosmic rays versus the primary energy as a result of this analysis. For the "light" group an average A of 2.5 is assumed, for the "medium" group A=14 and for the "heavy" group A=42. A comparable analysis based on the VENUS interaction model show a variance in the final result of around 10%. By replacing the fractal parameters in the neural net by hadronic parameters like number of reconstructed hadrons above 100 GeV, and the sum of the reconstructed energy of this hadrons, a conspicuous increasing of the mean mass is resulting. This corroborates the suspicion of an insufficient description by the high-energy hadronic interaction models in the extreme forward direction (see Antoni et al. 1999). However in the analysis of all shower variables in all analyses the tendency to increasing heavy primaries after with a slightly decreasing just before the "knee" is seen.

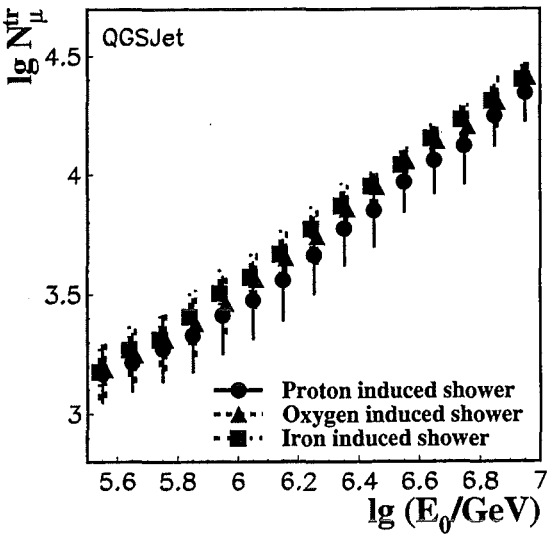

Figure 4: Dependence of the "energy estimator" N_μ^{tr} from the primary energy for different primary masses, based on the interaction model QGSJet including the detector simulation as well as all selection cuts. The error bars indicate the spread of N_μ^{tr} for each energy range.

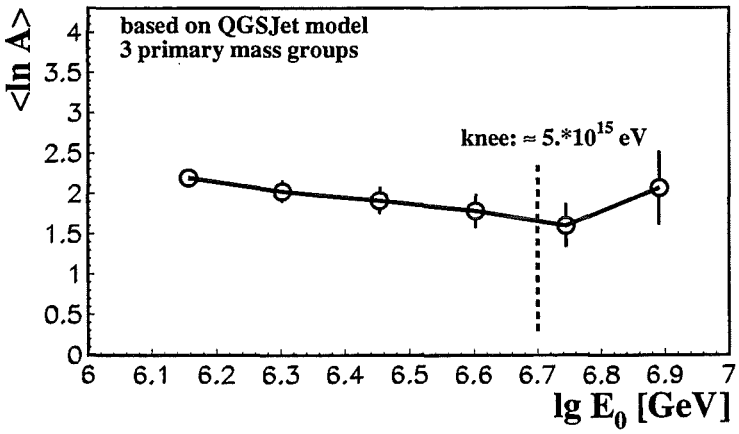

Figure 5: Mean of the logarithmic mass versus the primary energy. The position of the knee as estimated by the KASCADE experiment, is indicated.

References

Antoni, T. et al. 1999, submitted to Journal Phys. G; preprint astro-ph/9904287
Haungs, A. et al. 1996, Nucl. Instr. Meth. A 372, 515
Haungs, A. et al. 1998, FZKA-Report 6105, Forschungszentrum Karlsruhe, Germany
Heck, D. et al. 1998, FZKA-Report 6019, Forschungszentrum Karlsruhe, Germany
Klages H.O. et al. 1997, Proc. 25th ICRC (Durban, 1997), Vol 8, 297

HE 2.2.40

A Multivariate Approach for the Determination of the Mass Composition in the Knee Region

M. Roth[1]*, T. Antoni[1], W.D. Apel[1], F. Badea[4], K. Bekk[1], K. Bernlöhr[1], E. Bollmann[1], H. Bozdog[4], I.M. Brancus[4], A.A. Chilingarian[2], K. Daumiller[1], P. Doll[1], J. Engler[1], F. Feßler[1], H.J. Gils[1], R. Glasstetter[1], R. Haeusler[1], W. Hafemann[1], A. Haungs[1], D. Heck[1], J.R. Hörandel[1] †, T. Holst[1], K.–H. Kampert[1], J. Kempa[3], H.O. Klages[1], J. Knapp[1] ‡, H.J. Mathes[1], H.J. Mayer[1], J. Milke[1], D. Mühlenberg[1], J. Oehlschläger[1], M. Petcu[4], H. Rebel[1], M. Risse[1], G. Schatz[1], F.K. Schmidt[1], T. Thouw[1], H. Ulrich[1], A. Vardanyan[2], B. Vulpescu[4], J.H. Weber[1], J. Wentz[1], T. Wibig[3], T. Wiegert[1], D. Wochele[1], J. Wochele[1], J. Zabierowski[3]

[1]*Institut für Kernphysik and Institut für Experimentelle Kernphysik, Forschungszentrum and Universität Karlsruhe P.O. Box 3640, D–76021 Karlsruhe, Germany*

[2]*Yerevan Physics Institute, Cosmic Ray Division, Armenia*§

[3]*Institute for Nuclear Studies and Dept. of Experimental Physics, University of Lodz, PL–90950 Lodz, Poland*

[4]*National Institute of Physics and Nuclear Engineering, RO–7690 Bucharest, Romania*

Abstract

New results of a multivariate analysis to determine the chemical composition obtained with the KASCADE detector are presented. Taking the information of the electron-photon, the hadron, and the muon detectors for an event-by-event analysis into account the energy dependence of the primary cosmic ray composition in the *knee* region is estimated. Bayesian nonparametric and neural network methods are used. The investigated EAS events indicate a tendency to a heavier composition above the *knee*.

1 Introduction:

The origin of cosmic rays (CR) is still fraught with insufficient knowledge and uncertainty. The analysis of the energy spectrum and the chemical composition remains one of the most important constraints on theoretical models. To infer the primary mass not only the electromagnetic but also hadronic and muonic information provided by the KASCADE detector (Klages, 1997) is used in an event-by-event examination. The novelty of this approach is the possibility to study the mass composition contingent upon the used observables. Comparing the results the differences in various observables can be investigated.

2 EAS Reconstruction:

2.1 The detector setup: The basic concept of the KASCADE experiment is to measure a large number of observables for each individual event with good accuracy and high degree of sampling. For this purpose 252 detector stations form a detector array of 200 × 200 m^2 containing liquid scintillation detectors for detecting the electromagnetic component on the top of a lead/iron absorber plate as well as plastic scintillators below the shielding. A detector coverage of more than 1% for the electromagnetic and about 2% for the muonic component EAS is achieved. In combination with a precise measurement of the hadrons using an iron sampling calorimeter, the shower core can be investigated in great detail. The main part of the central detector system is a large hadron calorimeter. It consists of a 20 × 16 m^2 iron stack with eight horizontal gaps. 10,000 ionisation chambers are used in the six gaps and below the iron stack to measure of hadronic energy in a total of 40,000 electronic channels. The third gap is equipped with 456 scintillation detectors for triggering and timing purposes. Below the iron stack two layers of multiwire proportional chambers (MWPCs) measure muon tracks and allow to study structures of the muon lateral distribution in EAS cores.

*corresponding author: e-mail: roth@ik3.fzk.de

†now at: University of Chicago, Enrico Fermi Institute, Chicago, IL 60637

‡now at: University of Leeds, Leeds LS2 9JT, U.K.

§The work has been partly supported by a research grant (No.94964) of the Armenian Government and by the ISTC project A116.

2.2 Relevant Observables: The presented detailed analysis of EAS presented below benefits from the simultaneous measurement of a large number of quantities for each individual event. This enables multidimensional analyses for the reconstruction of the energy and the mass of the primary.

Specific EAS parameters measurable by the experiment KASCADE are used, like the number of electrons N_e, the truncated number of muons N_μ^{tr} (Glasstetter, 1997; Weber, 1997), the number of hadrons N_h^{100GeV} with an energy larger than 100 GeV, the sum of the energy of this hadrons $\sum E_h$, the energy of the most energetic hadron $\max E_h$ (Hörandel, 1997), and the number of muons $N_\mu^\star$ with an energy threshold of $E_\mu \geq 2$ GeV measured below the central calorimeter by the MWPCs (Haungs, 1996).

Two sets of data are used. "Selection I" uses the information from the array of field stations on electrons and muons. It permits to analyse the data with good statistical accuracy but has no information from the central detector. "Selection II" uses in addition many observables measured in the central detector but has the disadvantage of a reduced data sample (Roth, 1999).

Therefore 720,000 events with an energy larger than $E \approx 5 \cdot 10^{14}$ eV and a maximal core distance to the centre of the field array of 91 m are selected (set "selection I"). Approximately 8000 high-energetic ($E > 10^{15}$ eV), central showers are collected by cuts of N_μ^{tr} ($> 10^{3.6}$), the core location ($R_{core} < 5$ m from the centre of the central detector system), at least one Hadron with an energy above 100 GeV and 10 muons in the MWPCs (set "selection II").

2.3 Simulations: Simulations have been performed with the models VENUS and QGSJet in the energy range $10^{14} - 3.16 \cdot 10^{16}$ eV using the CORSIKA code (Heck, 1998).

For each primary (p, He, O, Si, and Fe) approximately 2000 EAS events have been simulated, distributed in the energy range with an decreasing particle flux. The core of the EAS lies within 5 m radius from the centre of the central detector. The response of all detector components is taken into account in detail using the GEANT code. Afterwards the simulated events are treated like measured ones. Therefore measured and simulated data reconstructed with the same procedures.

3 Mass Estimation:

The number of electrons as a classical EAS measure provide a very good ability to distinguish between light and heavy particles. In analyses performed for different other observables (see refs above) it has been shown that in general the signals obtained by the central detector contain mass sensitive parameters (e.g. N_h^{100GeV}, $\sum E_h$, $N_\mu^\star$, ...). The truncated number of muons N_μ^{tr} (the integration of the lateral distribution function limited to the range of the fit region caused by the array layout), however, is considered as a good energy estimator as it shows only marginal sensitivity to the mass of the primary particle according to simulations (Weber, 1997). Due to the limited statistics of simulated and measured events the analysis of measured data using information in the centre of the EAS core is restricted to at most three types of primaries: light (p), medium (O), and heavy (Fe). Table 1 shows, as an example, the nearly energy independent classification rates from a Bayesian analysis described in brief in (Chilingarian, 1998) for three groups of primaries, which are calculated for different sets of observables. They represent the possibility of correct classification $P_{i\to i}$ (or misclassification $P_{i\to j}$). As expected the combination of all observables together provides the best classification.

Table 1: The classification rates $P_{j\to i}$ for three groups of primary nuclei using different sets of observables (VENUS model).

$N_\mu^\star, \sum E_h$.

	p	O	Fe
$P_{p\to i}$	0.58	0.27	0.15
$P_{O\to i}$	0.34	0.33	0.32
$P_{Fe\to i}$	0.22	0.30	0.48

N_μ^{tr}, N_e.

	p	O	Fe
$P_{p\to i}$	0.68	0.26	0.06
$P_{O\to i}$	0.21	0.49	0.30
$P_{Fe\to i}$	0.09	0.31	0.60

$N_\mu^{tr}, N_e, N_\mu^\star, \sum E_h$.

	p	O	Fe
$P_{p\to i}$	0.71	0.24	0.05
$P_{O\to i}$	0.18	0.52	0.30
$P_{Fe\to i}$	0.07	0.26	0.67

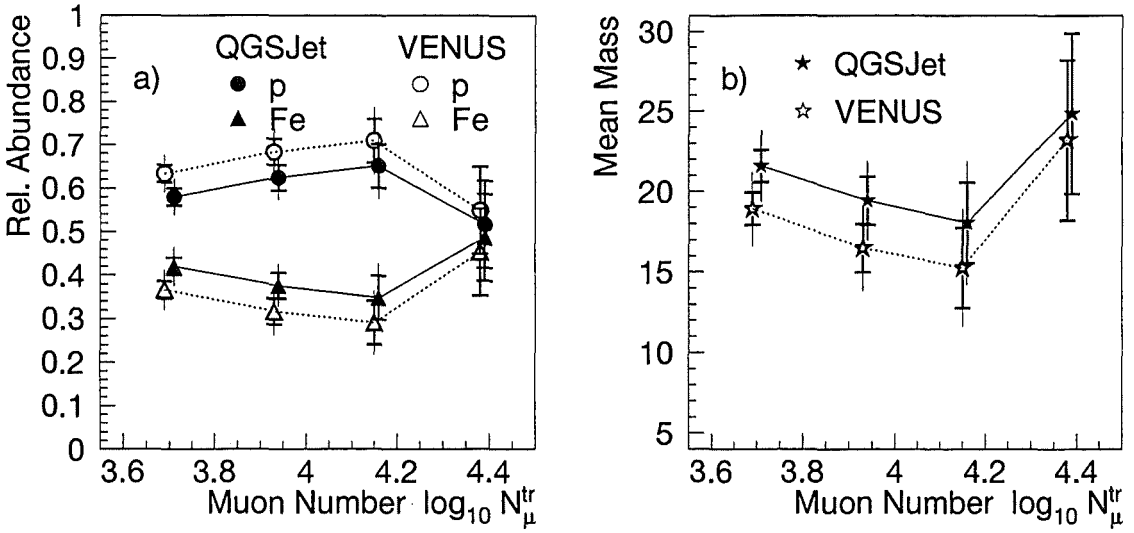

Figure 1: a) Reconstructed chemical composition for two class case and b) mean mass vs. number of muons(QGSJet and VENUS).

However, the increase of the $P_{i\to i}$ from the set $\{N_\mu^{tr},\ N_e\}$ to the set $\{N_\mu^{tr},\ N_e,\ N_\mu^{\star},\ \sum E_h\}$ is not very large, because the fluctuations of the correlations are large. The correlations of these parameters are strongly model dependent. Hence, applying different models in a nonparametric analysis can lead to completely different results. The geometric mean $\sqrt[N]{\prod_{i=1}^{N} P_{i\to i}}$ of the diagonal elements $P_{i\to i}$

Table 2: Geometric mean of correct classification as a measure of separability for different groups of primaries (VENUS model).

	5 groups	3 groups	2 groups
$N_\mu^{\star}, \sum E_h$	0.15	0.46	0.71
N_μ^{tr}, N_e	0.34	0.58	0.89
$N_\mu^{tr}, N_e, N_\mu^{\star}, \sum E_h$	0.38	0.63	0.89

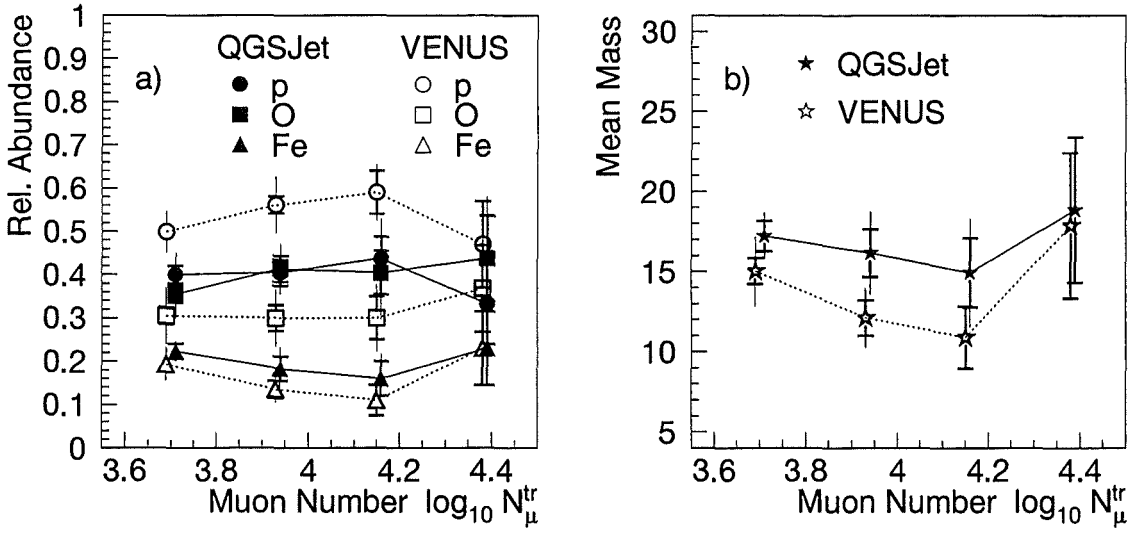

Figure 2: a) Reconstructed chemical composition for three class case and b) mean mass vs. number of muons (QGSJet and VENUS).

(see table 1) in table 2 reflects once more the increasing separability by taking into account more than two observables. Even when taking the full available information (i.e. four observables) into consideration the separability for five groups is a crucial point and must be studied in more detail.

As shown in figures 1 and 2 there is a tendency to have a lighter composition in the knee region ($log_{10}\ N_\mu^{tr} \approx 4.1$) using the Bayesian decision making procedure independently of the applied model and the number of chosen groups to divide in (2 or 3). At higher energies (i.e. muon number) the composition is getting heavier. In case of VENUS the composition seems to be in general lighter than in the QGSJet case. Results of different combinations of observables (N_μ^{tr}, N_e, $N_\mu^\star$,$\sum E_h$, and $\max E_h$) which show similar behaviour are combined to average values. The error of the misclassification is taken into consideration and also included as thin error lines in figures 1 and 2. Instead of only few thousand events in case of the set "selection II" the set "selection I" provides more than 700.000 events to be analysed by using only the muonic and electromagnetic components. The results of the different sets are shown in figure 3. They corroborate each other. The abscissa scale is the estimated energy which is calculated by a neural network for each single event (Chilingarian, 1999).

4 Conclusion:

The presented results on the energy dependence of the elemental composition are of preliminary character. A tendency of increasing heavy primaries beyond and a slightly decreasing before the *knee* is confirmed, like other KASCADE results. The two models indicate the same tendency on different scales of mean masses. Comparing figures 1 and 2 the mean mass depends obviously on the number of classes. One has to take as many classes as possible into account to minimise the biasing effect of too few classes, but bearing in mind the limitation of the classification accuracy.

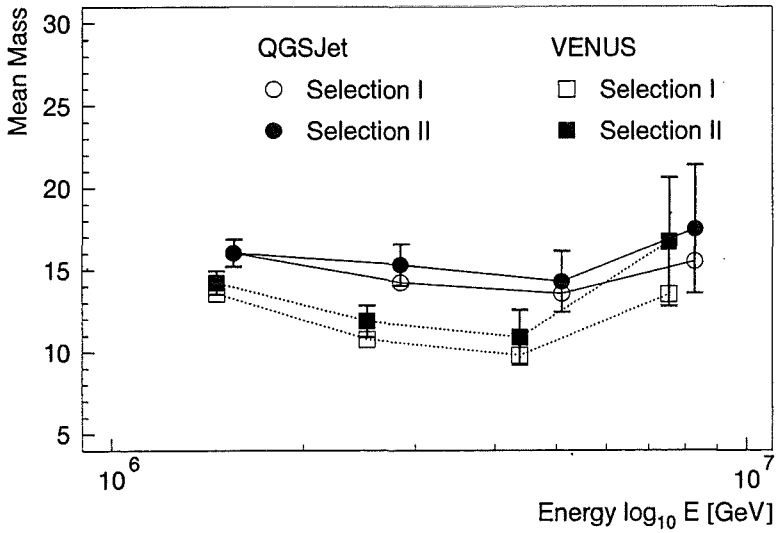

Figure 3: Reconstructed chemical composition for different data sets ("selections I+II") and the models QGSJet and VENUS vs. energy (see text for explanation).

References

Chilingarian, A. et al., Proc. 16th ECRS (Madrid, 1998), 571
Chilingarian, A.A. et al., Proc. 26th ICRC (Salt Lake City, 1999), HE 2.2.04
Glasstetter, R. et al., Proc. 25th ICRC (Durban, 1997), 6, 157
Haungs, A. et al. 1996, *Nucl. Inst. Meth.* A372, 515
Heck, D. et al. 1998, FZKA-Report 6019, Forschungszentrum Karlsruhe, Germany
Hörandel, J. et al., Proc. 25th ICRC (Durban, 1997), 6, 93
Klages, H.O. et al. 1997, *Nucl. Phys. B (Proc. Suppl.)*, 52B, 92
Roth, M. 1999, FZKA-Report 6262, Forschungszentrum Karlsruhe, Germany
Weber, J. et al., Proc. 25th ICRC (Durban,1997), 6, 153

HE 2.2.41

First Measurement of the Knee in the Hadronic Component of EAS

J.R. Hörandel[2,7] T. Antoni[1], W.D. Apel[1], F. Badea[3],K. Bekk[1], K. Bernlöhr[1], E. Bollmann[1], H. Bozdog[3], I.M. Brancus[3], A. Chilingarian[4], K. Daumiller[2], P. Doll[1], J. Engler[1], F. Feßler[1], H.J. Gils[1], R. Glasstetter[2],R. Haeusler[1], W. Hafemann[1], A. Haungs[1], D. Heck[1], T. Holst[1], K.H. Kampert[1,2], H. Keim[1], J. Kempa[5], H.O. Klages[1], J. Knapp[2,8], H.J. Mathes[1], H.J. Mayer[1], J. Milke[1], D. Mühlenberg[1], J. Oehlschläger[1], M. Petcu[3], H. Rebel[1], M. Risse[1], M. Roth[1], G. Schatz[1], F.K. Schmidt[2], T. Thouw[2], H. Ulrich[2], A. Vardanyan[3], B. Vulpescu [3], J.H. Weber[2], J. Wentz[1], T. Wibig[6], T. Wiegert[1], D. Wochele[1], J. Wochele[1], J. Zabierowski[6]

[1] *Institut für Kernphysik, Forschungszentrum Karlsruhe, D-76021 Karlsruhe, Germany*

[2] *Institut für Experimentelle Kernphysik, University of Karlsruhe, D-76128 Karlsruhe, Germany*

[3] *Institute of Physics and Nuclear Engineering, RO-7690 Bucharest, Romania*

[4] *Cosmic Ray Division, Yerevan Physics Institute, Yerevan 36, Armenia*

[5] *Department of Experimental Physics, University of Lodz, PL-90950 Lodz, Poland*

[6] *Soltan Institute for Nuclear Studies, PL-90950 Lodz, Poland*

Abstract

The number of hadrons and their energy sum in extensive air showers has been measured using the KASCADE hadron calorimeter. Shower size spectra of the hadronic component have been derived using both observables. The spectra can be described by a power law and exhibit a change in the spectral index at energies around 5 PeV. The primary cosmic–ray flux spectrum is derived from the measurements in the energy range from 0.2 PeV up to 50 PeV.

1 Proem:

The cosmic–ray primary–flux spectrum for all particles is well described by a power law in a large energy interval ranging from 10 GeV up to 100 EeV. The only fine structure between 10 GeV and 10 EeV is a break in the exponent at energies of about 3 to 5 PeV. This phenomenon is commonly called the "knee" where the all–particle differential energy spectrum changes from $E^{-2.7}$ before the knee to $E^{-3.1}$ beyond it.

The origin of this break is not yet clear in spite of being known for 40 years by now. Explanations of the knee usually assume astrophysical reasons, but it could be caused by new physics in the high–energy particle interaction as well, since the available interaction models are not able to predict the measurements in all observables satisfactorily (Hörandel et al. 1999a).

Direct observations at the top of the atmosphere run out of statistics well below the knee due to limited size of the instruments and short exposure times. The knee has been observed by ground–based extensive air shower experiments mainly in the electromagnetic size spectrum. Observations in the muonic size and by Čerenkov light are scare. To solve the problem of the origin of the knee, it is useful to measure the shower size spectra of all shower components. The KASCADE experiment (Klages et al. 1997) determines the shower size spectra of the electromagnetic, muonic and hadronic component. Using its large hadron calorimeter the number of hadrons and their energy sum in extensive air showers has been measured and size spectra of the hadronic component are derived as presented in the following.

2 Experimental Set up:

The fine segmented hadron calorimeter allows to measure individual hadrons in the core of an EAS. The 16×20 m^2 calorimeter is of the sampling type, the energy being absorbed in an iron stack and sampled in

[7]corresponding author, present address: The University of Chicago, Enrico Fermi Institute, 933 East 56^{th} Street, Chicago, IL 60637, USA; http://ik1au1.fzk.de/~joerg

[8]now at: The University of Leeds, Leeds LS2 9JT, U.K.

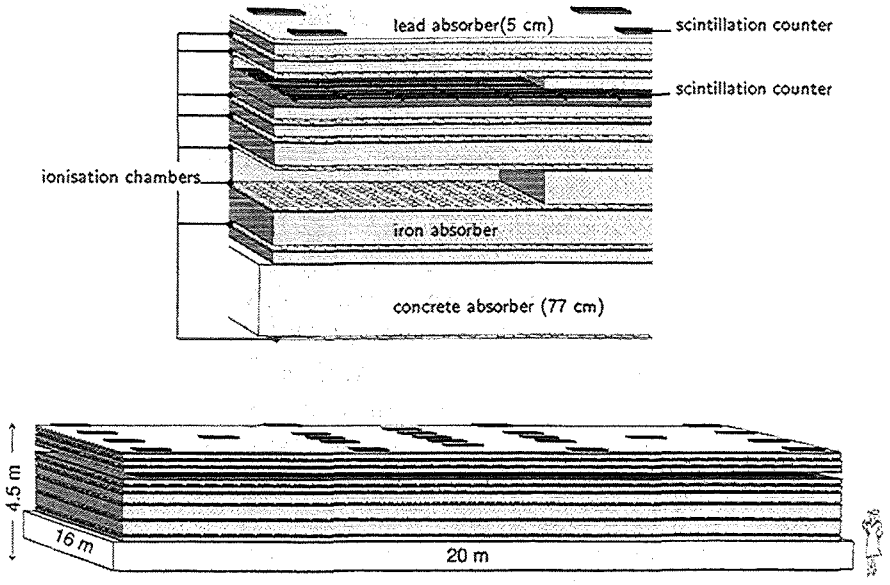

Figure 1: Sketch of the KASCADE hadron calorimeter. Detailed view (top) and total view (bottom).

eight layers by 10 000 ionization chambers (Engler et al. 1998). As sketched in Figure 1, the iron slabs are 12−36 cm thick, becoming thicker in deeper parts of the calorimeter. The energy resolution varies slowly from $\sigma/E = 20\%$ at 100 GeV to 10% at 10 TeV. The concrete ceiling of the detector building is the last part of the absorber and the ionization chamber below acts as tail catcher. In total, the calorimeter thickness corresponds to 11 interaction lengths λ_I for vertical hadrons. On top, a 5 cm lead layer filters off the electromagnetic component to a sufficient low level.

A ionization chamber contains four independent electronic channels with a dimension of 25×25 cm^2 each and is filled with the room temperature liquids tetramethylsilane or tetramethylpentane. Liquid ionization chambers exhibit a linear signal behaviour with a very large dynamic range. The latter is limited only by the electronics to about 5×10^4. The chambers are able to prove a signal of one traversing minimum ionizing particle up to an energy deposition of 10 GeV per channel without saturation. The latter corresponds to more than 10^4 passing muons. This ensures the energy of vertical incident individual hadrons to be measured linearly up to 25 TeV. The containment losses at this energy are about 2%. The energy calibration is performed by means of through–going muons, taking their energy deposition as standard. Due to the fine lateral segmentation, the minimal distance to separate two equal–energy hadrons with 50% probability amounts to 40 cm. The reconstruction efficiency for hadrons increases with energy from 70% at 50 GeV to almost 100% at 100 GeV.

A layer of plastic scintillators on top of the lead absorber and a second one below the third iron layer act as trigger for the ionization chambers.

The electromagnetic and muonic components are measured by a 200×200 m^2 array of 252 detector stations. The stations consist of 3.1 m^2 liquid scintillation detectors to prove the electromagnetic component and below a lead and iron shield, corresponding to 20 radiation lengths, 3.2 m^2 plastic scintillator to measure muons with an energy threshold of 300 MeV. The scintillator array allows to determine the electromagnetic and muonic shower size with a resolution of about 10% for electrons and 30% for muons at PeV energies as well as the position of the shower core with an accuracy of about 2 m and the angle of incidence.

3 Measurements and simulations:

From October 1996 to August 1998 about 10^8 events were recorded. After all cuts 40 000 showers were left for the final analysis. The event selection and simulations used for the present analysis are described elsewhere in these proceedings (Hörandel 1999a). The total number of hadrons and the hadronic energy sum in each shower are obtained by integration of the lateral distribution and the lateral energy density up to a distance of 24 m from the shower axis.

4 The hadronic size spectrum:

The hadronic size spectrum is presented in Figure 2. The normalized flux is multiplied by $N_H^{2.5}$ in order to accentuate any possible structure. A kink is clearly visible around a hadron number of 65. The data can be described by a power law $dN/dN_H \propto N_H^{\beta}$ with $\beta_1 = -2.81 \pm 0.04$ below and $\beta_2 = -3.12 \pm 0.11$ above the knee. Following CORSIKA simulations the knee position corresponds to a range from 2 PeV up to 5 PeV for a pure proton or iron composition, respectively (Antoni et al. 1999). The abscissa in Figure 2 extends up to 500 registered hadrons. Accordingly, the caveat arises that the lower flux may be caused by saturation effects in the number of reconstructed hadrons. For this purpose, the hadronic size spectrum has been analysed by restricting the calorimeter acceptance to different surface areas. The acceptance has been reduced by up to a factor of 3. Hence, if the knee is brought about by a deficiency in hadron pattern reconstruction, this should have an even stronger influence in these examinations. The sizes have been chosen as a square of 10×10 m^2, and rectangles of 10×12 m^2 and 10×16 m^2. In all three cases the knee showed up near $N_H = 65$ and the kink in the slopes stayed within the errors at the same hadron number with an identical change of slope. In addition, the position of the knee and the spectral indices are stable with increasing statistics, since the first evidence of a knee in the hadronic component in 1997 (Hörandel 1998) the number of events has been increased from 14 000 to 40 000.

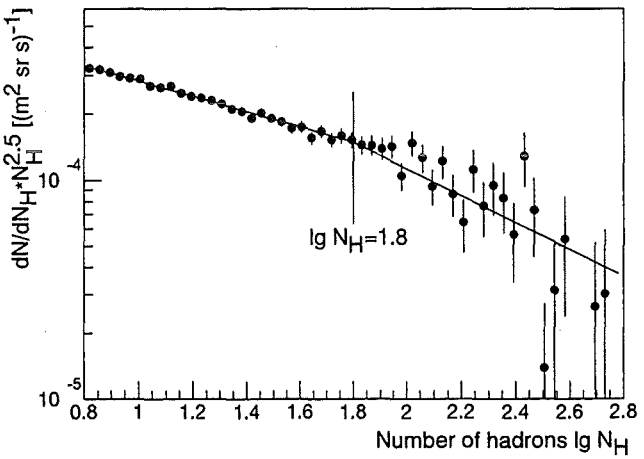

Figure 2: The hadronic shower size spectrum.

5 The hadronic energy spectrum:

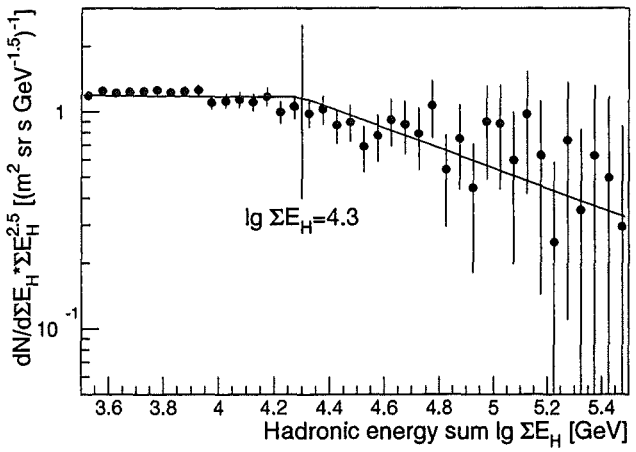

Figure 3: Frequency of showers detected versus total hadronic energy in the shower.

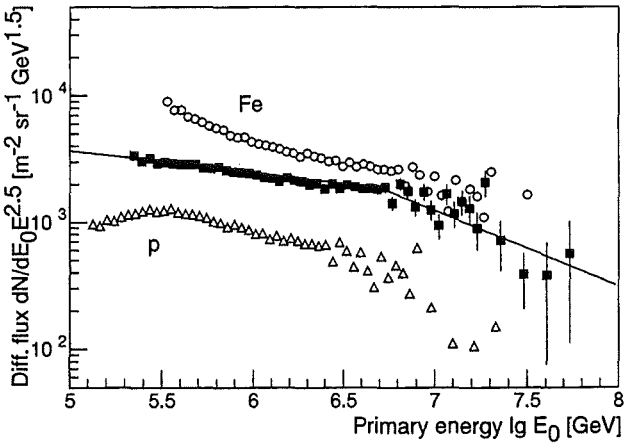

Figure 4: Differential all-particle flux versus primary energy as derived from the hadronic shower size spectrum.

Hitherto the knee has been observed in the spectra of particle numbers soley, apart perhaps from observations by means of Čerenkov light. The calorimeter allows in addition to the particle number, to measure the energy of the hadrons. Therefore, the knee can be investigated in the energy sum spectrum, too. The frequency of showers as function of their hadronic energy is presented in Figure 3. A kink in the spectrum at an energy sum of about 20 TeV is evident. Regarding the uncertainty in primary composition, the position of the knee corresponds to a primary energy of approximately 2 to 4 PeV. Once again a power law has been fitted to the data with spectral indices $\beta_1 = -2.5 \pm 0.1$ below and $\beta_2 = -2.9 \pm 0.2$ above the knee.

6 The primary energy spectrum:

When deriving the primary energy spectrum from the shower size spectrum, one encounters the uncertainty in primary composition. Since the currently available interaction models are not able to describe the measured observables in all respects, the mass composition depends on the observables used. Therefore, it is important to use for the calculation of the primary spectrum the mass composition as obtained from the observables used for the shower size spectrum, i.e. for the hadronic shower size spectrum a mass composition measured with the hadronic component has to be used. Almost all parameters which are sensitive to the primary's mass depend logarithmically on the mass number A (Hörandel 1998). The mean logarithmic mass as obtained from the hadronic component (Hörandel et al. 1999b) can be parametrised as a function of energy using a a straight line starting with $\langle \ln A \rangle = 1.5$ at 50 TeV increasing to $\langle \ln A \rangle = 3.3$ at 10 PeV.

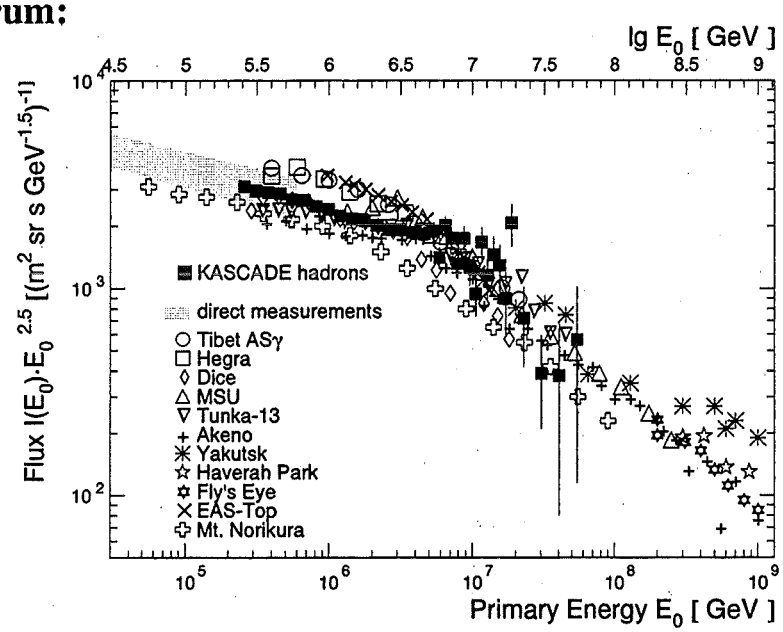

Figure 5: The all–particle primary energy spectrum as obtained from the hadronic component compared with world data. See (Antoni et al. 1999) for references.

The primary particle flux obtained by using the measured composition is plotted in Figure 4 together with results assuming a pure proton or pure iron composition. The straight lines represent fits of a power law to the data. A value of 5.0 ± 0.5 PeV is found for the knee position, and an energy scaled absolute flux of $1880/(\mathrm{m}^2\ \mathrm{sr\ s\ GeV}^{-1.5})$. The slopes of the primary spectrum are $\gamma_1 = -2.66 \pm 0.12$ below the knee and $\gamma_1 = -3.03 \pm 0.16$ above. The primary spectrum as obtained from the hadronic component is in good agreement with other measurements as can be seen in Figure 5.

References

Antoni, T. et al. (KASCADE Collaboration) 1999, "First observation of the knee in the hadronic component of EAS", submitted to Astrop. Phys.

Engler J. et al. 1998, "A warm–liquid calorimeter for cosmic–ray hadrons", to be publ. in Nucl. Instr. Meth.

Hörandel, J.R. 1998, Report FZKA 6015, Forschungszentrum Karlsruhe

Hörandel, J.R. et al. (KASCADE Collaboration) 1999a, Proc. 26^{th} ICRC (Salt Lake City), HE 1.3.01

Hörandel, J.R. et al. (KASCADE Collaboration) 1999b, Proc. 16^{th} ECRC, Alcalá, 579

Klages, H.O. et al. (KASCADE Collaboration) 1997, Nucl. Phys. B (Proc. Suppl.) 52B, 92

HE 2.2.42

Analysis of the Muon/Electron Ratio in EAS

J.H.Weber[1]*, T. Antoni[2], W.D. Apel[2], F. Badea[3], K. Bekk[2], K. Bernlöhr[2], E. Bollmann[2], H. Bozdog[3], I.M. Brancus[3], A. Chilingarian[4], K. Daumiller[1], P. Doll[2], J. Engler[2], F. Feßler[2], H.J. Gils[2], R. Glasstetter[1], R. Haeusler[2], W. Hafemann[2], A. Haungs[2], D. Heck[2], J.R. Hörandel[1‡], T. Holst[2], K.-H. Kampert[1,2] J. Kempa[5], H.O. Klages[2], J. Knapp[1§], H.J. Mathes[2], H.J. Mayer[2], J. Milke[2], D. Mühlenberg[2], J. Oehlschläger[2], M. Petcu[3], H. Rebel[2], M. Risse[2], M. Roth[2], G. Schatz[2], H. Schieler[2], F.K. Schmidt[1], T. Thouw[2], H. Ulrich[2], A. Vardanyan[4], B. Vulpescu[3], J. Wentz[2], T. Wibig[5], T. Wiegert[2], D. Wochele[2], J. Wochele[2], J. Zabierowski[6]

[1] *Institut für Experimentelle Kernphysik, University of Karlsruhe, D-76021 Karlsruhe, Germany*

[2] *Institut für Kernphysik, Forschungszentrum Karlsruhe, D-76021 Karlsruhe, Germany*

[3] *National Institute of Physics and Nuclear Engineering, RO-7690 Bucharest, Romania*

[4] *Cosmic Ray Division, Yerevan Physics Institute, Yerevan 36, Armenia*

[5] *Department of Experimental Physics, University of Lodz, PL-90950 Lodz, Poland*

[6] *Soltan Institute for Nuclear Studies, PL-90950 Lodz, Poland*

Abstract

The detector array of the KASCADE experiment measures the electromagnetic and muonic component of extended air showers. More than 100 million air showers have been analysed in narrow zenith angle bins. The muon number in extended air showers enables a good estimation of the energy of the primary particles, while the number of electrons in the shower depends strongly on the mass of the primary particle as well as on the primary energy and the zenith angle of the event. The reconstructed muon and electron numbers for each event are converted into primary energy using the results of MC-simulations (CORSIKA). The distributions of the muon/electron ratio within small energy bins are compared with the predictions for primary particles of different masses. An energy dependant mass composition was obtained favouring a decrease of light elements above the knee.

1 Experimental Setup and Observables

For the measurement of lateral electron and muon distributions the detector array of the KASCADE experiment comprises about 500 m^2 electron and 620 m^2 muon detectors which are distributed over 252 detector stations (Klages, 1997). The stations house electron detectors and muon detectors that are shielded by slabs of lead and iron. The measured energy deposits in both detector types are corrected to the mutual deposits of all other particles in an extensive air shower to obtain correct electron and muon numbers. This correction is done with lateral correction functions, that mainly depend on primary energy and zenith angle. These functions are based on simulations with the CORSIKA event generator (Heck,1998) followed by a tracking to the KASCADE experiment at observation level. This allows to convert energy deposits into particle numbers using an iterative method.

2 Determination of Electron and Muon Numbers

The data evaluation is performed in 3 levels. In a first level shower core, zenith angle, electron and muon sizes are estimated using short algorithms. The obtained parameters are used to apply the correction functions in a first way and to give start parameters for fits in the following level. A conus fit to the arrival times of the electrons gives the zenith angle. The lateral electron distributions are fitted with a NKG function using a Moliere radius of 89 m that describes the data best. This fit gives the core position and the form parameter (age) of the distribution, too. The lateral muon distribution is fitted with a NKG function as well, using a

*corresponding author; e-mail: weber@ik1.fzk.de

‡present address: University of Chicago, Enrico Fermi Institute, Chicago, IL 60637

§now at: University of Leeds, Leeds LS2 9JT, U.K.

Moliere radius of 420 m in a fit range of 40 m - 200 m. The lower cut is due to uncorrectable punch through from hadrons and photons in the muon detectors near the shower core. This fit uses the shower core obtained by the previous fit and a parametrization of the muon form parameter (age_μ) as a function of the electron size. This parametrization is obtained from simulations. In a third level a combined fit to the lateral electron distribution is performed using the fit result of the lateral muon distribution as a background function. With the knowledge of the lateral electron distribution the deposit in the muon detectors is corrected again and the resulting lateral distribution is fitted again. The muon distribution is integrated within the fit range of 40 m - 200 m resulting in the truncated muon number N_μ^{tr}. This parameter has the advantage to be free of systematical errors caused by extrapolations outside the experimentel acceptance and is in addition a good estimator of the primary energy irrespective of the primary mass. The electron size and the truncated muon size can be obtained with a systematic error less then $\sim 8\%$.

3 Determination of the Mass Composition with the Muon/Electron Ratio

The data presented here were taken out of $\sim$ 140 million reconstructed events. Several cuts were applied to the reconstructed events in order to ensure reliable results. An energy threshold of $\sim 10^{15}$ eV guarantees 100% trigger and reconstruction effciency. Due to the influence of the atmospherical depth on the shower parameters the data were subdivided into narrow zenith angle bins. To be comparable with simulations the zenith angle of the data shown in all following figures was restricted to $18^o < \theta < 25^o$. The resulting sample consists of 380.000 measured events after all cuts. As simulations with the hadronic interaction model QGSJET turned out to show the best agreement with the data analysis using this model only will be presented. All simulated showers have been tracked through the experiment und reconstructed like the measured data, so systematic errors due to the reconstruction methods can be neglected. The simulated showers have been given a weigth in energy corresponding to the mesured energy flux. In a first step the data were divided into 12 energy intervals in a range from $5.9 \leq \log(E_o/\mathrm{GeV}) \leq 7.1$. The energy binning is performed according to a function of the muon size N_μ^{tr} and the electron size N_e as obtained from simulations. The muon size is the dominant energy estimator while the electron size is used as a small correction to reduce the slight mass dependance of N_μ^{tr}. Figure 1 shows the quality of the energy reconstruction. The line indicates a perfect reconstruction accuracy. Systematic errors in the energy determination between proton and iron induced showers are not larger then the energy intervals. The error bars represent the spread of the reconstructed energy that mainly results from the spread in muon and electron sizes themselves. The good reconstruction accuracy implements the possibilty to divide the data in nearly mass-independant energy intervalls without prior knowledge of the mass composition.

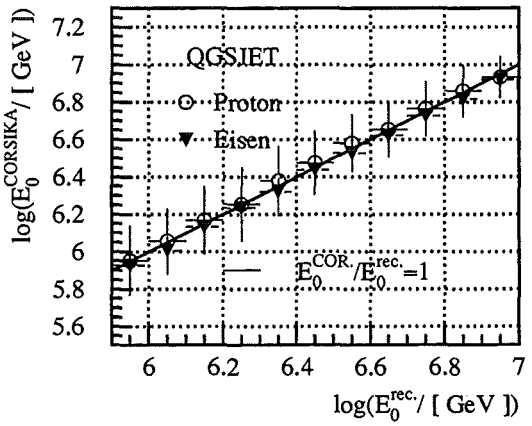

Figure 1: The primary energy from simulations as function of the reconstructed energy for proton and iron induced showers.

The ratio $\log(N_\mu^{tr})/\log(N_e)$ has been found to be the most sensitive mass parameter. The distributions of

this parameter can be described in good approximation with a Gaussian function. The mean values and spread of the distributions of four mass groups (proton, helium, oxygen, and iron) were parametrized as functions of the reconstruced energy. The sum of these four functions was fitted for each energy bin to the data distribution giving directly the fractions of the 4 mass groups as the fit result. Figure 2 shows two examples of such a fit for energy bin (a) $6.2 < \log(E_0/\mathrm{GeV}) < 6.3$ and (b) $6.7 < \log(E_0/\mathrm{GeV}) < 6.8$ on a logarithmic scale. The points represent the data, the black line represents the fit and the lines from light to dark grey show the simulated distributions of the mass groups (from proton to iron) normalized to the fit result. The figure reveals a very good agreement between the fit and the measured data. No shift of the simulations to one side of the data distribution or an error in the total integral can be found. The relative fractions of the four mass groups for all energy bins are shown in Figure 3 a).

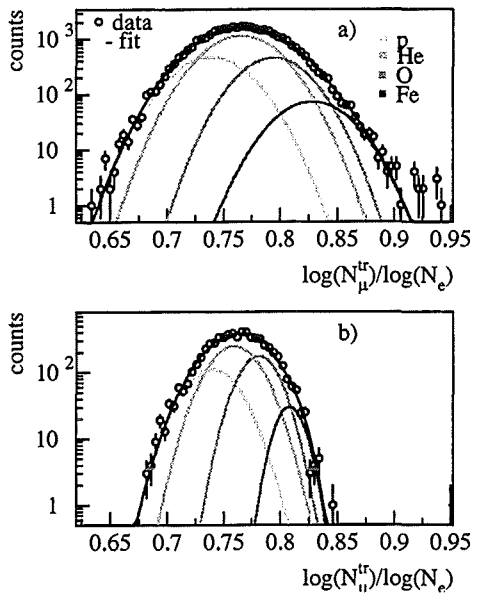

Figure 2: The muon/electron ratio for two different energy bins

4 The Mass Composition

The light grey area indicates the fraction of proton induced showers. The colours darken with increasing mass up to iron induced showers. There is little change in the composition which is clearly light mass dominated up to an energy at 6.5-6.6 $\log(E_0/\mathrm{GeV})$ After that energy which corresponds to the knee position of the all-particle spectrum the composition shows a decrease of light elements with increasing energy. In order to compare our result with other experiments we calculated a mass parameter λ that is defined as $\lambda = \sum_{i=p,He,O,Fe}^{i} ln(A_i) \cdot P_i$ with P_i being the relative fraction of mass group i. The mass parameter is about 1.4 $\pm$0.3 below the knee and increases to 2.1 $\pm$0.3 at 10^{16} eV as shown in Figure 3 b). The shaded area represents the systematical uncertainties that result from the Gaussian parametrization of the simulated distributions. Due to the (relative to measured data) small statistics of the simulated showers the widths of the distributions shown in Figure 2 are not very accurately known, resulting in a systematical dependency of the resulting mass parameter. The statistical error of the data can be neglected.

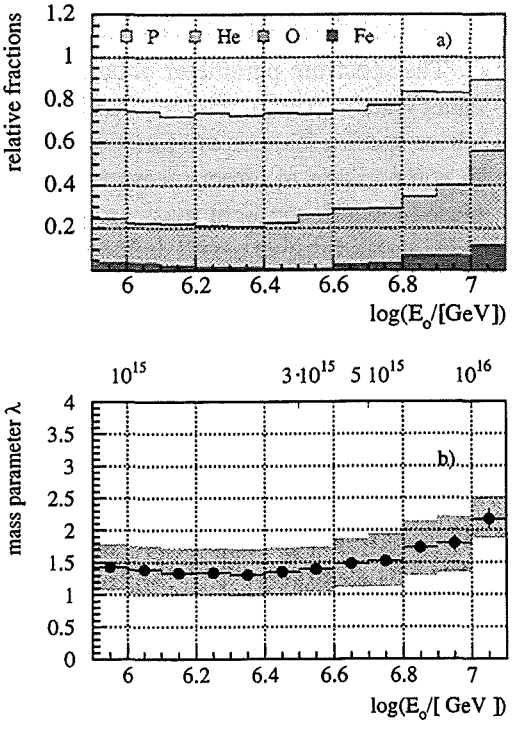

Figure 3: The mass composition (a) and the mass parameter λ (b) as function of the energy

For the following analysis of the primary all-particle flux the data were divided into a light mass group (protons and helium) and a heavy mass group (oxygen and iron). The spectrum was obtained straight forward by using the counts in the energy bins. Small changes of the energy axis due to the steep slope of the energy spectrum have been taken into account. This differential spectrum was weighted once with the percentage of the light mass group and once with that of the heavy mass group. The result is shown in Figure 4. The overall spectrum is plotted in the same figure. It shows clearly a knee position at 6.5-6.6 in $\log(E_0/\mathrm{GeV})$ (corresponding to 3.2-4 $\cdot 10^{15}$ eV) as one would expect from Figure 3 and 4.

The light and heavy mass groups have comparable slopes up to the knee region, but beyond this energy the light mass group shows a significant increase in the slope, while the slope of the heavy mass group remains nearly unchanged. The knee position and the slopes before and after the knee have been fitted using a function described in (Glasstetter,1998). This leads to following results: The knee position is found at 3.7 PeV. The index before the knee is about 2.65 and 2.93 after the knee. The systematic errors we estimate to approximately 13%. The knee position of the light mass group is at a comparable region while the heavy mass group shows no significant knee. The index of the light mass group changes from 2.67 to 3.31, the index of the heavy mass group stays constant at 2.51 The large errors are due to the systematical uncertainties, illustrated in Figure 4 by the shaded area.

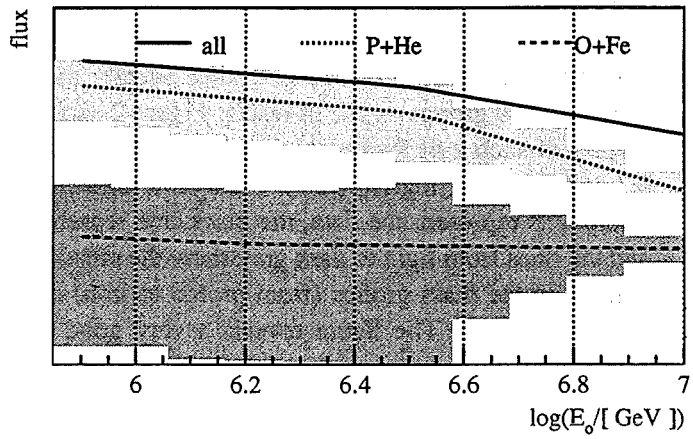

Figure 4: The flux (arbitrary units) for light and heavy masses as function of the energy. The ordinate is multiplied by a factor of $E_0^{2.5}$ to illustrate the shape of the spectrum.

5 Conclusions and Outlook

The spectrum parameter obtained with the hadronic interaction model QGSJET compare well with world data (Watson, 1997). The results of the analysis are in good agreement with acceleration/propagation models where spectra features are functions of the rigidity (Wiebel-Sooth, 1998).

In comparision to direct measurements at lower energies the mass composition obtained appears somewhat biased towards the light mass group. The ratio of the logarithmic sizes is a very sensitive parameter. Though the simulations give a well defined mean of this parameter a shift of the mean by only 2 % (that means $\sim$ 15% less electrons or $\sim$ 15% more muons) can change the value of the mass parameter λ from 1.4 to a value of 1.8 at 1 PeV which one would extrapolate from direct measurements. Due to the iterative corrections of the lateral electron distributions with the extrapolated lateral distributions of the muons, that are only defined in a region of 40 m - 200 m, the parametrization of the muon form parameter age$_\mu$ as a function of the electron size (see section 2) becomes a crucial point. Though the simulated parametrization fits the data reasonably within the fit region, a fit to the mean measured lateral distributions, that are collected as a function of the truncated muon size, gives a slightly different age$_\mu$. In a further analysis the parametrization of the muon age will be obtained from the data and not from simulations. First studies with low statistic show a an increase of the ratio of $\sim$ 1%. A careful study of this effect continues.

References

Heck, D. et al., 1998, FZKA 6019 Forschungszentrum Karsruhe (1998)
Glasstetter, R. et al., Proc. 25th ICRC (Durban 1997), 157
Klages, H.O. et al., Nucl. Phys. B (Proc Suppl.) 52b (1997) 922
Watson, A.A., Proc. 25th ICRC (Durban 1997) 8, 257
Wiebel-Sooth, B. et al, A & A, 330 (1998) 389-398

HE 2.2.43

EAS Muon Arrival Time Distributions Measured in the KASCADE Experiment

I.M. Brancus[1]*, T. Antoni[2], W.D. Apel[2], A.F. Badea[1], K. Bekk[2], K. Bernlöhr[2], E. Bollmann[2], H. Bozdog[1], A. Chilingarian[3], K. Daumiller[4], P. Doll[2], J. Engler[2], F. Feßler[2], M. Föller[2] H.J. Gils[2], R. Glasstetter[4], R. Haeusler[2] †, W. Hafemann[2], A. Haungs[2], D. Heck[2], T. Holst[2], J.R. Hörandel[2] K.-H. Kampert[2,4], J. Kempa[5], H.O. Klages[2], J. Knapp[4] H.J. Mathes[2], H.J. Mayer[2], J. Milke[2], D. Mühlenberg[2], J. Oehlschläger[2], M. Petcu[1], U. Raidt[2] H. Rebel[2], M. Risse[2], M. Roth[2], G. Schatz[2] F.K. Schmidt[4], T. Thouw[2], H. Ulrich[2], A. Vardanyan[3], B. Vulpescu[1], J. Weber[4], J. Wentz[2], T. Wibig[5], T. Wiegert[2], D. Wochele[2], J. Wochele[2], J. Zabierowski[6], S. Zagromski[2],

[1]*National Institute of Physics and Nuclear Engineering, Bucharest, Romania*

[2]*Forschungszentrum Karlsruhe, Institut für Kernphysik, D-76021 Karlsruhe, Germany*

[3]*Cosmic Ray Division, Yerevan Physics Institute, Yerevan, Armenia*

[4] *Institut für Experimentelle Kernphysik, University of Karlsruhe, Germany*

[5]*University of Lodz, Institute of Physics, Lodz, Poland*

[6] *Soltan Institute for Nuclear Studies, Lodz, Poland*

Abstract

The temporal structure of the EAS muon component, given by median, first and third quartile of the single distributions is studied with the muon detection facilities of the KASCADE central detector. Data have been analysed for EAS core distances up to 130 m and for primary energies of the knee region. The EAS muon time profile and disc thickness have been studied along their dependence on the angle-of-incidence and on the energy indicative muon number N_μ^{tr}, particular attention is paid to which extent EAS muon arrival time distributions at larger radial distances display features indicating a change of the mass composition of primary cosmic rays around the knee. The experimental results are compared with EAS Monte-Carlo (CORSIKA - CRES) simulations including the detector response.

1 Experimental setup and general procedures:

Using the timing and muon detection facilities of the KASCADE central detector (Klages et al., 1997), in particular the trigger layer of 456 scintillation detectors (placed as the third active layer of the hadron calorimeter) and the position sensitive large area multiwire proportional chambers (MWPC) installed below the hadron calorimeter, the muon arrival time distributions ($E_\mu \geq 2$ GeV) have been measured. Their dependence on different shower quantities: the distance from the shower center R_μ, the zenith angle θ of the shower incidence and the muon shower content N_μ^{tr} (representing the muon content with $E_\mu > 250$ MeV, integrated in a limited range of 40 - 200 m from the centre of the lateral muon distribution and considered as an identifier of the primary energy) have been studied (Brancus et al., 1998). The total number of collected events amounts to c. 200 000 with the requirement that at least 3 timing detectors of the timing facility of the central detector must have fired per event. The muon component at energies > 2 GeV is measured as correlated signals of the trigger layer and the MWPC and associated by the general KASCADE trigger to an EAS event.

Measurements of the relative muon arrival time refer to an experimentally defined zero-time, usually the arrival time τ_{cor} of the shower core. These quantities are called *global times* furtheron:

$$\Delta\tau_1^{glob} = \tau_\mu^1 - \tau_{\rm cor}, \tag{1}$$

τ_μ^1 being the arrival time of the foremost muon. The global times are affected by the limited accuracy of the reconstruction procedures of the arrival time of the electromagnetic component, hence we prefer to analyse

*corresponding author; e-mail: iliana@muon2.nipne.ro

†presenting author

local times which refer to the arrival time of the foremost muon, registrated in the timing detector at a particular distance from the center R_μ, defined in a plane perpendicular to the shower axis:

$$\Delta\tau^{loc}(R_\mu) = \tau_\mu(R_\mu) - \tau^1_\mu(R_\mu) \quad (2)$$

We characterize the single local arrival time distributions by different moments T: *the median* ($\Delta\tau_{0.50}$), *the first* and *the third quartile* ($\Delta\tau_{0.25}$ and $\Delta\tau_{0.75}$). In order to supress faked muons from hadron events (noticeable at $R_\mu \leq 30$ m), a condition for the energy deposit in the scintillator detectors has been applied.

2 The EAS muon shower profile and disc thickness:

We consider the muon arrival time distributions in different intervals of the core distance $R_\mu = 20 - 30$ m, ... up to 130 m for different ranges of zenith angles and for 5 ranges of the $\log_{10} N^{tr}_\mu$. From the local arrival time distributions determining the mean values and the standard deviations one obtaines the muon shower profile and the disc thickness.

Fig. 1 presents the variation of the median muon arrival time distributions with the distance from the shower core, compared with a description by a Γ-probability distribution function (Woidneck et al., 1975):

$$\Gamma(T) = aT^b exp(-cT) \quad (3)$$

with a mean value

$T(R_\mu) = (1+b)/c$ and the standard deviation $\sigma^\Gamma = (1+b)^{1/2}/c$.

It is obvious that the muon arrival time distributions become broader with increasing radial distances and narrower with increasing $\log_{10} N^{tr}_\mu$ size.

Fig. 2 shows the muon shower profile and the disc thickness comparing the mean values and the standard deviations extracted directly from the experimental (histograms) distributions for different $\log_{10} N^{tr}_\mu$ to those fitted by a Γ-Form. The shape of the EAS profile has been approximated by a parabolic form (Ambrosio et al., 1997):

$$T(R_\mu) = t_1 + t_2(R_\mu/R_m)^\beta \quad (4)$$

with $R_m = 100$ m, the scaling radius for muon lateral distribution. Some limitations of the used parametrization are observed, in particular for the variances of the slower

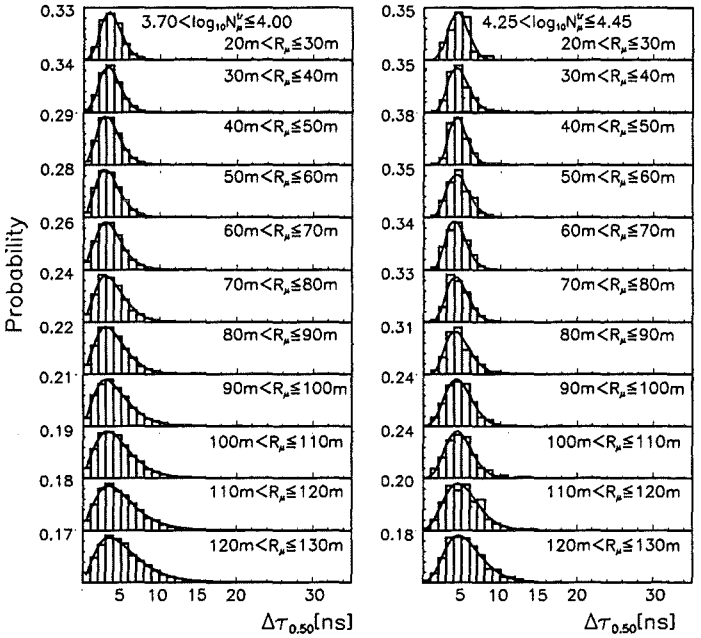

Figure 1: The variation of the shape of the median distribution with the core distance R_μ for two $\log_{10} N^{tr}_\mu$ ranges and for $5^o < \theta \leq 30^o$. The distributions are normalised to the maximum number of particle per time-bin. The lines give the fits by the Γ-form.

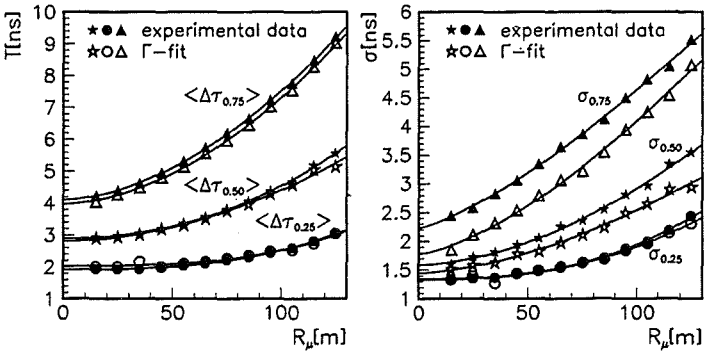

Figure 2: The mean values and standard deviations of the median, first and third quartiles distributions extracted from the distributions (Fig. 1) and compared with those from fitting the distributions with a Γ- form

muon component, but the deviations are much smaller than that observed for the charged particle component (Agnetta et al., 1997).

3 The variation of the muon shower profile with N_μ^{tr}:

As Monte-Carlo simulations show, for the KASCADE experiment the quantity $\log_{10} N_\mu^{tr}$ is approximately proportional $\log_{10} E_0$ and independent from the primary mass. Thus the use of EAS classification along $\log_{10} N_\mu^{tr}$ instead of $\log_{10} N_e$ avoids preparing samples mixing different energy ranges of different primary masses (Haungs et al., 1998).

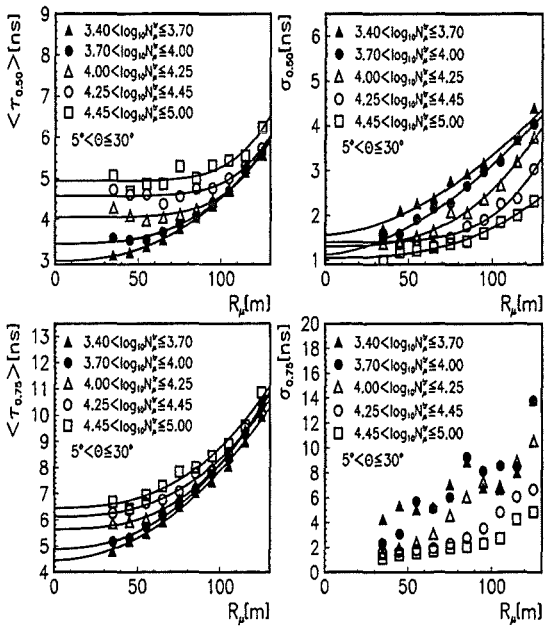

Figure 3: The R_μ dependence of the mean values and of the standard deviations of the median and the third quartile distributions for different ranges of $\log_{10} N_\mu^{tr}$ in the zenith-angle range of $5^o < \theta \leq 30^o$. Full lines are approximations of the time profile by a parabolic shape

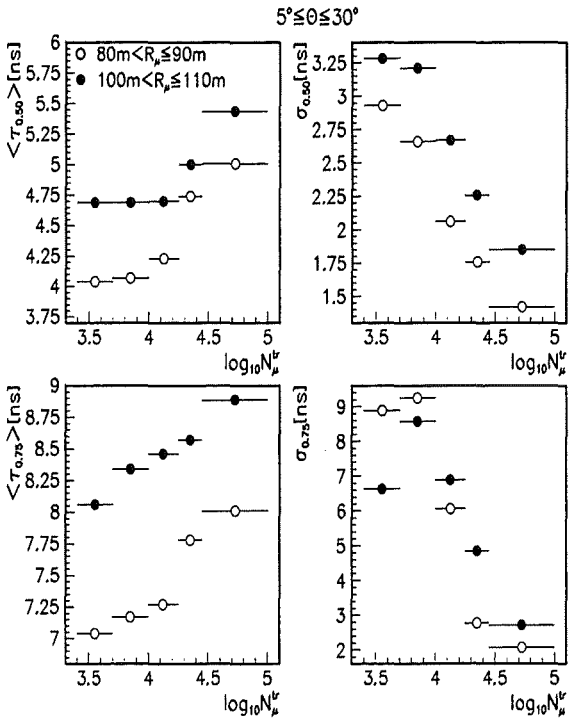

Figure 4: The $\log_{10} N_\mu^{tr}$ dependance of the time moments and their standard deviations for the zenith angle $5^o < \theta \leq 30^o$ and for two ranges of radial distances: $80\ m < R_\mu \leq 90\ m$ and $100\ m < R_\mu \leq 110\ m$

In the present analysis we classified 5 different $\log_{10} N_\mu^{tr}$ ranges covering an energy range from about $8 \cdot 10^{14}$ eV to $3.4 \cdot 10^{16}$ eV. Fig. 3 shows the profiles for different $\log_{10} N_\mu^{tr}$ ranges for the median and the third quartile. It is obvious that the standard deviations of the distributions decrease with increasing primary energy.

Fig. 4 displays the variation of the mean arrival time and of the standard deviations of the median and the third quartile distributions with $\log_{10} N_\mu^{tr}$, indicating a decrease of fluctuations, especially for the last two ranges corresponding to primary energies above the knee. This might be an indication for the appearance of an increasingly heavier primary component in the cosmic rays.

4 Comparison with predictions of Monte-Carlo EAS simulations:

The experimental muon arrival time distributions are compared with simulations of the air shower development, calculated by use of the Monte-Carlo simulation program CORSIKA (Heck et al., 1998). The actual simulation calculations (based on QGSJET model) cover an energy range of $5 \cdot 10^{14} - 1 \cdot 10^{16}$ eV (divided in 5 overlapping energy bins for three mass groups: H = protons, O = CNO group, Fe = heavy group) for an energy distribution of a spectral index of -2.7. They comprise a set of 2000 showers for each case. The response of the KASCADE detector system and the timing qualities have been simulated using the CRES programm, dedicately developed by the KASCADE group on basis of the GEANT code.

Fig. 5 display simulated median distributions of the arrival times for EAS for the $\log_{10} N_\mu^{tr}$ range of 3.7- 4.0. A mass composition H : O : Fe = 4 : 1 : 2 has been adopted. The good agreement of the simulated and the experimental observed distributions (see fig. 1 left side) is remarkable.

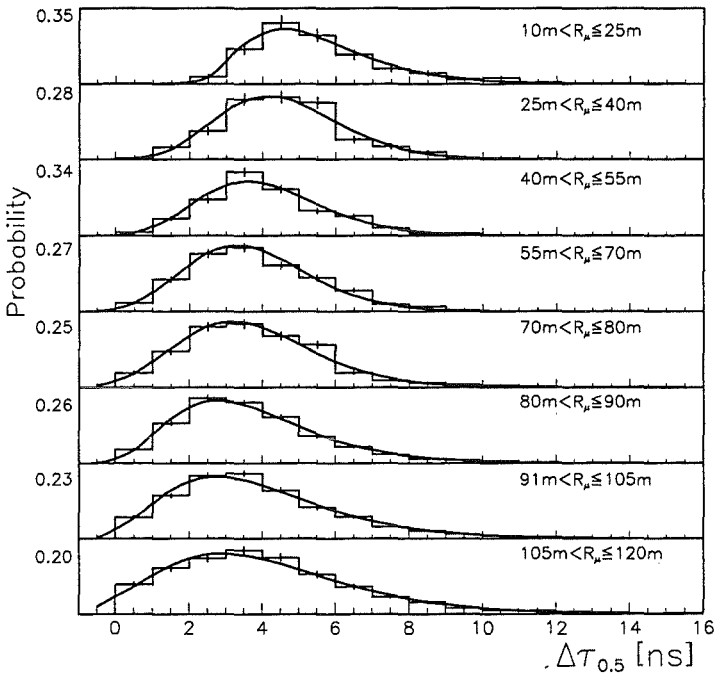

Figure 5: Simulated median muon arrival time distributions, $\Delta\tau_{0.5}$ for different distances from the shower core for a $\log_{10} N_\mu^{tr}$ range of 3.7- 4.0. The lines represents the fit by the Γ-form.

5 Concluding remarks:

With the present studies of the time structure of the EAS muon component inferred from data measured with the KASCADE detector, the phenomenological features of the muon arrival time distributions and of the shower profile and disc thickness are reported. As compared to the results of studies of the charged particle component the time profiles of the EAS muon component appears to be flatter. The time dispersion of the EAS disc conspicuously decreases with higher energies of the primaries, above the knee, possibly indicating a change in the composition. First exploratory comparisons with Monte-Carlo simulations exhibit a remarkably good agreement of the measured data with the theoretical predictions, thus confirming that the CORSIKA simulations describe the longitudinal EAS development quite realistically.

References

Agnetta, G. et al., 1997, Astropart. Phys. 6, 301
Ambrosio, M. et al., 1997, Astropart. Phys., 7, 329
Brancus, I.M. et al., 1998, FZKA-Report 6151, (Forschungszentrum Karlsruhe)
Haungs, A. et al., 1998, FZKA-Report 6105, (Forschungszentrum Karlsruhe)
Heck, D. et al., 1998, FZKA-Report 6019, (Forschungszentrum Karlsruhe)
Klages, H.O. et al., 1997, Nucl. Phys. B (Proc.Suppl.), 52B, 92
Woidneck, C.P. et al., J. Phys. A Math. Gen., 8, 997

HE 2.2.44

Estimation of the Primary Mass with Hadronic Observables in EAS Cores

J. Engler[1], T. Antoni[1], W.D. Apel[1], F. Badea[2], K. Bekk[1], K. Bernlöhr[1], E. Bollmann[1], H. Bozdog[2], I.M. Brancus[2], A. Chilingarian[3], K. Daumiller[4], P. Doll[1], F. Feßler[1], H.J. Gils[1], R. Glasstetter[4], R. Haeusler[1], W. Hafemann[1], A. Haungs[1], D. Heck[1], J.R. Hörandel[1‡], T. Holst[1], K.-H. Kampert[1,4], H. Keim[1], J. Kempa[5], H.O. Klages[1], J. Knapp[4§], H.J. Mathes[1], H.J. Mayer[1], J. Milke[1], D. Mühlenberg[1], J. Oehlschläger[1], M. Petcu[2], H. Rebel[1], M. Risse[1], M. Roth[1], G. Schatz[1], F.K. Schmidt[4], T. Thouw[1], H. Ulrich[1], A. Vardanyan[3], B. Vulpescu[2], J.H. Weber[4], J. Wentz[1], T. Wibig[5], T. Wiegert[1], D. Wochele[1], J. Wochele[1], J. Zabierowski[6]

[1]*Institut für Kernphysik, Forschungszentrum Karlsruhe, D-76021 Karlsruhe, Germany*

[2]*Institute of Physics and Nuclear Engineering, RO-7690 Bucharest, Romania*

[3]*Cosmic Ray Division, Yerevan Physics Institute, Yerevan 36, Armenia*

[4]*Institut für Experimentelle Kernphysik, University of Karlsruhe, D-76021 Karlsruhe, Germany*

[5]*Department of Experimental Physics, University of Lodz, PL-90950 Lodz, Poland*

[6]*Soltan Institute for Nuclear Studies, PL-90950 Lodz, Poland*

Abstract

The primary cosmic-ray mass composition is estimated using the hadronic component of EAS measured by the large hadron calorimeter of the KASCADE experiment. Methods for evaluating the mean mass are described, model dependences are discussed and results are presented. The data indicate an increase of the mean mass with rising primary energy, especially beyond the *knee*.

1 Proem

The experiment KASCADE (Klages et al., 1997) has in its centre of array stations a large hadron calorimeter to study the core of EAS in the energy region around the *knee*. In the following, observables are presented which allow to infer the primary mass composition from particle distributions in the hadronic core. However, a correct modelling of the interactions in the atmosphere is mandatory to extract reliable conclusions about the primary mass. The procedure is very prone to even small changes in the interaction mechanism. Two interaction models, namely QGSJET (Kalmykov & Ostapchenko, 1993) and VENUS (Werner, 1993) as implemented in the EAS simulation code CORSIKA (Heck et al., 1998) are used. These two models, based on the Gribov Regge theory, have been chosen because their solid theoretical ground allows best to extrapolate from collider measurements to higher energies, forward kinematical regions and nucleus-nucleus interactions. They have been proven to describe the hadronic observables reasonably well (Antoni et al., 1999).

2 Experimental Set-up and Measurements

KASCADE measures all three components of an EAS simultaneously, i.e. the electromagnetic, the muonic, and the hadronic part. The latter is studied with the 320 m^2 large iron calorimeter which is 11 interaction lengths deep and interspersed with eight layers of active detectors. These are ionization chambers filled with the room temperature liquids tetramethylsilane and tetramethylpentane. The electrodes of 25 $\times$ 25 cm^2 size are matched to the mean lateral spread of hadronic cascades in iron and allow the resolve individual hadrons with 40 cm separation. For hadrons above a threshold energy of 50 GeV impact point, energy, and direction of incidence are reconstructed. Details of the calorimeter performance are given in (Engler et al., 1999).
For the investigations presented below, events had to fulfill the following requirements: More than two hadrons are reconstructed, the zenith angle of the shower is less than 30° and the core, as determined by the array

‡corresp. author; e-mail: jrh@ik1.fzk.de, pres. address: The University of Chicago, Enrico Fermi Institute, Chicago, IL 60637

§now at: University of Leeds, Leeds LS2 9JT, U.K.

stations with a resolution of about 2 m, hits the calorimeter or lies within 1.5 m distance outside its boundary. About 40 000 showers meet these conditions.
The showers are classified according to their truncated muon size N_μ^{tr} as measured by the array. N_μ^{tr} is obtained experimentally by integrating the muon lateral distribution in the range 40-200 m. N_μ^{tr} is a good estimator of the primary energy E_0, because for selected showers hitting the calorimeter $E_0 \propto N_\mu^{tr\,0,98}$, nearly irrespective of the primary mass.

3 Simulations

Simulations were performed using the CORSIKA version 5.2 and 5.62. A sample of 7000 p and Fe events were simulated with QGSJET, and 2000 showers were generated with VENUS, each for p, He, O, Si and Fe primaries. The showers were distributed in the energy range of 0.1 to 31.6 PeV according to a power law with a differential index of 2.7 and were spread in the zenith angle in the intervall of 15° to 20°. The shower axes were distributed uniformly over the calorimeter surface extended by 2 m beyond its boundary.

4 Results

In Fig.1 two examples of hadronic observables are presented which both distinctly depend on the primary mass. The graph on the left–hand shows the lateral hadron density and on the right–hand the distance distributions in *minimum-spanning trees* (MST), both for N_μ^{tr} intervalls that correspond to primary energies around 1.2 and 2 PeV, respectively. A MST connects all hadrons to each other in a plane perpendicular to the shower axis. It is that configuration where the sum of all connections weighted by the inverse energy sum of its neighbours has a minimum. Presented are results from the simulations for primary protons and Fe nuclei. The shaded area, hence, presents the region allowed for any primary mass composition. The measured data, indeed, fall in-between, and the distance to the two extrema determines the mean mass. Actually, in this way the logarithmic mass $\langle \ln A \rangle$ is obtained, because most of the observables depend only on the mass logarithmically. This can be infered from Fig.2 where the mean distance between the extrema is plotted versus $\ln A$ for the lateral hadron density, see the left–handed graph in Fig.1.

In a similar manner four other observables are investigated, namely the lateral energy density, the en-

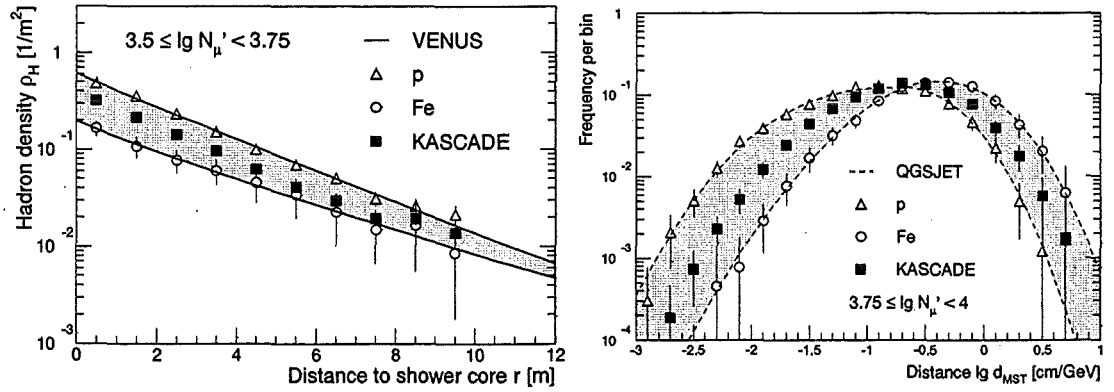

Figure 1: Lateral hadron density (left–hand) and distances in a MST (right–hand) for a muon number interval as indicated. The data are compared with simulations using VENUS and QGSJET for primary protons and iron nuclei.

ergy spectrum of hadrons, the energy of the most energetic hadron and the distribution of the fractional energy of hadrons with respect to the most energetic hadron in the shower. The latter and the MST indicate to some extent the granularity in a hadronic core, the first in energy, the second in space. For heavy primaries these two observables are expected to exhibit a rather uniform distribution whereas primary protons should show up with pronounced fluctuations.

For all six observables a mean mass parameter λ is calculated from the distance to the two extreme compositions: $\lambda = 0$ for a pure proton and $\lambda = 1$ for a pure iron composition. Fig. 3 shows this parameter as a function of N_μ^{tr}, i.e. approximately the primary energy. A steady rise with energy can be noticed for all six variables. The fluctuations, however, are large. For this reason the mean values $\langle\lambda\rangle$ of these observables and for both interaction models are combined and the corresponding $\langle \ln A\rangle$ determined.

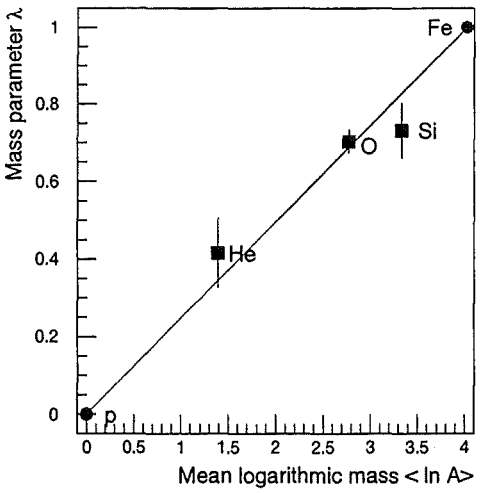

Figure 2: The mass parameter λ as obtained from CORSIKA simulations using VENUS.

Fig.4 presents the results in context of a compilation of recent world data. Plotted are KASCADE figures of the present analysis using the hadrons. In addition, two further analyses are given, viz. investigations utilizing electrons and muons as measured in the array detectors (Weber et al., 1999) and a Bayes classification on an event–by–event basis employing seven observables from both the array and the central detector (Roth et al., 1999).

Direct measurements above the atmosphere are presented by the shaded area as taken from (Wiebel-Sooth, 1998). The two points at 1 PeV are extrapolations from direct measurements given in recent review talks, (Shibata 1998) and (Watson 1997). The hadron analysis yields relative high values of $\ln A$ following the trend indicated by the RUNJOB data and the measurements on the Chacaltaya. One notices that around 1 PeV the Bayes classification using all components measured in the KASCADE experiment matches the extrapolations best. The hadrons alone seem to yield a too heavy and the electrons a too light composition.

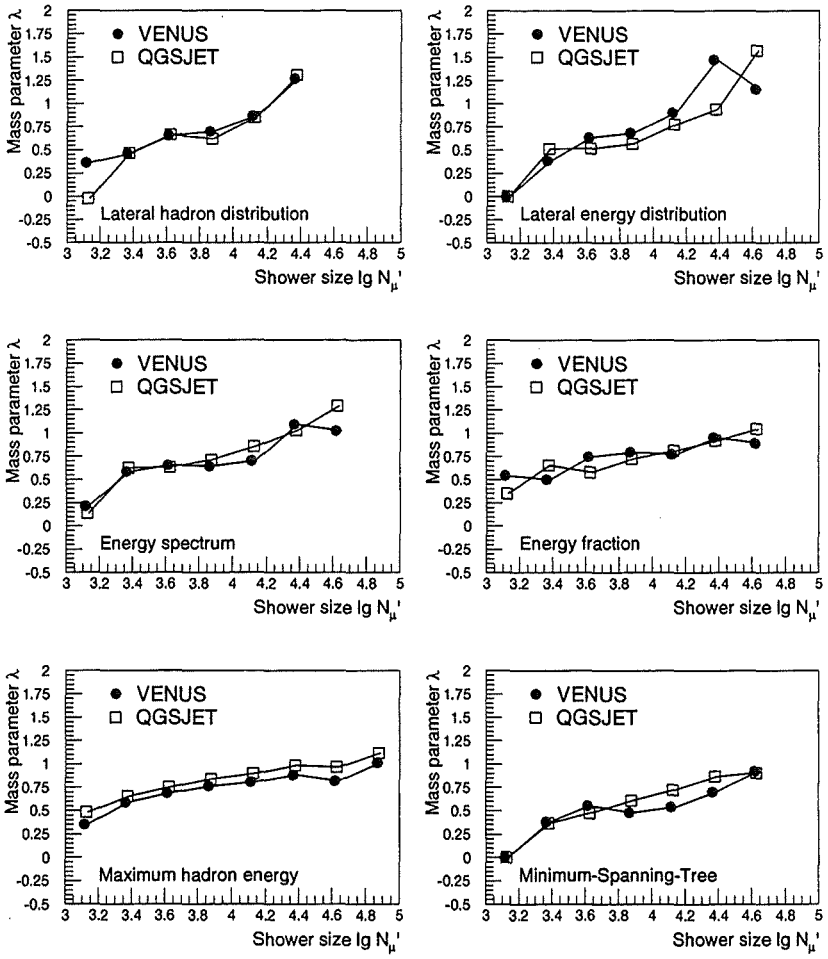

Figure 3: The mass parameter obtained from six observables vs. the truncated muon number. Values at $N_\mu^{tr} = 3.1$ are not corrected for trigger efficiency of the array.

Several other investigations have revealed that the simulations generate too many hadrons at observation level, see e.g. (Antoni et al., 1999) or (Risse et al., 1999). One, therefore, is tempted to conjecture that the missing hadrons are interpreted by the present analysis as a heavy composition. Vice versa the simulations seem to generate too few electrons which would account for the light composition found in the analysis using the electromagnetic component only. Whether the interaction codes really generate such an imbalance between the hadronic and electromagnetic component cannot be decided at the moment but we endeavour to study the effect by forthcoming measurements.

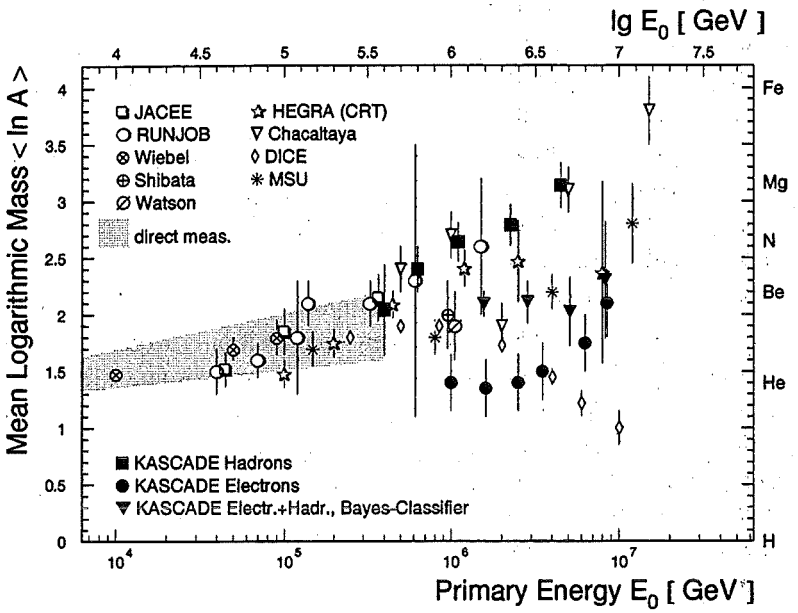

Figure 4: Mean logarithmic mass vs. primary energy. The shaded area represents direct measurements, compilation (Wiebel-Sooth, 1998), EAS measurements Chacaltaya (Shirasaki et al., 1997), HEGRA (Bernlöhr et al., 1998), DICE (Swordy 1998), MSU (Fomin et al., 1998).

References

T. Antoni et al., KASCADE Collab., "Test of Interaction Models with Hadrons", 1999, subm. to J.Phys.G, preprint astro-ph/9904287, also these Proceedings HE 1.3.01

K. Bernlöhr et al., Astrop.Phys. 8(1998) 253

J. Engler et al., "Warm-Liquid Calorimeter for Cosmic-Ray Hadrons", to be publ. Nucl.Instr.Meth.

Yu.A. Fomin et al., Proc. 16th ECRS, Alcala (1998) 261

D. Heck et al., Report FZKA 6019 (1998) Forschungszentrum Karlsruhe

N.N. Kalmykov & S.S. Ostapchenko, Yad. Fiz 56(1993) 105

H.O. Klages et al., KASCADE Collab., Nucl.Phys.B (Proc. Suppl.)52B (1997) 92

M. Risse et al., KASCADE Collab., Proc. 26th ICRC, Salt Lake City, HE 1.3.02

M. Roth et al., KASCADE Collab., Proc. 26th ICRC, Salt Lake City, HE 2.2.40

T. Shibata, talk at 10th ISVEHCRI, Gran Sasso 1998

S.P. Swordy, Proc. 16th ECRS, Alcala (1998) 265

Y. Shirasaki et al., Proc. 25th ICRC Durban 4(1997)53

A.A. Watson, rapporteur talk, Proc. 25th ICRC Durban 8(1997)257

J. Weber et al., KASCADE Collab., Proc. 26th ICRC, Salt Lake City, HE 2.2.42

K. Werner, Phys.Rep. 232(1993)87

B. Wiebel-Sooth, "All-particle Energy Spectrum Measured at HEGRA", thesis, University of Wuppertal WUB-Dis 98-9.

HE 2.5.28

Recent Additions to the Extensive Air Shower Simulation Code CORSIKA*

D. Heck[1†], F. Schröder[2‡],
T. Antoni[1], W.D. Apel[1], F. Badea[3], K. Bekk[1], K. Bernlöhr[1], E. Bollmann[1], H. Bozdog[3], I.M. Brancus[3],
A. Chilingarian[4], K. Daumiller[5], P. Doll[1], J. Engler[1], F. Feßler[1], H.J. Gils[1], R. Glasstetter[5],
R. Haeusler[1], W. Hafemann[1], A. Haungs[1], J.R. Hörandel[5§], T. Holst[1], K.-H. Kampert[1,5], J. Kempa[6],
H.O. Klages[1], J. Knapp[5¶], H.J. Mathes[1], H.J. Mayer[1], J. Milke[1], D. Mühlenberg[1], J. Oehlschläger[1],
M. Petcu[3], H. Rebel[1], M. Risse[1], M. Roth[1], G. Schatz[1], F.K. Schmidt[5], T. Thouw[1], H. Ulrich[1],
A. Vardanyan[4], B. Vulpescu[3], J.H. Weber[5], J. Wentz[1], T. Wibig[6], T. Wiegert[1], D. Wochele[1],
J. Wochele[1], J. Zabierowski[7],

[1]*Institut für Kernphysik, Forschungszentrum Karlsruhe, D-76021 Karlsruhe, Germany*
[2] *Fachbereich Physik, Bergische Universität Wuppertal, D-42097 Wuppertal, Germany*
[3]*National Institute of Physics and Nuclear Engineering, RO-7690 Bucharest, Romania*
[4]*Cosmic Ray Division, Yerevan Physics Institute, Yerevan 36, Armenia*
[5] *Institut für Experimentelle Kernphysik, University of Karlsruhe, D-76021 Karlsruhe, Germany*
[6]*Department of Experimental Physics, University of Lodz, PL-90950 Lodz, Poland*
[7] *Soltan Institute for Nuclear Studies, PL-90950 Lodz, Poland*

Abstract

The Monte Carlo program CORSIKA simulates the evolution of extensive air showers in the atmosphere initiated by photons, hadrons or nuclei. Besides the already available 5 models DPMJET, HDPM, QGSJET, SIBYLL, and VENUS describing hadronic interactions at high energies we have added the new model NEXUS. Based on the universality hypothesis of the behavior of high energy interactions, NEXUS in its unified approach combines Gribov-Regge theory and perturbative QCD, including Reggeons, soft Pomerons, semi-hard Pomerons as a QCD-evolution of soft Pomerons, and parton-parton scattering.

A further CORSIKA addition is the 'curved' option which allows a correct treatment of showers incident at large zenith angles $> 70^o$. At those angles a deviation from a planar atmosphere caused by the curvature of the Earth's surface must be taken into account. The new extensions and features of CORSIKA are described.

1 Introduction:

The extensive air shower simulation code CORSIKA (**CO**smic **R**ay **SI**mulation for **KA**SCADE) (Heck et al., 1998) originally was developed to understand and interpret the data measured by the KASCADE experiment (Klages et al., 1997; Kampert et al., 1999). By various additions and extensions for, e.g. neutrinos, Cherenkov radiation, highest energies including Landau-Pomeranchuk-Migdal effect and thin sampling, various computing systems etc. (Heck & KASCADE collaboration, 1997) during the last decade CORSIKA has become a multi-purpose working horse for cosmic ray investigations and is now employed by $\approx$ 200 users in more than 60 laboratories around the world.

2 The NEXUS Interaction Model:

NEXUS (Drescher et al. 1998) is the result of a common effort of the authors of VENUS (Werner, 1993) and QGSJET (Kalmykov & Ostapchenko, 1993). It combines basic treatments of these two codes in a new approach, creating a new generation interaction model. Many additions and new ideas are included which

*presented by M. Risse

†corresponding author; e-mail: heck@ik3.fzk.de

‡supported by BMBF, FRG under contract No. 08 107 206

§present address: University of Chicago, Enrico Fermi Institute, Chicago, IL 60637
¶now at: University of Leeds, Leeds LS2 9JT, U.K.

	DPMJET	HDPM	NEXUS	QGSJET	SIBYLL	VENUS
Gribov-Regge	+		+	+		+
Minijets	+		+	+	+	
Sec. Interactions			+			+
N-N Interaction	+		+	+		+
Superposition		+			+	
Max. Energy (GeV)	$> 10^{11}$	10^8	2×10^8	$> 10^{11}$	$> 10^{11}$	2×10^7
Memory (Mbyte)	52	8	123	10	9	21
CPU time/shower (min)	2.6	1.0	35	1.0	0.75	4.5

Table 1: Basic features of hadronic interaction models. CPU times for: p primary, $E_0 = 10^{15}\ eV$, vertical, $E_h \geq 0.3\ GeV$, $E_\mu \geq 0.3\ GeV$, 110 m a.s.l., NKG option, DEC 3000/600 AXP (175 MHz); NEXUS values preliminary.

should allow an extension for an appropriate and reliable description of hadronic interactions also at highest energies with $E_{lab} > 10^{20}\ eV$.

Basically, NEXUS starts from the universality hypothesis (Drescher et al., 1999) saying that *the behavior of high-energy interactions is universal.* The nucleon-nucleon interaction for instance, is deduced from the lepton-nucleon scattering with photon exchange, ordering the ladder of partons emitted from the nucleon according increasing virtuality such that the parton with highest virtuality comes closest to the photon. In the nucleon-nucleon interaction the ladder is ordered to have the partons with highest virtuality in the middle, such as two lepton-nucleon ladders fused at their photon side. This ladder representing the semihard Pomeron can be treated by QCD evolution and is coupled to the nucleon by a soft Pomeron or a Reggeon, as described in (Werner et al., 1997). Parameters for the string fragmentation are obtained from e^+e^--data employing the 'kinky string' method. By this approach the modeling of the complicated mechanism of hadron-hadron interaction is decomposed into separate 'building blocks' which are deduced from simpler systems like the deep inelastic lepton-nucleon scattering. Tab. 1 compiles the basic features of the hadronic interaction models. NEXUS combines the advantages of VENUS with its detailed treatment of N-N interactions respecting possible interactions of the produced secondaries, and the QGSJET program treating the hard processes. However, the improvements go on the expenses of intense CPU resources.

Preliminary tests of extensive air shower simulations with CORSIKA/NEXUS showed the need for small final corrections in the NEXUS programming to obtain reasonable agreement with experimental data in a quality which resembles the parent programs VENUS and QGSJET as compared in (Knapp, Heck & Schatz, 1996; Knapp, 1998).

3 'Curved' Option:

In the CORSIKA standard version a plane atmosphere is assumed and the penetrated thickness increases with $1/\cos\theta$. This limits simulations to zenith angles $\theta < 70^o$. Above this value the difference between a flat atmosphere and a true spherical atmosphere becomes more and more important and at $\theta = 90^o$ the thickness of a planar atmosphere reaches infinity, compared with $\approx 37000\ g/cm^2$ for the true spherical case. Therefore, for large zenith angles $\theta > 70^o$ the Earth's curvature must be taken into account.

To avoid lengthy formulas for a treatment in a spherical coordinate system with corresponding long CPU times the description of particle transport in a Cartesian coordinate system is kept, but the horizontal step size is limited to $< 20\ km$. Longer transport distances are divided into appropriate segments to be treated in a local flat atmosphere. After each traversed segment the particle coordinates are transferred into the next local Cartesian coordinate system with its vertical axis pointing to the middle of Earth. Thus the curved Earth's

surface is approximated piece by piece by flat segments with limited horizontal extension. A similar treatment has been described by (Sciutto, 1998).

A comparison of simulations performed at $\theta = 70^o$ for hadrons and muons with the 'standard' and with the 'curved' version revealed an increase of CPU time by $\approx 30\%$. The validity of the coordinate transformations at the segment boundaries has been checked by the deviation of the particle trace from the detector center after penetrating the complete atmosphere without interaction and without magnetic deflection, impinging on the detector with $\theta = 89^o$. This needs a horizontal transport over a distance of $\approx 1100\ km$ corresponding with a movement over 10^o degrees along an Earth's meridian. The test revealed a missing of the detector center by $< .0003\ mm$ caused by rounding errors in double precision calculations.

4 Other Modifications and Additions:

4.1 Inelastic cross-sections for QGSJET: Motivated by discrepancies between the observed hadron rates and CORSIKA/QGSJET simulations (Risse et al., 1999) the QGSJET code (Kalmykov & Ostapchenko, 1993) has been modified (Ostapchenko, 1998) to increase the inelastic hadron-proton cross-sections within the error bars of collider data. Following a μ trigger with $n_\mu \geq 9$ in the KASCADE calorimeter fewer hadrons with $E_{had} > 100\ GeV$ are observed than predicted by the simulations. In the QGSJET modifications the cross-section values at $E_{lab} = 100\ GeV$ are kept largely unchanged, but with slightly steeper slopes they arrive at 5% higher values at $E_{lab} = 1\ PeV$. With these modified cross-sections the simulated hadron rates are lowered by $\approx 22\%$, but they are still higher than the rates observed in the calorimeter. A further slight improvement of QGSJET is attained by omitting the restriction of diffractive collisions to diffractive masses $m_D < 5\ GeV$. This leads to a minor increase of average inelasticity. The hadron rates predicted by CORSIKA simulations employing other interaction models exceed the CORSIKA/QGSJET prognosis clearly (Risse et al., 1999).

4.2 Improved EGS4 coding: Double precision calculation is now used throughout in the EGS4 package (except for EGS4 cross-section files). By suitable means the large ($\approx 100\ \%$) fluctuations in the probability for direct $\gamma \rightarrow \mu^+\mu^-$-pair formation - resulting from inadequate numerical representation in the cross-section file - could be reduced by a factor of 10. As side effect, the photonuclear probability became a much more smoothed function of energy. The trigonometric functions gained by interpolation from precalculated tables with limited precision ($\approx 10^{-5}$) are now replaced by intrinsic double precision functions improving the angular precision by several orders of magnitude on the expenses of $\approx$ 30% enlarged computing times.

4.3 Atmospheres: To adapt to the atmospheric conditions at various geographic places and at various seasons, sets of atmosphere parameters are available for: U.S. standard, 8 seasonal conditions as measured for middle Europe, tropical (annual average), mid-latitude summer and winter, sub-arctic summer and winter, and South pole at 4 seasons. Additional atmospheres may be introduced by the user in tabular form of altitude dependent densities and mass overlays. For some of the atmospheres also the refractive index for precise correction of Cherenkov photon ray tracing is available (Bernlöhr, 1998), as it is needed for imaging atmospheric Cherenkov telescopes with observation at large zenith angles.

4.4 Energy Balance: Detailed tables are added to the CORSIKA output giving the energy contained within the various particle species (γ, e^+, e^-, μ^+, μ^-, hadrons, all charged particles, and nuclei) as a function of atmospheric thickness in intervals specified by the user. A second table gives the energy deposit within each interval by ionization and by energy or angular cuts, listed separately for γ, $e^\pm$, $\mu^\pm$, and hadrons. Also the energy carried away by neutrinos is counted. The longitudinal sum of these deposits completes the energy balance.

4.5 Imaging Atmospheric Cherenkov Telescopes: A set of C-routines (Bernlöhr, 1999) has been implemented to treat the Cherenkov photons as registered by imaging atmospheric Cherenkov telescopes.

5 Program Distribution:

The CORSIKA program files including an up-to-date version of the User's Guide (Knapp & Heck, 1993) are available via anonymous ftp from ftp-ik3.fzk.de (restricted access). Interested users should contact the corresponding author. Further details are given on the web page **http://www-ik3.fzk.de/~heck/corsika/** .The next release of CORSIKA comprising these additions and improvements is planned for end of 1999.

Acknowledgments:

We thank K. Werner for the permission to use NEXUS, for his assistance in coupling it with CORSIKA and for many helpful discussions. Special thanks go to S. Ostapchenko for preparing the modified cross-sections of QGSJET. The contribution of South pole atmosphere parameters by D. Chirkin is acknowledged as well as the EGS4 cross-section file improvement by P. Steffen. We would like to thank all colleagues, who have contributed to the development of CORSIKA by reporting detected errors, suggestions and experiences.

References

Bernlöhr, K. 1999, to be published in Astrop. Phys.
Drescher, H.J. et al. 1998, preprint hep-ph/9806407
Drescher, H.J. et al. 1999, preprint hep-ph/9903296 (to be published)
Heck, D., KASCADE Collaboration 1997, Proc. 25th ICRC (Durban, 1997), Vol. 6, 245
Heck, D. et al. 1998, Report FZKA 6019, Forschungszentrum Karlsruhe
Kalmykov, K.K. & Ostapchenko, S.S. 1993, Yad. Fiz. 56, 105
Kampert, K.-H., et al., 1999, Proc. 26th ICRC (Salt Lake City, 1999) OG 1.2.11
Klages, H. 1997, Nucl. Phys. B (Proc. Suppl.), 52B, 92; Proc. 25th ICRC (Durban, 1997), Vol. 8, 297
Knapp, J. & Heck, D. 1993, Report KfK 5196B, Kernforschungszentrum Karlsruhe; for an up-to-date version see http://www-ik3.fzk.de/~heck/corsika/
Knapp, J., Heck, D., & Schatz, G. 1996, Report FZKA 5828, Forschungszentrum Karlsruhe
Knapp, J. 1998, Proc. X Int. Symp. Very High Energy Cosmic Ray Interactions, Gran Sasso (Italy)
Ostapchenko, S.S. 1998, private communication
Risse, M. et al. 1999, Proc. 26th ICRC (Salt Lake City, 1999) HE 1.3.02
Sciutto, S. 1998, Auger technical note GAP-98-032
Werner, K. 1993, Phys. Rep. 232, 87
Werner, K. et al. 1997, Proc. 3rd Int. Conf. Physics & Astrophysics of Quark-Gluon Plasma, Jaipur (India)

OG.4.5.01

The Auger Fluorescence Detector Prototype Telescope

H. Bluemer[6], V. Bocci[4], J. Castro[2], R. Cester[3], A. Cordero[2], P. Facal[4], B.E. Fick[1], R. Fonte[5], H.O. Klages[6], M. Kleifges[6], J. Kleinfeller[6], G. Matthiae[4], E. Menichetti[3], H. Nogima[1], J.M. Nunez[2], N. Pastrone[3], P. Privitera[4], P. Sommers[1], and the Pierre Auger Collaboration.

[1]*Physics Department, University of Utah, Salt Lake City, UT 84112, USA*
[2]*Benemerita Universidad Autonoma de Puebla, Puebla, Mexico*
[3]*University of Torino, Dipartimento di Fisica, Torino, Italy*
[4]*University of Roma 2, Dipartimento di Fisica, 00133 Roma, Italy*
[5]*Inst. Nazionale di Fisica Nucleare, 95129 Catania, Italy*
[6]Inst. fur Kernphysik, Forschungszentrum Karlsruhe, 76021 Karlsruhe, Germany

Abstract

The Pierre Auger Cosmic Ray Observatory will study cosmic rays above 10 EeV using both atmospheric fluorescence measurements and ground level particle detectors. A demonstration hybrid observatory will commence operation in Argentina's Mendoza Province next year (2000). This paper documents the design for the prototype fluorescence telescope whose field of view is 30x30 degrees. The large field of view is made possible by using a Schmidt diaphragm that eliminates coma aberration. Reflective light collectors at the focal surface resurrect dead spaces between PMT cathodes. The nearly uniform focal surface simplifies the translation of FADC data to fluorescence light flux as a function of time, and hence shower size as a function of atmospheric depth. The primary objective for the Auger fluorescence detector is to measure accurately the longitudinal development profiles of showers that are detected in conjunction with the surface array.

1 Introduction

In development since 1992, the Pierre Auger Project is a collaboration of physicists in 19 different countries, dedicated to the construction of a powerful new observatory for studying the highest energy cosmic rays (Cronin et al., 1992; Auger Collaboration, 1997). The detector will have good sensitivity to all cosmic rays above the spectrum's ankle, with constant aperture above 10^{19} eV. In order to achieve nearly uniform exposure to the full celestial sphere, the plan calls for two matching sites – one in Argentina's Mendoza Province and the other in Millard County of Utah. Work has begun at the southern site. The full-time aperture will be 7000 km^2·sr at each site, provided by arrays of water Cherenkov detectors on the ground. Atmospheric fluorescence measurements of the air shower longitudinal profiles will be made at night using optical telescopes. The symbiotic operation of the surface array and fluorescence detectors (FDs) will provide a "hybrid" data set with redundancy, cross checks on systematics, and unprecedented sensitivity to primary particle types. This paper describes the present design for the Auger FD telescopes and plans for a prototype to become operational next year. Information about the Auger Project is available at *www.auger.org*, and further details about the FD can be found at *www.physics.utah.edu/~sommers/hybrid/*.

2 The telescope design

The Auger FD telescope design is based on the successful Fly's Eye and HiRes detectors (Baltrusaitis et al., 1985; HiRes Collaboration, 1997). There are significant innovations, however, including

Schmidt optics and a new electronics design. (Plans for the FADC electronics and trigger system are reported separately.) In order to minimize measurement uncertainties due to the variable atmosphere, multiple "eyes" will be built so that showers will be seen at closer range and smaller factors will be required to correct for atmospheric attenuation by Rayleigh and Mie scattering. With the present layout plan for the southern site, the median R_p is 14 km, where R_p is the perpendicular distance between eye and shower axis.

Figure 1 is a schematic diagram of an Auger telescope. The field of view is approximately $30° \times 30°$. An aperture stop (diaphragm) eliminates coma aberration. With its spherical focal surface, the system is almost spherically symmetric about the point at the diaphragm's center. The spot size (point spread function) is governed by spherical aberration and is nearly the same for any arrival direction within the field of view. (There is some variation of the camera's obscuration.) Specific optical parameters and properties of this design are summarized in Table 1.

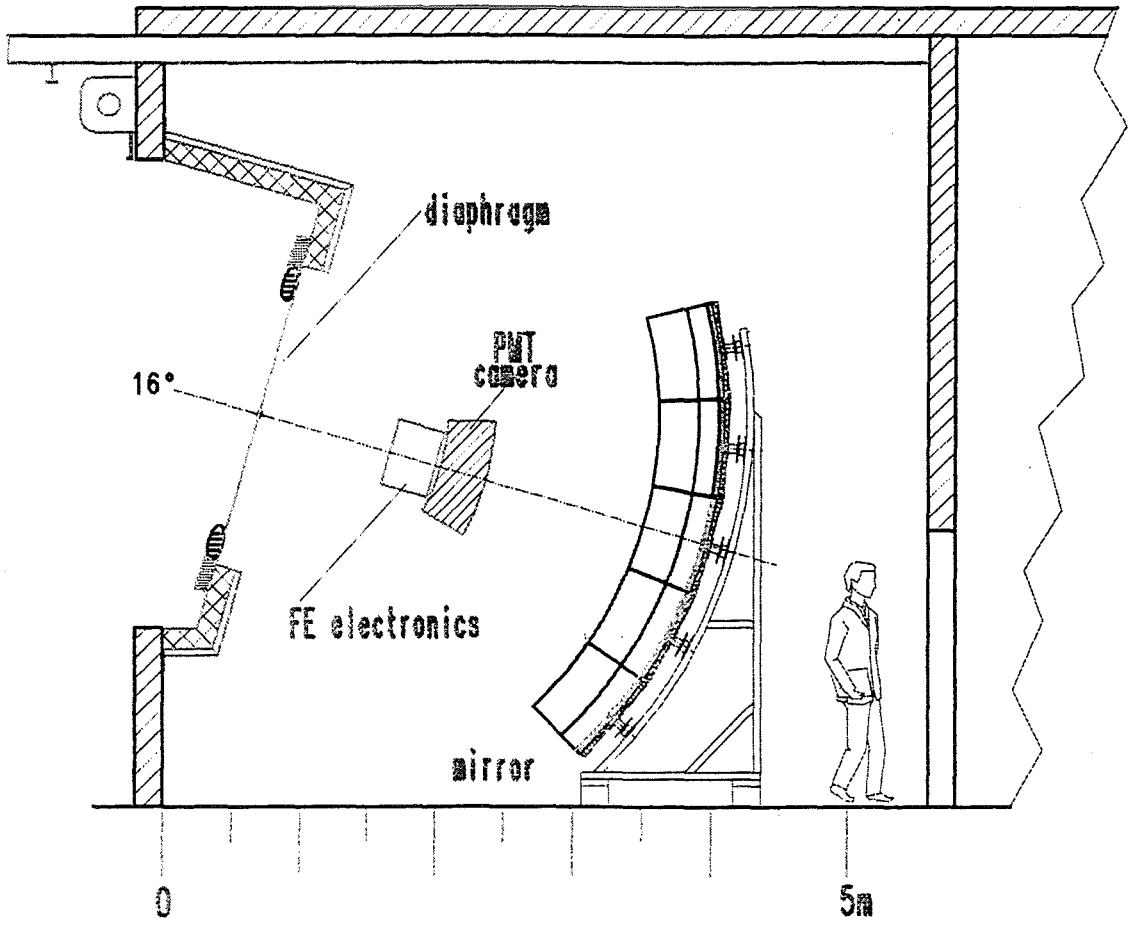

Figure 1: Diagram of Auger telescope design.

Table 1: FD Telescope Specifications

Field of view (FOV)	30° azimuth ×28.6° elevation
Diaprhagm aperture	1.7-m diameter
Mirror radius of curvature	3.4 m
Mirror size	$3.5m \times 3.5m$ (square)
Mirror segmentation (probable)	5 × 5 almost square segments
Focal surface radius of curvature	1.743 m
Coma aberration	None
Spherical aberration	0.5°
Optical filter in diaphragm	UV transmitting 320-400 nm
Camera pixellation	22 rows with 20 hexagonal pixels each
Camera size	93 cm in azimuth, 86 cm in elevation
Camera shadow	35% at center of FOV, 20% at corners
Hexagonal pixels	1.5° (45.6 mm) side-to-side
Hexagonal PMT candidates	Photonis XP3062 or Electron Tube 9974

The task of the FD is to measure air shower longitudinal development profiles. Exploiting only some timing information from the surface array, the geometry of the shower axis is accurately determined by a single eye (Sommers, 1995; Dawson et al., 1996). The place of light emission in the atmosphere is therefore known for the arriving light flux at each instant. Knowing the distance and atmospheric attenuation from that place, one can infer from the light flux the amount of emitted fluorescence light and therefore the shower size at that atmospheric depth. An accurate measurement of the light flux as a function of time is the paramount objective since it gives the longitudinal profile in this way.

The optical spot size (0.5°) will be small compared to the pixel size (1.5°), so the entire signal from a distant shower is normally captured by a single PMT at any instant. Signals (and backgrounds) need to be combined from multiple PMTs only when the spot is on the boundary between pixels. (With 100-ns FADC time slices, the duration of increased background noise can be accurately delimited.)

Uniformity of detector response over the focal surface is critical for achieving the paramount objective: a reliable measurement of light flux as a function of time. In particular, it is important that the response not depend strongly on whether the spot is near a pixel center or straddling the boundary between pixels. Highly reflective sloping walls will be positioned over the (dead) edges of PMTs to deflect the signal photons at pixel boundaries onto active cathodes.

The Schmidt optics (suggested first by the Auger group in Puebla) has some important advantages:

- Large field of view (reduced number of telescopes, fewer edge effects).
- Uniformity (no off-axis coma).
- Dust, temperature, humidity, and rodent control (using the optical filter as a window in the diaphragm).
- Relatively small shutters in front of the diaphragm suffice to close the telescope during the day-

light.

• The reduced number of telescopes makes it practical to house an entire eye within a single building.

The prototype will test the reference design and also some minor variations:

o By incorporating a Schmidt corrector plate, it may be possible to increase significantly the light collecting area (diaphragm) without degrading the spot size.

o All-aluminum mirrors and polished glass mirrors will be compared against simple slumped glass mirrors.

o Bonding small optical filters to the PMTs may have advantages over a large filter in the diaphragm.

3 Plans for the prototype

The FD prototype telescope will make hybrid measurements of air showers in conjunction with an "engineering surface array" consisting of 40 water Cherenkov tanks. The water tanks will have the 1.5-km separation of the reference design and will be arranged in a hexagonal pattern centered at a distance of 10 km from the prototype telescope. With a 10% duty factor for dark sky and good weather, the expected number of hybrid showers with this engineering array is 386 above 10^{18} eV in one year, with 9 of those showers above 10^{19} eV.

In addition, controlled tests of the FD telescope will be performed using a "laserscope" that can produce (upward-going) artificial shower tracks of arbitrary direction from arbitrary points on the ground. Light scattered from the laserscope's beamed UV pulse mimics the fluorescence emission from an air shower front. At the Argentine site's altitude, a 10^{19} eV shower at maximum size corresponds to Rayleigh scattering from a laser pulse of 210 μJ. These laser studies will test the telescope's important properties:

• Trigger efficiency. Does the telescope trigger on 210-μJ laser pulses over the part of the final surface array that it is expected to cover?

• Angular resolution. How well is the track-detector plane determined? Is the laser axis within that plane well determined using the "hybrid" timing information of the FD pixels together with the laser position and time of firing? The expected angular resolution is about 0.5°.

• Longitudinal profile resolution. Lidar instrumentation operating in conjunction with the laserscope will provide a vertical profile of light that is scattered backward. This can be corrected for the combined Rayleigh and Mie differential scattering cross section to give the longitudinal profile that should be measured by the telescope.

References

Auger Collaboration, 1997, Design Report, 2nd edition, available from Fermilab.

Baltrusaitis, R.M. et al., 1985, Nuclear Instrumentation and Methods A240, 410.

Cronin, J.W. et al., 1992, Proceedings of the workshop on a giant ground array (Paris), Nucl. Phys. (Proc. Suppl) B28.

Dawson, B.R. et al., 1997, Astroparticle Physics, vol. 5, pp. 239-247.

HiRes Collaboration, 1997, Proc. Int. Cosmic Ray Conf. (Durban), vol. 5, pp. 321-366 (OG.10.6.1 – OG.10.6.12).

Sommers, P., 1995, Astroparticle Physics, vol. 3, pp. 249-360.

OG 4.3.32

Simulation Studies on the Characterization of Cerenkov Images by Fractal and Wavelet Parameters *

A. Haungs[1]†, A.K. Razdan[2], C.L. Bhat[2], R.C. Rannot[2], and H. Rebel[1]
[1]*Forschungszentrum Karlsruhe, Institut für Kernphysik, D-76021 Karlsruhe, Germany*
[2]*Bhabha Atomic Research Centre, Nuclear Research Laboratory, Mumbai - 400 085, India*

Abstract

Based on Monte Carlo simulations using the CORSIKA code, it is shown that Cerenkov images produced by ultrahigh energy γ-rays and cosmic ray nuclei (proton, Neon and Iron) have a fractal nature. The resulting multifractal and wavelet moments as inputs to a properly-trained artificial neural network are found to provide an efficient characterization scheme of the cosmic EAS primaries.

1 Introduction:

The atmospheric Cerenkov imaging technique reflects the current state-of-art for the observation of γ-rays in the TeV region. Apart from performing γ-ray astronomy investigations, this technique may hopefully pave the way for set in imaging Cerenkov telescopes eventually in a supplementary mode of operation for independent cosmic-ray mass-composition studies in the ultra-high energy region – an important problem of its own right. Motivated by this topic, we investigate here the possibility of subjecting the Cerenkov image data to perhaps more general, albeit as-yet untried, multifractal and wavelet analyses of deriving independent parameters which can supplement the presently-in-use Hillas moments for event-characterization. The paper discusses here first results of exploratory studies, based on Cerenkov image data simulated for the Imaging Element of the 4-element TACTIC (TeV Atmospheric Cerenkov Telescope with an Imaging Camera) array, using the CORSIKA air-shower code (Heck et al. 1998).

2 TACTIC:

The TACTIC instrument consists of an array of 4 atmospheric Cerenkov elements each using a tessellated optical collector of 9.5 m^2 light collection area and a synchronized, computer-controlled alt-azimuth drive system. The central (imaging) element (IE) of this compact telescope array is located at the centroid of an equilateral triangle of 20 m-side and the 3 Vertex Elements (VE) are placed at the vertices of this triangular configuration (Bhatt et al. 1997). The IE has a fast photomultiplier tube (PMT)-based 349-pixel Imaging Camera in its focal-plane, covering a field-of-view (FoV) of $\sim 6^\circ \times 6^\circ$ truncated squarewith a pixel resolution of $\sim 0.31^\circ$ diameter. The VE's front-end instrumentation, apart from yielding a significantly lower trigger threshold energy for the VE's, provides information on the polarization state, spectral content and time-profile of the recorded ACE. Extensive Monte Carlo simulation studies are presently underway to provide specific guidelines for optimizing event characterization strategies and thereby enable this instrument to carry out VHE γ-ray astronomy and UHE cosmic-ray mass-composition investigations through the atmospheric Cerenkov detection route.

3 CORSIKA-based Cerenkov Image data-bases:

The data-bases for carrying out the present feasibility studies were generated using the CORSIKA (Version 4.5) air-shower code (Heck et al. 1998) with Cerenkov option, and the use of the high energy interaction model VENUS and the model GHEISHA for interactions at lower energies ($E_{lab} < 80$ GeV). A rectangular matrix of 60×4 detector elements, each 5 m $\times$ 5 m in dimensions, is folded into the CORSIKA simulation programme

*The work is embedded in the Indian-German bilateral agreement of scientific-technical cooperation (WTZ INI-205).
†corresponding author; e-mail: haungs@ik3.fzk.de

for this purpose, in conformity with the actual geometrical configuration of the TACTIC array and the size of its 4 light-collectors. The Cerenkov data bases of 100 showers each for γ-rays, proton and Neon and Iron nuclei have been generated. These simulated data bases are valid for the altitude (1700 m) and magnetic field values of Gurushikhar, Mt. Abu, the permanent location of the TACTIC in the Western Indian state of Rajasthan. The zenith angle Θ of the primary is fixed at 40° for gamma and 40° $\pm$ 2° for protons, Neon and Iron, larger Θ being preferred to achieve twin benefits of a higher primary threshold energy and a larger effective collection area. γ-rays of energy 50 TeV and protons, Neon and Iron nuclei of 100 TeV energy (the factor of two higher energy for nuclear-progenitors being chosen to have roughly comparable average Cerenkov photon densities in all the 4 cases) have been considered. To keep computer time and the Cerenkov photon file size within manageable limits for a given event, the Cerenkov photons are generated in the restricted wavelength region, $\lambda \sim (300 - 320)$ nm. Cerenkov photons likely to be received at a given element with λ outside the above-referred sample window are generated off-line, using the well-known Cerenkov radiation spectral law $\sim \lambda^{-2}$. Other exercises done subsequently in the off-line mode include (i) taking proper account of the λ-dependent atmospheric extinction suffered by the individual Cerenkov photons emitted in the overall wavelength interval $\lambda \sim (300 - 600)$ nm, (ii) ray-tracing Cerenkov photons, incident on each 60 cm-diameter facet of the IE mirror into the focal-plane of the light receiver, and (iii) deriving the number of photo-electrons (PE) likely to be registered by each of the 349 photomultiplier (PMT) pixels of the IE camera after accounting for the reflection coefficient of the mirror and the quantum efficiency of the PMT pixels. Each of these 256 pixels, (which also include the pixels with information on the simulated Cerenkov image) have been injected with a photomultiplier noise component $\sim$ 4 PE. The noise injected in the image follows Poissonian distribution.

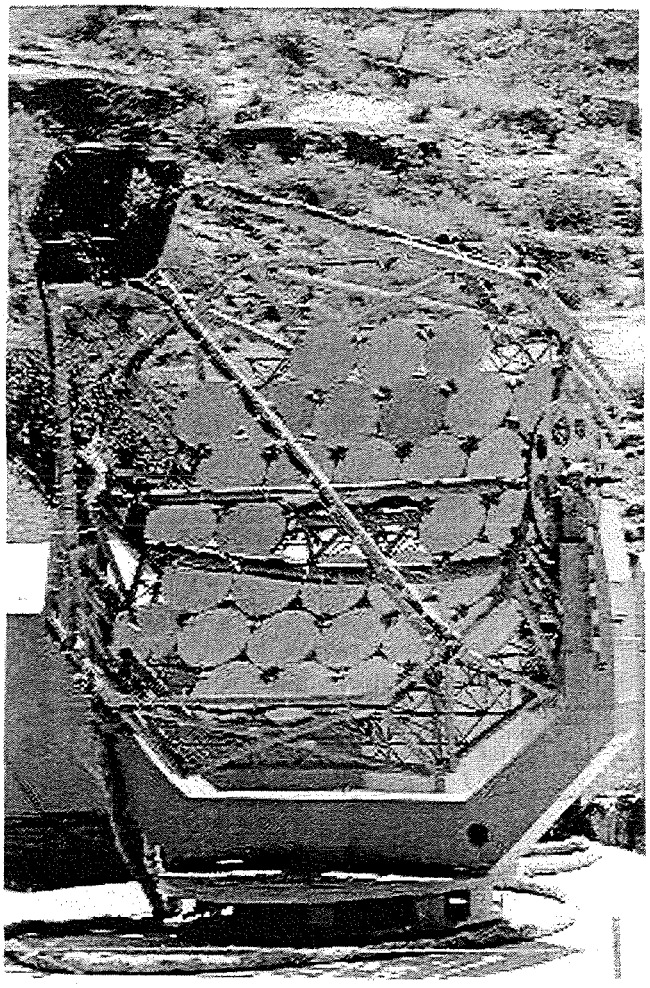

Figure 1: Photograph of the TACTIC central telescope installed at Gurushikar on Mt. Abu, Rajasthan, India (1700 m a.s.l.).

4 Imaging Parametrisation:

4.1 Multifractals: Fractals are structures which display a self similar behavior, and the fractal nature is quantitatively characterized by fractal dimensions. It is possible to calculate multifractal moments which quantify structures of multidimensional density distributions (Aharony 1990). In anticipation of the requirements of the associated analysis procedure, only the square-grid, comprising the innermost 16 x 16 pixels of the TACTIC Imaging camera, has been considered. Only images with a total number of $\geq$ 1800 PE have been used. We have calculated multifractal moments of each simulated Cerenkov image by dividing the image into M = 4, 16, 64 and 256 equally sized parts and by calculating the number of photoelectrons in each part. M is related to the fractal scale-length ν by $M = 2^{\nu}$.

The multifractal moments given by the following expression have been computed $G_q(M) = \sum_{j=1}^{M}(k_j/N)^q, N \neq 0$, where N is the total number of PE in the image, k_j is the number of PE in the j^{th} cell and q is the order of the fractal moment. If the Cerenkov image exhibits a self similar behavior the fractals moments G_q show a power law relation of the parameter of the length scale M: $G_q \propto M^{\tau_q}$ The exponent τ_q is determined from G_q by using the formula $\tau_q = \frac{1}{\ln 2}\frac{d\ln G_q}{d\nu}$. The slope has been obtained from $\nu = 1$ to $\nu = 4$. This exponent τ_q is related to the generalized multifractal dimensions, D_q by $D_q = \frac{\tau_q}{q-1}, q \neq 1$, where q is the order of the moment and varies over the range -6 $\leq$ q $\leq$ 6. For $q = 1$, D_1 is defined as equal to one. The value of $D_{q_{max}}$ characterizes the location and the size of the largest irregularity in the image structure. This means that, more regular the image, the closer is D_6 to 1. A more detailed description of this procedure is given in (Haungs et al. 1999). In Figure 2, we compare the distributions of the multifractal dimension D_6 for the four progenitor species comprising the data-base used in the present work. D_6 reflect the overall regularity of the image structure. As γ-ray images produce the most regular images amongst the four particle types considered here, D_6 have the largest peak values for γ-ray progenitors. Iron images are more regular than proton images, since, for the same total energy per nucleus, iron events have lesser energy per nucleon. This results in a smaller interaction length for iron primaries (as in the case of γ-rays) and hence more secondaries with lesser energy for particle than what is expected in the case of proton events. This leads to destroy a visible hadronic core in the image of an Iron progenitor, while it survives in the case of a proton image.

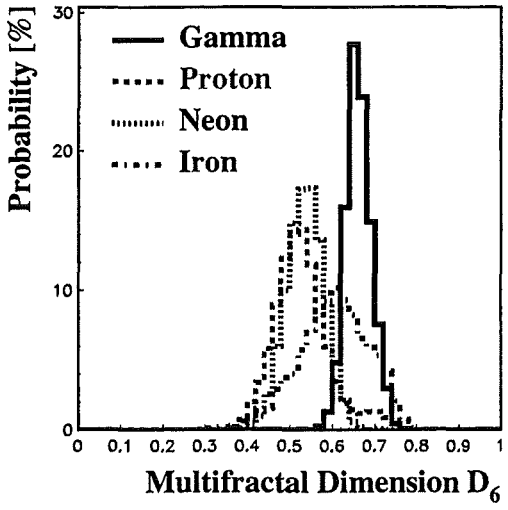

Figure 2: Distributions of the multifractal dimension D_6 for all simulated images in the range of PE from 1800 to 3000 for the different progenitor particles of the ACE.

4.2 Wavelets: A pattern analysis in terms of wavelets can be regarded as a sequence of filtering processes in order to examine the presence of local structures on different scale-lengths. In some aspects it is a generalization of a Fourier analysis, using localized functions, called wavelets instead of sine and cosine functions. When applied to the TACTIC images, the wavelet moment (Kantelhardt, Roman and Greiner 1995) W_q is used, given by: $W_q(M) = \sum_{j=1}^{M-1}(\frac{|k_{j+1}-k_j|}{N})^q$; k_j is the number of PE in the j^{th} cell in a particular scale. The wavelet moments have been obtained by dividing the Cerenkov image into $M = 4, 16, 64, 256$ equally sized parts and counting the number of photoelectrons in each part. The difference of probability in each scale gives the wavelet moment. Again a proportionality $W_q \propto M^{\beta_q}$ is given for the electron distribution in the Cerenkov images. The two wavelet dimensions which we have used for examining the structures of the Cerenkov images are the slopes β of the best-fit regression line for the double logarithmic distribution W_q vs. M for $q = 2$ and $q = 6$ obtained for each image. Figure 3 gives the distribution of the wavelet parameter β_6 for the simulated data-bases

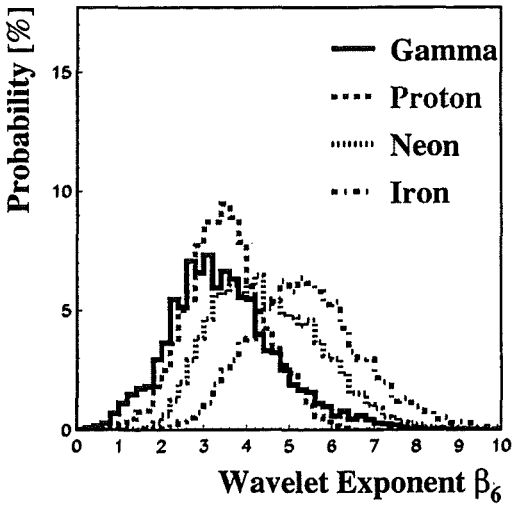

Figure 3: Distributions of the wavelet parameter β_6 for the same images as in Fig.2.

associated to the 4 progenitor species used in this work. It is well known that wavelet moments are sensitive to differences in the average numbers of photoelectrons in neighboring pixels on different length scales. With vanishing differences, i.e. regular images, the the slope of the best-fit (lnW_q vs. lnM) regression line gets flatter. As Fe and Ne events are associated with a relatively larger number of muons compared with proton (and γ-ray) events, the Cerenkov images produced by these high Z nuclei are characterized by local intensity peaks, resulting in higher values for the slope parameter in case of high Z nuclei compared with protons (and γ-rays). This feature, which may be present in the structure of a Cerenkov image, is not exploited as source of information by the use of Hillas parameters.

5 Artificial Neural Network-based Classification

We use the well known pattern recognition capabilities of an artificial neural network (ANN), in order to display the degree to which extent the event-classification potential of the fractal and wavelet parameters can be used. From a statistical modeling point of view, the ANN technique represents a non-parametric event classification scheme. Two hidden layers were used with backpropagation mode in this exercise alongwith optimized learning parameters. A sample of 12000 events was used in the training steps of the network, and the output values demanded are 0.0 for γ-rays, 0.33 for protons, 0.67 for Neon nuclei and 1.0 for Iron nuclei. The test data set comprises a total of 24000 events, belonging to γ-ray, proton, Neon and Iron species, all 4 in an equal proportion. The network was trained with two fractal (D_2 and D_6) and two wavelet (β_2 and β_6) parameter values as inputs to the net. It is clear from Figure 4 that γ-rays and hadrons are well separated, but the protons and Neon display overlapping distributions while Iron is very well separated.

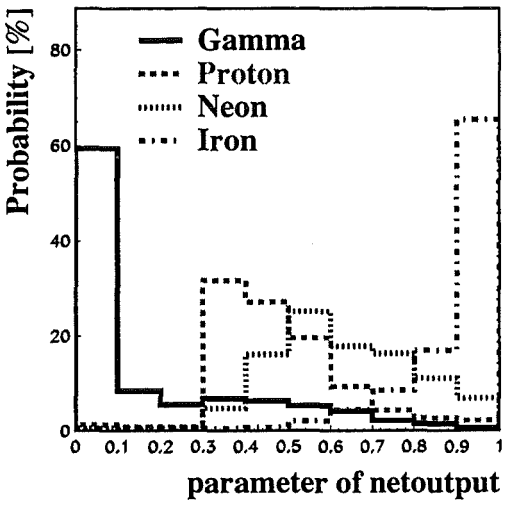

Figure 4: Distributions of the different primaries in the output parameter of a neural net analysis.

6 Conclusions

It has been shown that Cerenkov images have a fractal structure. Multifractal dimensions and wavelet moments can be used along with Hillas parameters to discriminate more efficiently amongst gamma-rays, protons, Neon and Iron progenitor species through a properly-trained artificial neural net. The multifractal and wavelet approach for analyzing Cerenkov images has been discussed for the first time in context of gamma-ray astronomy. This (preliminary) work suggests the prospects of the resulting discrimination parameters as supplementary classifiers for cosmic-ray mass-composition studies in the UHE bracket is quite promising.

References

Aharony, A. 1994, Physica A 168, 479
Bhatt, N. et al. 1999, Proc. 26th ICRC (Salt Lake City, 1999), OG 2.4.20
Haungs, A. et al. 1999, submitted to Astrop. Phys.
Heck, D. et al. 1998, FZKA-Report 6019, Forschungszentrum Karlsruhe, Germany
Kantelhardt, J.W., Roman, H.E. & Greiner, M. 1995 Physica A 220, 219

HE 1.2.23

On the Optical Density Spectrum of the PAMIR Emulsion Experiment

A. Haungs[1]*, J. Kempa[2]†, and J. Malinowski[2]†

[1]*Forschungszentrum Karlsruhe, Institut für Kernphysik, D 76021 Karlsruhe, Germany*

[2]*University of Lodz, Department of Experimental Physics, PL 90950 Lodz, Poland*

Abstract

The optical density spectrum of electromagnetic particles, measured at the high-altitude emulsion experiment PAMIR, is compared with distributions obtained by Monte Carlo simulations. The extensive air shower simulations are based on the CORSIKA program including different high energy interaction models, like QGSJET, SIBYLL and VENUS. Additionally the Monte Carlo calculations include a detailed simulation of the detector response for the electromagnetic particles based on the GEANT code. This enables to discuss in details the energy resolution and threshold efficiency of the Pamir emulsion calorimeter, as well as comparisons of the interaction models.

1 Introduction:

Direct measurements of the cosmic rays by balloon-borne or satellite experiment provide accurate knowledge of the slopes of the differential primary spectrum up to $\approx 10^{14}$ eV for different nuclei (Wiebel-Sooth, Biermann, and Meyer 1998). The Pamir emulsion experiment (4370 m a.s.l.) could measure the flux of electromagnetic particles in the energy range $4 - 100$ TeV and of hadrons ($7 - 100$ TeV) created by interactions of the primaries in the upper atmosphere. The particle flux is estimated by the optical density of the measured spots at the emulsions and the zenith angle of the particles (Bayburina et al. 1983). Detailed Monte-Carlo simulations of both the flux of the particles at high altitudes and the detector effects of the experiment should be helpful to understand the measured distributions. The task of this paper is to compare the measured density distributions of the electromagnetic particles with simulations in the low energy region, where the chemical composition of the primary cosmic rays is known. This additionally gives the possibility to test the air shower simulation program package CORSIKA (Heck et al. 1998) and the different high-energy interaction models included at the energy region around $\approx 10^{14}$ eV especially at the extreme forward direction.

2 Simulations:

For the following consideration 500000 events are generated for three different nuclei (H,He,Fe) and three interaction models (VENUS vers.4.12, QGSJET, SIBYLL vers.1.6), used as generators in the CORSIKA version 5.62 (see Heck et al. 1998). In the case of primary protons the simulations cover the energy spectrum of 10^{13} eV - 10^{16} eV with $dN/dE_0 \propto E_0^{-\gamma}$ ($\gamma_H = 2.75$) and isotropic incidence up to 40°. In the case of primary Helium (Iron) the used slope is $\gamma_{He} = 2.62$ ($\gamma_{Fe} = 2.60$) in the energy range $2 \cdot 10^{13}$ eV - 10^{16} eV (10^{14} eV - 10^{16} eV). All secondary particles with energies larger than 1 TeV at the observation level of the Pamir experiment are taken into account for the further examination. Figure 1 shows the differential energy spectra of the secondary electromagnetic particles at the Pamir level for different primaries and interaction models. The primary flux of the components are normalized to the flux of the primary protons. In general an increasing slope with increasing primary mass is seen, but the role of primary iron nuclei for the total flux of the electromagnetic particles with $E_{e/\gamma} > 1$ TeV for the Pamir observation level is negligible. The slopes of the spectra are nearly model independent, but the total number of particles is nearly a factor two larger in case of the SIBYLL model than in case of VENUS or QGSJET. In comparison with the experimentally observed slopes there is a good agreement with the simulated ones (Haungs and Kempa 1998).

*corresponding author; e-mail: haungs@ik3.fzk.de

†partly supported by the Polish State Committee for Scientific Research (KNB grant No PB 929/P3/95/07) and partly by the Rector of the Lodz University (grant 1999/505/030240)

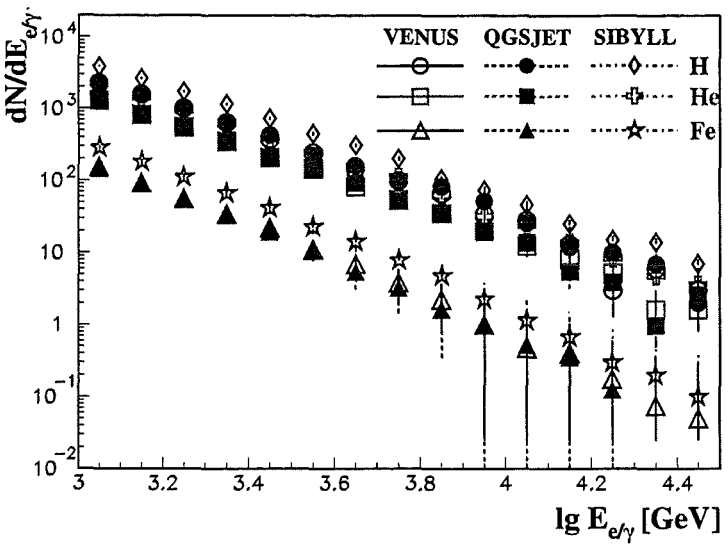

Figure 1: The energy spectra of the simulations for all electromagnetic particles for three different high-energy interaction models. The distributions for primary helium and iron are normalized to the flux of the simulated protons.

For the electromagnetic particles detector simulations are performed based on the GEANT detector simulation tool package. Gamma rays for different fixed energies in the range of 2 to 50 TeV and for four different zenith angles ($0°, 10°, 20°, 30°$) are tracked through the experimental setup. The obtained electron densities at each layer of the X-ray films in bins of $10 \times 10\ \mu m^2$ are considered for the calculation of the optical densities of the spots at the emulsions in $r < 50\,\mu m$. Fluctuations of the densities at fixed energies and fixed angle-of-incidences are taken into account with high statistical accuracy in the detector simulation (Haungs and Kempa 1997). Following the resulting density distributions for each electromagnetic particle from the EAS simulations with given energy and angle-of-incidence an optical density is calculated by interpolation. Figure 2 shows the average optical density and its variance for all particles as obtained by the CORSIKA simulations.

3 Optical Density Spectrum:

The measured optical density spectrum of single electromagnetic particles for an exposure time $ST = 11.5\,m^2yr$ is obtained from the so called working layer (12 c.u.) at the Pamir experiment. The spectrum contains a total number of 1469 electromagnetic particles (Bialobrzeska et al. 1998). Figure 3 shows this optical density distribution compared with simulated distributions, including the detector response described above, the normalization to the exposure time of the measurements, and the well known chemical composition of the primaries in this energy region (Wiebel, Biermann and Meyer 1998). The negligible part of particles coming from primary iron nuclei and the small differences in the slope for different primaries are to be noted.

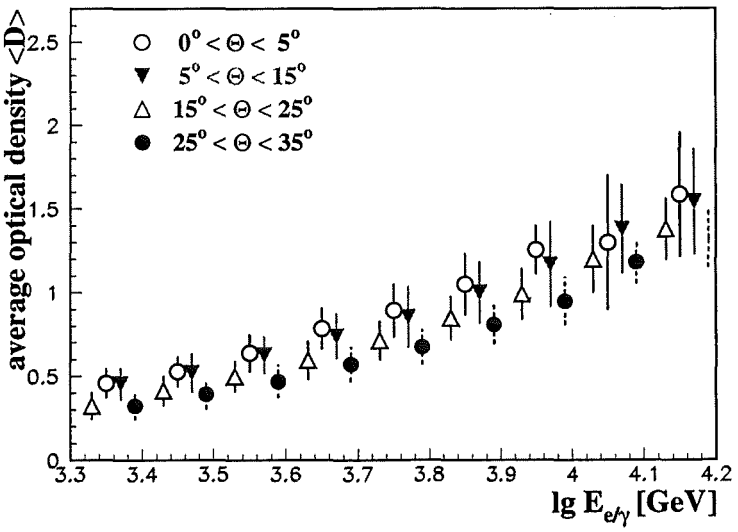

Figure 2: Dependence of the simulated optical density from the particle energy and angle-of-incidence. The error bars represent the variance of the density in each energy range.

Even if there exists a relatively large part of medium primaries (which are not simulated for these considerations), it would not change the distribution and total number of the "all simulation" distribution of the density spectrum. The relevant primary energy for this particles are between 10^{14} eV and 10^{15} eV. Differences of the two models VENUS and QGSJET are found to be negligible at the comparison of the optical density spectrum. For both models there is an excellent agreement between measurements and simulations. It exists a good agreement in the slope of the spectrum and in the total number of particles, but there are some differences at very small optical densities (low energies). In the simulated distributions particles with a "true" energy of larger than 3 TeV are taken into account, only. But following the calculations based on GEANT there are some particles with lower energy which can fluctuate to a optical density larger than 0.2 . This would lead to an enhancement of the simulated density spectrum at low values. On the other hand, there exists a "scanning" efficiency smaller than 100% for the density around the threshold at the experiment, i.e. some single particles are not scanned after the development of the emulsion films. Comparing darkness distributions for different films and years the uncertainty can be evaluated to $\approx 20 - 30\%$ at the first three data points. The SIBYLL model is unable to reproduce the data. The flux of high energetic electromagnetic particles in forward direction is too large, especially in the well simulated range of darkness $0.5 < D < 1.2$ (Figure 3 lower panel). The differences at high optical densities in all comparisons is due to the limitation of the simulations to high primary energies.

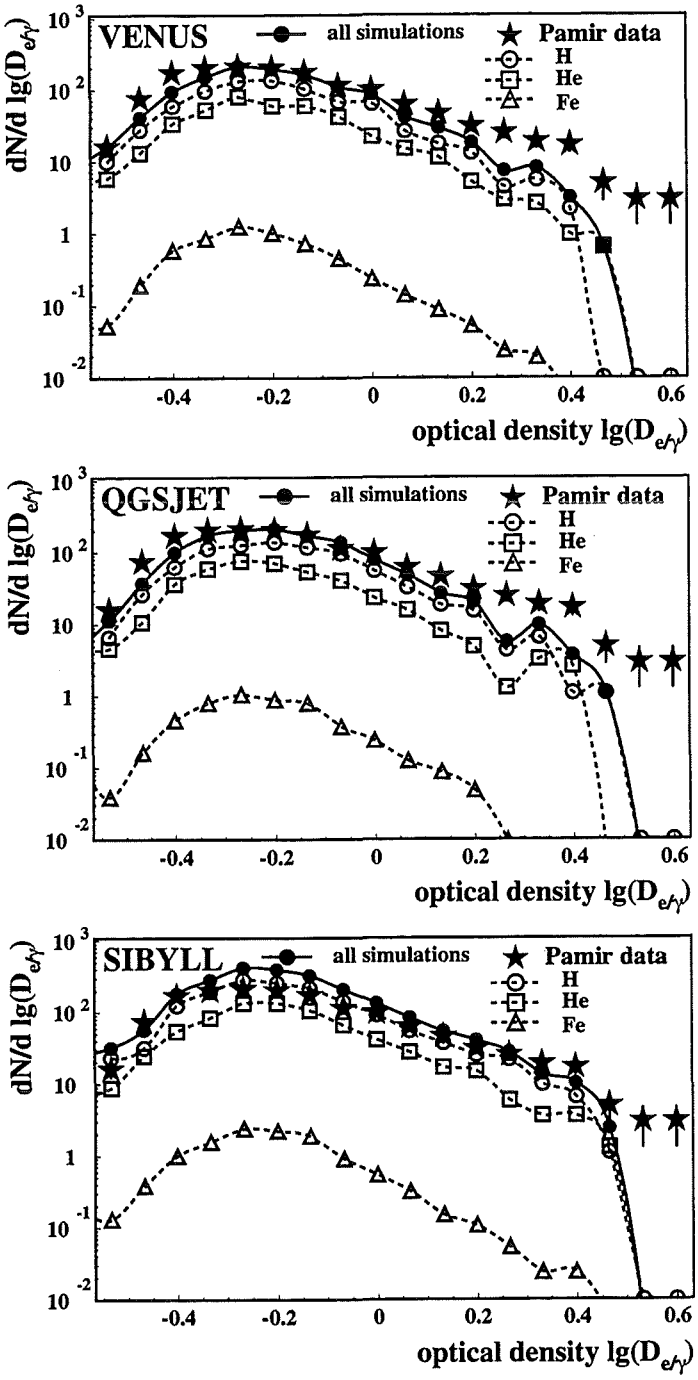

Figure 3: Measured optical density spectrum ($ST = 11.5\,\mathrm{m^2yr}$) of single particles in the working layer (12 c.u.) of the Pamir experiment ($N_{e,\gamma} = 1469$) compared with the simulated spectra of different primaries normalized to the measured exposure time for three different interaction models.

4 Energy Reconstruction:

After the simulation of the optical density the primary energy of the single particle can be reconstructed using the reconstruction procedures of the Pamir experiment. For each particle the energy is reconstructed from the optical density for the $r = 48\,\mu$m diaphragm according to the functions of Roganova and Ivanenko 1987 including the zenith angle of the particle. Figure 4 shows the quality of the energy reconstruction of this procedure for all particles with an integral optical density larger than 0.2. In spite of the high fluctuations in average the reconstruction quality is quite good and nearly independent of the species of the particle: gamma or electron. At low energies near the threshold the reconstructed energy seems to be larger than the true one. This could be due to systematic effects at the threshold of the Pamir experiment which are not included in the calibration procedure. At energies above 10 TeV a small underestimation of the energy is obvious.

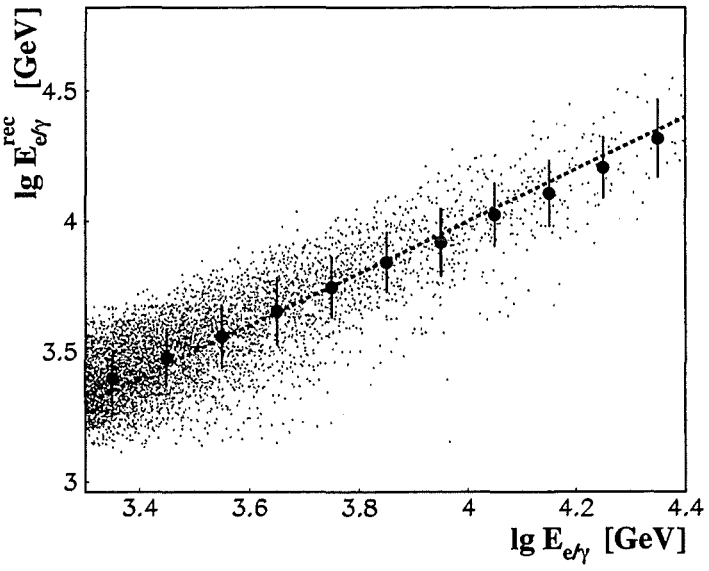

Figure 4: Comparison of the reconstructed energy with the true energy of all electromagnetic particles. Each small dot represents a single particle, the big dots are the reconstructed mean energy with its variance for each bin. For guiding the eyes, a line for $E^{rec} = E^{true}$ is printed.

5 Conclusions:

The quality of the interpretation of cosmic ray experiments at high altitudes is improved by the combination of the air shower simulation in the atmosphere (by CORSIKA with different high-energy interaction models) and the simulation of the detector response (by GEANT). Especially a proof of the energy reconstruction in the Pamir experiment is now possible. It shows a good reconstruction quality, in particular in the "medium" energy range, but with unexpectedly large fluctuations in the optical density for fixed energies. The good agreement between the measured and the simulated density spectrum shown in this study is an additional hint for a reasonable extrapolation of the interaction models to the extreme forward direction at low energies ($E \approx 10^{13} - 10^{15}$ eV), at least for the QGSJET and VENUS model, whereas the SIBYLL model (version 1.6) is unable to reproduce the data.

We wish to acknowledge useful discussions with Gerd Schatz, Heinigerd Rebel and Tom Thouw.

References

Bayburina, S.G. et al. 1983, Proc. 18th ICRC (Bangalore, 1983) Vol.5, 420
Bialobrzeska, H. et al. 1998, Proc. 10th ISVHECRI (Assergi, 1998), Nucl. Phys. B (Procl. Suppl.), in press
Haungs, A. & Kempa, J. 1997, Proc. 25th ICRC (Durban, 1997) Vol.6, 101
Haungs, A. & Kempa, J. 1998, Proc. 16th ECRS (Madrid, 1998) 497
Heck, D. et al. 1998, FZKA-Report 6019, Forschungszentrum Karlsruhe, Germany
Roganova, T. & Ivanenko, I.P. 1987, private communication
Wiebel-Sooth, B., Biermann, P.L. & Meyer, H. 1998, A&A, 330, 389

HE 2.5.29

A Simulation Study of Linsley's Approach to infer Elongation Rate and Fluctuations of the EAS Maximum Depth from Muon Arrival Time Distributions

A.F. Badea[1], H. Rebel[2†], M. Zazyan[3], I.M. Brancus[1], A. Haungs[2], and J. Oehlschläger[2]

[1]*National Institute of Physics and Nuclear Engineering, Bucharest, Romania*

[2]*Forschungszentrum Karlsruhe, Institut für Kernphysik, Karlsruhe, Germany*

[3]*Cosmic Ray Division, Yerevan Physics Institute, Yerevan, Armenia*

Abstract

An indirect approach to deduce the elongation rate D_e and the fluctuations of the atmospheric depth X_m of the EAS maximum from muon arrival time distributions has been scrutinized on basis of Monte Carlo simulations of the EAS development and of the longitudinal profile of various EAS parameters. Special attention is made to the behaviour of a scaling parameter relating the variations at the height of the shower maximum to the arrival time of muons at observation level.

1 Introduction:

The early development of extensive air showers induced by high-energy cosmic particles, is critically influenced by the basic parameters of the particle-air interaction, i.e. by the mean free path, the interaction inelasticity and the multiplicity of secondary-particle production. A shorter initial free path, high inelasticity or high multiplicity can be also associated to a primary particle with high atomic number. The early stages, difficult to be directly observed, influence the position of the atmospheric depth of the maximum EAS development. Thus experimental studies which are able to observe the EAS maximum, like the observation of the fluorescence light of the atmospheric nitrogen do provide important information on the nature of the primary and of its interaction properties.

The average depth of the maximum X_m of the EAS development depends on the energy E_0 and the mass of the primary particle, and its dependence from the energy is traditionally expressed by the so-called elongation rate D_e defined as change in the average depth of the maximum per decade of E_0:

$$D_e = dX_m/dlog_{10}E_0$$

Invoking the superposition model approximation i.e. assuming that a heavy primary (A) has the same shower elongation rate like a proton, but scaled with energies E_0/A

$$X_m = X_{init} + D_e log_{10}(E_0/A)$$

or for a mixed composition, characterized by $< log_{10}A >$

$$< X_m >= X_{init} + D_e(log_{10}E_0 - < log_{10}A >)$$

As long as D_e is only weekly dependent from the energy, X_m shows practically a linear dependence from $log_{10}E_0$, and any change in this dependence is indicative for a change either of D_e or of the composition ($< log_{10}A >$).

In 1977 (Linsley 1977, Linsley and Watson 1981) an indirect approach studying D_e has been suggested. This approach can be applied to shower parameters which do not depend explicitely on the energy of the primary

†corresponding author: e-mail: rebel@ik3.fzk.de

particle, but do depend on the depth of observation X and on the depth X_m of shower maximum. EAS quantities like arrival times and their dispersions characterizing the time structure of the muon shower disc and mapping the longitudinal EAS development, are of this type. Actually the basic idea arises from the simple fact that the muon arrival time distributions reflect largely the time-flight of the muon travelling through the atmosphere i.e. being dependent on distance (path length) of the observation level X from X_m. Hence adequately defined arrival time parameters T do implicitely depend on the primary energy E_0 and the angle-of-EAS incidence Θ.

Prompted by recent experimental investigations of these dependences by the KASCADE collaboration (Brancus 1998, Antoni 1999) we did scrutinize Linsley's approach on basis of Monte Carlo simulations of the EAS longitudinal development of the muon component. The interest in such studies arises from the question, how various influences of the muon propagation (Coulomb scattering e.g.) may obscure the information expected from the observation of muon arrival time distributions and if the basic assumptions involved are correct. From the calculated longitudinal profiles of the shower size N_e and the muon number N_μ the corresponding maxima $X_m^{(e,\mu)}$ and their fluctuations $\sigma(X_m^{(e,\mu)})$ are determined. These results are subsequently compared with the application of a procedure, essentially based on the relation between the variation of EAS time dispersion (characterised by various adequate moments T of the muon arrival time distributions like the mean or the median values e.g.) with the primary energy and the variation with the zenith angle of incidence.

2 Basic relations:

The distribution of the EAS muon arrival times, measured at a certain observation level relatively to the arrival time of the shower core reflect the pathlength distribution of the muon travel from locus of production (near the axis) to the observation locus. The basic a-priori assumption is that we can associate the mean value or median T of the time distribution to the height of the EAS maximum X_m, and that we can express $T = f(X, X_m)$. Here X is slant depth at the observation level X_v (the vertical atmospheric thickness X_v)

$$\partial T/\partial log_{10}E_0|_X = D_e \partial T/\partial X_m|_X$$

The change of T with the energy E_0 at a given $X = X_v/cos\Theta$ is proportional to the variation of T with X_m for a given energy. However, at observation level we do not observe $\partial T/\partial X_m$, which could be related, if specifying the function $f(X, X_m)$ and

$$F = -(\partial T/\partial X_m)_X/(\partial T/\partial X)_{X_m}$$

respectively. Thus

$$\partial T/\partial log_{10}E_0|_X = -F \cdot D_e \cdot 1/X_v \cdot \partial T/\partial sec\theta|_{E_0}$$

In order to derive from the energy variation of the arrival time quantities information about elongation rate, some knowledge is required about F, in addition to the variations with the depth of observation and the zenith-angle dependence, respectively.
In a similar way the fluctuations $\sigma(X_m)$ of X_m, may be related to the fluctuations $\sigma(T)$ of T

$$\sigma(T) = -\sigma(X_m) \cdot F_\sigma \cdot 1/X_v \cdot \partial T/\partial sec\theta|_{E_0}$$

with F_σ being the corresponding scaling factor for the fluctuation of F. In previous applications (Walker and Watson 1981 and Blake 1990) of this concept on basis of data measured with the Haverah Park water Cerenkov detectors simple assumptions have been made for two extreme forms of $f(X, X_m) = f(X - X_m)$ or $f(X, X_m) = f(X/X_m)$ leading to $F = 1$ or $F = X/X_m$, respectively. At a closer look these assumptions appear to be not very convincing, since the arrival times are related directly only to the travel distances of the muons rather than to the differences in the traversed grammage of the atmosphere. That fact will complicate the dependence from X and X_m. We try to scrutinize this aspect on basis of detailed EAS Monte Carlo simulations.

3 Monte Carlo simulations:

The simulations of the air shower development have been performed by use of the Monte Carlo air shower simulation program CORSIKA (Heck 1998) (vers.5.621). The actual set of simulations calculations (based on the QGSJET model) comprise the EAS development of proton and iron induced EAS for three different primary energies (10^{15} eV, $3.16 \cdot 10^{15}$ eV, 10^{16} eV) and three different angles-of-incidence ($\Theta = 15°, 25°, 35°$) with a set of 1000 simulated EAS for each case. The EAS quantities of interest are evaluated at six different observation levels, in the case of the EAS muons generally with two different energy thresholds of 0.25 and 2.0 GeV. The longitudinal profiles of the electromagnetic and the muon component develop differently.

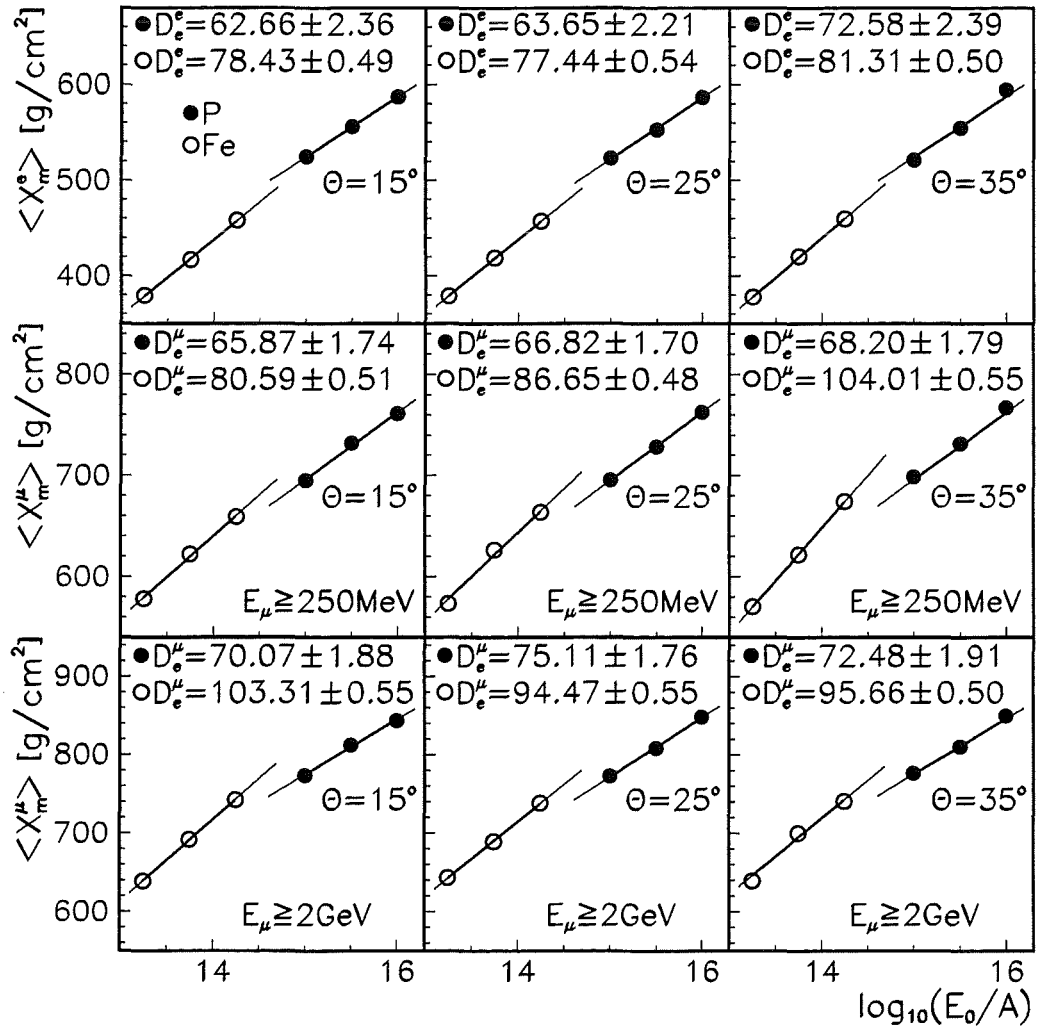

Figure 1: $D_e^{e,\mu}[g/cm^2/dec]$ for electromagnetic and muon components.

While the electromagnetic component exhibits a relatively well pronounced maximum of the shower size N_e, characterized in the Greisen parametrisation by the shower age $s = 1$, the maximum of the penetrating muon component (N_μ) appears to be shifted deeper and rather shallow, since the muon losses, after reaching a kind of plateau of N_μ, are relatively small, especially for higher energy muons. As the maximum depths are not necessarily identical, we discriminate between X_m^e and X_m^μ, D_e and D_μ, respectively. The fluctuations $\sigma(X_m)$ (standard deviation of the X_m distributions) prove to be practically energy independent, but they are different for different cases: $\delta(X_m^e)(p) \approx 80 g/cm^2$, $\delta(X_m^e)(Fe) \approx 17 g/cm^2$, $\delta(X_m^\mu)(p) \approx 100 g/cm^2$, $\delta(X_m^\mu)(Fe) \approx 30 g/cm^2$. There is a trend of slightly increasing values D_e^e (60-70 g/cm/dec for protons) with the zenith angle, which can be understood as effect of the different path lengths of the particles traversing

the same grammage layers at different zenith angles. Fig.1 illustrates the features of D_e. Though there are differencies for different primaries, globally the superposition model appears to be a good approximation.
In deriving the muon arrival time distributions from the EAS simulations we restrict our considerations to the cases of distributions of the mean ($T = \Delta\tau_{mean}$) and median ($T = \Delta\tau_{0.5}$) arrival time of EAS registrated relatively to the foremost muon in an interval of a distance from the shower core of $R_\mu = 90 - 110$ m with a detection multiplicity $n \geq 4$, for different energies E_0 and zenith angles Θ of incidence, and for different observation levels, especially for the level of the KASCADE experiment, Germany (Brancus 1998) on sea level and for the ANI installation on Mt.Aragats, Armenia (3250 m a.s.l.). The variations display a linear dependence, and $\epsilon_E = \partial T/\partial sec\theta|_{E_0}$ and $\epsilon_\theta = \partial T/\partial log_{10}E_0|_{sec\theta}$ can be determined.

4 The scaling factor F deduced from arrival time parameters:

Using the coefficients ϵ_E and ϵ_Θ characterising the variation of the mean or median distributions with the energy and the angle of EAS incidence and adopting the value of the elongation rate, as predidicted by the simulations, we infer for different observation levels and different primaries the values of the scaling parameter F, whose knowledge would be in turn a prerequisite to evaluate experimental data in terms of the elongation rate and fluctutions of the height of EAS maximum.
The results display a rather complex dependence of F from X, X_m, from the type of the primary (p or Fe: $F_{fe} > F_p$) and from the energy threshold of the detected muons, varying between ($\approx 0.9 - 2.0$). Within all uncertainties and fluctuations of the results, eventually arising from the fact that the longitudinal development $T = f(X, X_m)$ can be never fairly expressed by a single form f for each observation level X_v, there may be a tendency with

$$F(X_v^1)/F(X_v^2) \propto X_v^1/X_v^2 \cdot sec\theta \quad \text{and} \quad F(Fe)/F(p) \propto X_m(p)/X_m(Fe).$$

5 Summary:

The relation between the arrival time observables and the changes of the longitudinal EAS profiles implies a scaling factor F, which depends from the height of the shower maximum, the observation level and zenith angle of EAS incidence. On basis of Monte Carlo simulations of the EAS development the ingredients for a determination of F have been deduced, and the variation of F has been studied for a number of cases. In the present status of our understanding we have to conclude that the scaling factor has a rather complex behaviour.It is affected by the EAS fluctuations and, though there are some trends, the dependences of average values are not yet established. In conclusion, unfortunately the Linsley approach does not provide a way to relate muon arrival time observations directly to the elongation rate and fluctuations of X_m without invoking detailed Monte Carlo simulations.

We thank for the encouraging discussions with our colleagues of the KASCADE collaboration, in particular with A. A. Chilingarian, D. Heck , R. Haeusler and G. Schatz. Some clarifying remarks of M. Nagano and K. Honda are particularly acknowledged.

References

Antoni T. et al. (KASCADE collaboration) 1999, Astrop. Phys. (to be published)
Blake P.R. et al. 1990, Journ.Phys.G: Nucl.Phys. 16, 775
Brancus, I.M. et al. (KASCADE collaboration) 1998, FZKA Report 6151, Forschungszentrum Karlsruhe
Heck, D. et al. 1998, FZKA Report 6019, Forschungszentrum Karlsruhe
Linsley, J. 1977, Proc 15th ICRC (Plodiv, 1977), Vol.12, 89
Linsley, J. and Watson, A.A. 1981, Phys. Rev. Lett. 46, 459
Walker, R. and Watson A.A. 1981, Journ.Phys.G: Nucl.Phys. 7, 1297

HE 3.1.16

WILLI, a Detector for Measuring the Charge Ratio of Cosmic Muons

I.M. Brancus[1], B. Vulpescu[1†], J. Wentz[2], H. Rebel[2], A.F. Badea[1], H. Bozdog[1], M. Duma[1], A. Haungs[2], H.J. Mathes[2], M. Petcu[1], M. Roth[2]

[1] *National Institute of Physics and Nuclear Engineering, Bucharest, Romania*

[2] *Forschungszentrum Karlsruhe, Institut für Kernphysik, Karlsruhe, Germany*

Abstract

The WILLI (Weakly Ionising Lepton Lead Interactions) detector is a small compact device for performing measurements of the charge ratio of cosmic muons by detecting the life time of the muonic atoms. This method gives precise results on the charge ratio in the energy range relevant for the atmospheric neutrino anomaly, avoiding usual difficulties of measurements with magnetic spectrometers. The results can be used to check and to improve interaction models for calculating neutrino fluxes. The technique of the instrument, its performance and the results on the charge ratio measurements are presented.

1 The relevance of the charge ratio of atmospheric muons for hadronic interaction models and the atmospheric neutrino anomaly:

With the propagation of cosmic rays (CR) in the atmosphere, pions and kaons are produced by the interactions with air nuclei. Muons and neutrinos are resulting from their decay:

$$\begin{aligned} A_{CR} + A_{Air} \rightarrow \quad & \pi^{\pm},\ K^{\pm},\ K^{0} \ldots \\ \pi^{+} \rightarrow \quad & \mu^{+} + \nu_{\mu} \rightarrow e^{+} + \nu_{e} + \overline{\nu}_{\mu} \\ \pi^{-} \rightarrow \quad & \mu^{-} + \overline{\nu}_{\mu} \rightarrow e^{-} + \overline{\nu}_{e} + \nu_{\mu} \end{aligned} \tag{1}$$

(and with a similar decay chain for the charged kaons). The ratio of the numbers of positive to negative muons, called muon charge ratio, provides important information on the interactions of the primary cosmic particles with the atmosphere nuclei, since it reveals detailed features of the multiplicity distributions and production cross sections of the parent particles and is a sensitive test quantity of hadronic interaction models. Hence at low energies (GeV range) studies of the muon charge ratio are related to predictions of the atmospheric neutrino fluxes and with the so-called atmospheric neutrino anomaly (Wentz 1999). This anomaly is the observation that the measured ratio of the neutrino fluxes $F(\nu_{\mu} + \overline{\nu}_{\mu})/F(\nu_{e} + \overline{\nu}_{e})$ appears to be significantly lower than the expected value ≈ 2 (Gaisser and Stanev 1988, Honda 1995). The experimental deficit of muonic neutrinos (KAMIOKANDE: Fukuda 1998) has been interpreted to be due to flavour oscillations of $\nu_{\mu} \rightarrow \nu_{\tau}$. As the muon charge ratio, observed in the range 0.1 – 2 GeV, directly reflects the ratio of the numbers of electronic neutrinos and

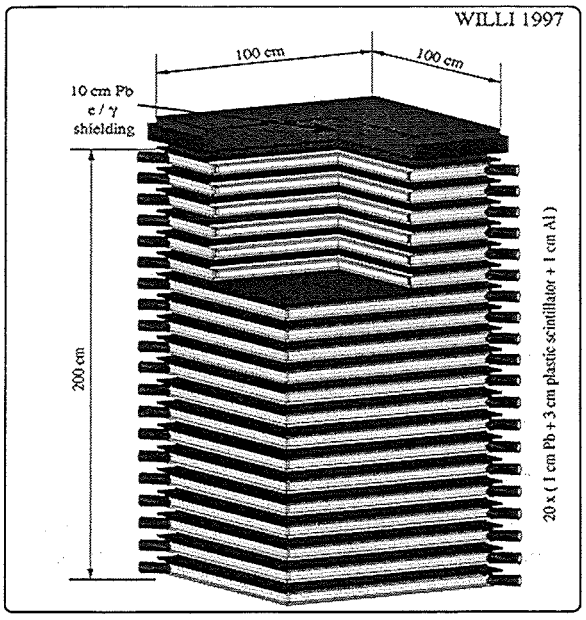

Figure 1: The sampling calorimeter configuration of the WILLI detector.

†corresponding author; e-mail: bogdan@muon1.nipne.ro

antineutrinos: $\nu_e/\overline{\nu}_e \approx \mu^+/\mu^-$ (Honda 1995), and since neutrinos and antineutrinos do interact with matter in a different way, the charge ratio is also an important information for evaluating neutrino detector responses. The observed muon charge ratio originates from the interaction of primary particles mainly of the GeV range. Consequently the propagation of the primaries and of the secondaries is noticeably influenced by the Earth's magnetic field and eventually by solar modulations. Thus additionally to the particle physics aspects there are further perspectives of muon charge ratio studies which establish a general interest in this observable of our environment.

2 Observation of the decay electrons for measuring the muon charge ratio with the WILLI detector:

Many experiments for the muon charge ratio have used magnetic spectrographs. Instrumental effects of different acceptance, scattering and detection efficiency for particles of different charges need careful consideration and are sources of uncertainties. This paper reports measurements of the muon charge ratio at low energies, avoiding the difficulties of a magnetic spectrometer with a relatively compact, small, flexible and mobile apparatus based on the observation of the decay electrons by delayed coincidence.

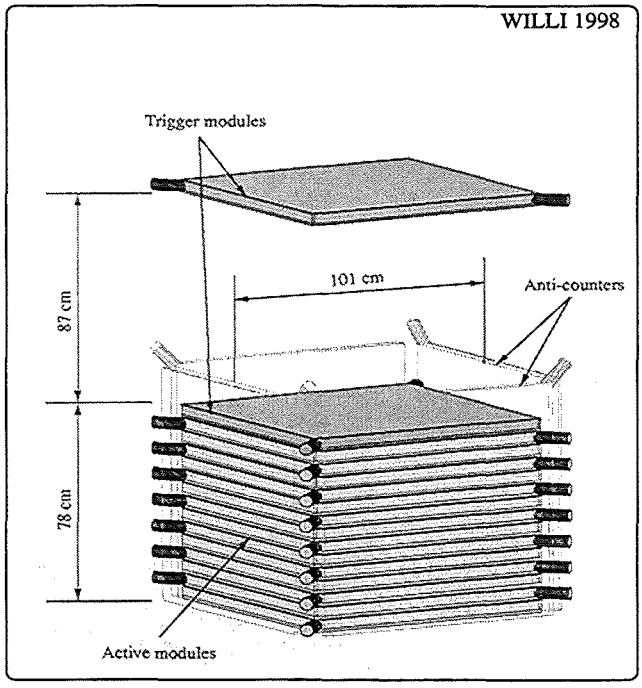

Figure 2: The modified configuration of the WILLI detector.

This instrument, a small sampling calorimeter (90 x 90 cm^2 area), has been built up in NIPNE Bucharest, (44°26′ N latitude, 26°04′ E longitude and sea level) for some prototype studies of cosmic muon interactions with the matter (Vulpescu 98) in context with the air shower experiment KASCADE. In the first stage of realisation (Fig. 1), the detector consisted of 20 layers of lead (1 cm thickness), separated by 20 active layers of NE114 scintillators (3 cm thickness) placed in between aluminum layers (1.2 cm thickness), being used for both exploratory studies of muon energy spectroscopy (Brancus 1998) and for muon charge ratio measurements (Vulpescu 1998). In a subsequent configuration (Fig. 2) the detector has been optimized for muon charge ratio measurements, by removing the Pb layers and improving the geometrical set-up and background rejection by use of anticounters (Vulpescu 1999).

The principle of the measurement is based on the different behaviour of positive and negative muons in matter. Stopped positive muons decay by the lifetime of free muons. Negative muons are captured in atomic orbits, where they may decay or are absorbed by the atomic nucleus. This leads to a reduced life time of stopped negative muons, depending on the stopping material. The total decay curve of all muon decays in the detector is a superposition of several decay laws:

$$dN/dt = [N_0/(R+1)][R\, c_0\, 1/\tau_0\, \exp(-t/\tau_0) + \sum c_j\, 1/\tau_j\, \exp(-t/\tau_j)], \qquad (2)$$

where $j = 1, 2, 3$, indicates the different absorber materials, $R(\mu^+/\mu^-) = N^+/N^-$, represents the muon charge ratio, N^+, N^- being the number of positive and negative muons, respectively and $N_0 = N^+ + N^-$.

3 The measurements of the muon charge ratio with WILLI detector:

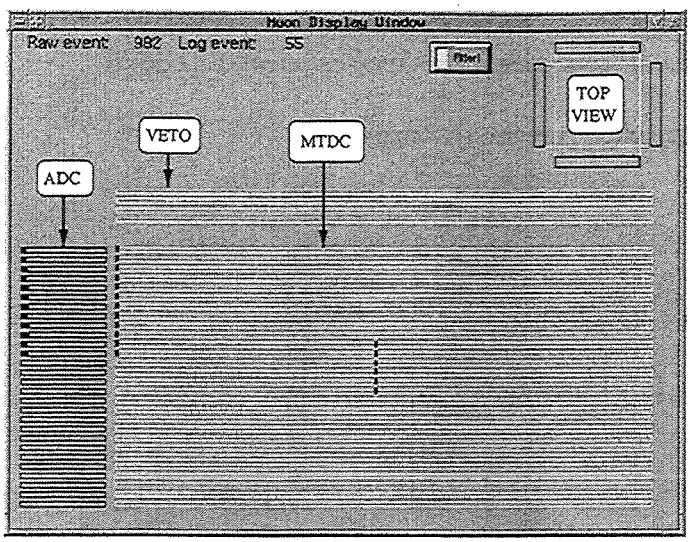

Figure 3: The offline display of a single event.

The light of the scintillators is collected by two photomultipliers via wavelength shifters. The mean energy loss of the minimal ionising muons (vertical incidence) of 6 MeV is used for the energy calibration of the detector (Vulpescu 1998). The energy signals taken from the anode and the third dynode are conducted to an ADC. A timing signal, given by the first dynode is analysed by a Multiple Time Digital Converter. A first trigger from the first layers starts the time measurement when the muon enters and the delayed signal from the decay electron is recorded in the remaining layers.

The signature of a stopped and decaying muon is a particle triggering the telescope, but not penetrating till the bottom of the detector, together with the appearance of a delayed particle, produced in the surrounding where the muon stopped (Fig. 3). With registrating the time interval of the incoming and decaying particle, the spectrum of the decay times is measured. The background of the decay curve is in the order of less than a per mille of the used signal.

The measured time spectrum is a superposition of four decay curves, the parameters c_0, c_i $(i = 1, 2, 3)$ which take into account the stopping power of the materials, the decay probability of muons bound in muonic atoms, detection efficiencies, detector geometry, laboratory walls, thresholds and angular acceptance, have been determined by extensive detector simulations using the GEANT code (Fig. 4). The dependence of the decay time on the absorber material is obvious. Aluminium reduces significantly the effective mean life time of negative muons as compared to that of the free decay of positive muons. Though the effective life time get even shorter for higher Z materials, the absorption is correspondingly larger and implies low rates of decay electrons. The decay probability for Al is 39.05% while for Pb only 2.75%. Hence aluminum proves to be the optimum choice under all practical aspects. Fig. 5 displays a compilation of world- wide measured results at different energies. The average value

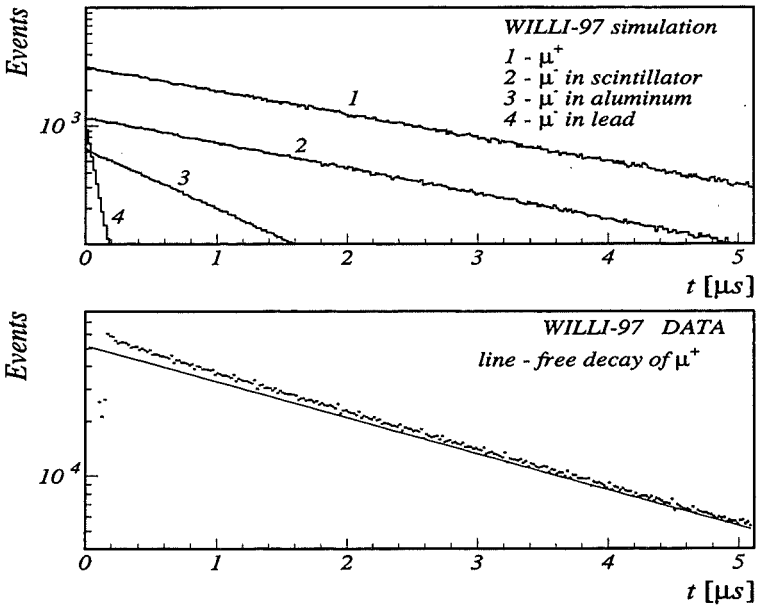

Figure 4: Monte Carlo simulation results of the contributions of different materials to the total decay curve, and the experimental decay curve compared with the decay curve expected for positive muons ($\tau = 2.2\mu$s).

of about 1.20 at energies < 20 GeV slightly increases with the energy. Our results:

WILLI 1997 experiment: $R(\mu^+/\mu^-) = 1.30 \pm 0.05$ for a mean muon momentum of 0.86 GeV/c
WILLI 1998 experiment: $R(\mu^+/\mu^-) = 1.27 \pm 0.01$ for a mean muon momentum of 0.53 GeV/c

concern the low energy part relevant for the atmospheric neutrino anomaly.

4 Concluding remarks:

The present study demonstrates a simple and efficient procedure to measure muon charge ratio with a small and compact detector, reaching accuracies in the order of few percent and excluding systematic errors of magnetic spectrometers. The reported results are obtained with two different geometrical configurations permitting two different muon energy ranges. It has been shown (Tsuji 1998) that the variation of muon fluxes, known as the east-west effect of the geomagnetic field, is more important for the low-momentum region and for larger zenith angle. In the future our device will be modified into a rotatable configuration for the observation of muons with different angles of incidence in zenithal and azimuthal plane.

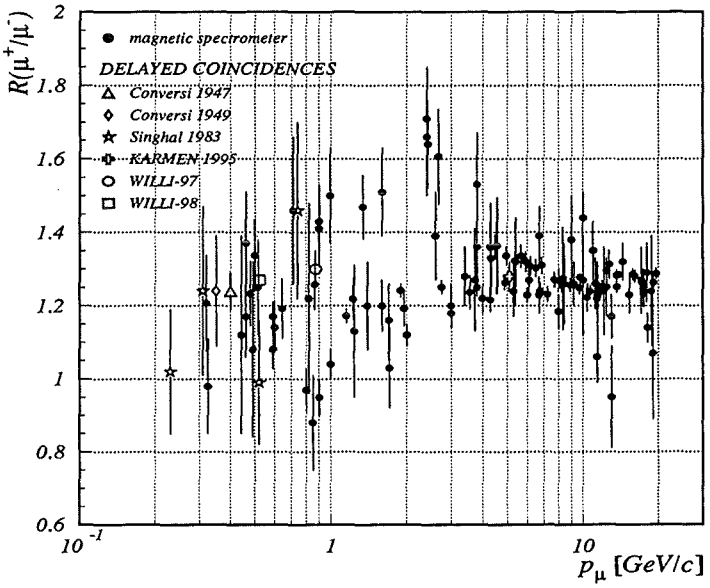

Figure 5: The present experimental knowledge on muon charge ratio.

Acknowledgements

The set up of the calorimeter in NIPNE Bucharest was realized with the support of Romanian Ministry for Research and Technology, the International Bureau Bonn and the Forschungszentrum Karlsruhe, Germany. We thank Prof. Dr. D. Müller for useful discussions.

References

Brancus, I.M. et al., 1998, Roum. Journ. Phys. vol. 43 no. 7-8
Fukuda, Y. et al., Phys. Lett. 1998, B436, 33; Phys. Rev. Lett. 81, 1562
Gaisser, T.K. & Stanev, T., 1998, Phys. Rev. D38, 85
Honda, M. et al., 1995, Phys. Rev. D52, 4985
Tsuji, S. et al., 1998, J. Phys. G: Nucl. Part. Phys. 24, 1805
Vulpescu, B. et al., 1998, Nucl. Instr. Meth. in Phys. Res. A414, 205
Vulpescu, B., 1999, PhD thesis
Wentz, J. et al., 1999, Proc. 23rd ICRC (Salt Lake City) HE 3.2.07

HE 3.2.07

Simulation of the flux of muons at energies relevant for the atmospheric neutrino anomaly

J. Wentz[1†], B. Vulpescu[2], D. Heck[1], and H.J. Mathes[1]

[1]*Forschungszentrum Karlsruhe, Institut für Kernphysik, D-76021 Karlsruhe, Germany*

[2]*National Institute of Physics and Nuclear Engineering, RO-7690 Bucharest, Romania*

Abstract

The feasibility of calculating fluxes and the charge ratio of muons relevant for the atmospheric neutrino anomaly with CORSIKA is investigated. It is shown that the differential fluxes and directional intensities are in good agreement with experimental data. But the hadronic interaction model GHEISHA used for $E_{lab} <$ 80 GeV/u fails to calculate the charge ratio of muons. The ratio between produced positive and negative pions and muons, respectively, is compared for different high energy hadronic interaction models.

1 Introduction:

Atmospheric neutrinos are produced in the interaction of the primary cosmic rays, consisting of protons and nuclei up to iron, with the Earth's atmosphere. Thereby pions, kaons, baryons and nuclear fragments are produced. Mainly the decay of the charged pions:

$$\begin{aligned} \pi^+ &\rightarrow \mu^+ + \nu_\mu \\ \pi^- &\rightarrow \mu^- + \overline{\nu_\mu} \end{aligned} \tag{1}$$

and the subsequent decay of the muons:

$$\begin{aligned} \mu^+ &\rightarrow e^+ + \nu_e + \overline{\nu_\mu} \\ \mu^- &\rightarrow e^- + \overline{\nu_e} + \nu_\mu \end{aligned} \tag{2}$$

are the sources of atmospheric neutrinos. At higher energies where the production of kaons becomes important, also the decay of K^+ and K^- contributes to the neutrino flux. A rough adding of the flavours involved in eqs 1 and 2 lead to the ratio:

$$R_\nu = \frac{\nu_\mu + \overline{\nu_\mu}}{\nu_e + \overline{\nu_e}} = 2 \tag{3}$$

This relation fails at high energies when a larger number of muons reach sea-level without decaying. The ratio of muon to electron neutrinos is measured by the Super-Kamiokande experiment, with the result that the expected ratio is considerable less than the theoretical expectation (Fukuda 1998a, Fukuda 1998b). Moreover, data for neutrinos from above show agreement, while the disagreement increases with the angle of the neutrinos, reaching its maximum for neutrinos which passed the whole Earth. This seems to be a clear evidence for neutrino oscillations, i.e. a non-zero rest mass of the neutrinos.

The interpretation of the experiment is based on Monte Carlo simulations of the neutrino fluxes. Various simulations have been made with quite different codes using such different approaches like diffusion equations for the transport of the particles, or complete Monte Carlo simulation of air shower development in atmosphere. The results of all calculations agree more or less in the ratio of ν_e/ν_μ, but there are considerable differences in the ratio of $\nu_e/\overline{\nu_e}$ and the absolute fluxes of all neutrino flavours. These differences play an important role in the interpretation of the oscillation feature. Even the strongly disfavoured oscillation $\nu_\mu \rightarrow \nu_e$ cannot be ruled out, due to large uncertainties in calculation of the absolute ν_e-fluxes.

A second difficulty arises from the flavour dependent cross-sections in the detection. For energies for which most of the Super-Kamiokande data exist, the cross-section for interactions of neutrinos is about 3 times higher than for antineutrinos. Therefore the theories must give a precise calculation for the fluxes of neutrinos and antineutrinos, in order to correct the experimental results.

[†]corresponding author; e-mail: wentz@ik3.fzk.de

In case of the muon neutrinos the different theories agree in a ratio of 1, what is understandable from eqs 1 and 2, where ν_μ and $\overline{\nu_\mu}$ are produced symmetrically in the production and the decay of muons. A small distortion originates from different energies of π^+ and π^- produced by p+n and p+p collisions, leading to a different number of decaying muons.

In case of the electron neutrino the situation is more difficult. The primary radiation as well as the atmosphere consist only of matter, i.e. of positive or neutral charged hadrons. The number of π^+ is considerable higher than the number of π^- produced. As can be seen in eq. 2 the ratio $\nu_e/\overline{\nu}_e$ is reflected in the ratio of μ^+/μ^-, which is known to be about 1.3 for $p_\mu > 2$ GeV. At lower energies the situation is less clear and the simulations show large differences. New experiments like WILLI (Vulpescu 1998) will give precise results for the muon charge ratio for $p_\mu < 1$ GeV, in the region interesting for Super-Kamiokande. The intention of this work is to study various hadronic interaction models in view of their feasibility of calculating the fluxes and the charge ratio of muons, as base of future calculations for atmospheric neutrino fluxes.

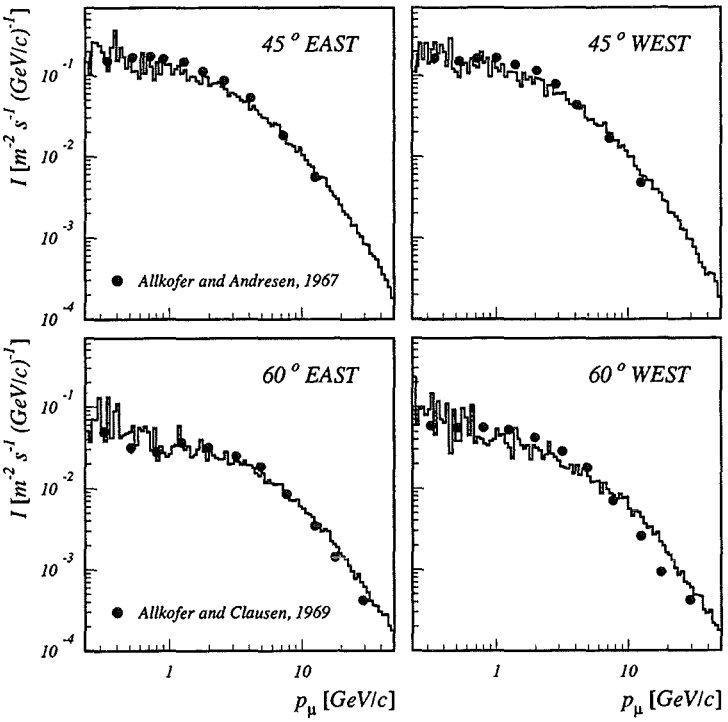

Figure 1: CORSIKA simulation of differential momentum spectra for muons from different direction at sea level compared with measurements (Allkofer 1967, Allkofer 1969). The absolute values result from integration over a solid angle of 10°.

2 Simulation of Muons on Sea-Level with CORSIKA:

CORSIKA is a complex Monte Carlo code, developed originally for the simulation of extended air showers (Heck 1998). It contains different interaction models for the simulation of hadron-hadron collisions for $E_{lab} > 80$ GeV/u. Below, all reactions are simulated by GHEISHA (Fesefeldt 1985) as implemented in GEANT 3 (CERN 1993). CORSIKA handles the tracking in the Earth's magnetic field and the decay of all unstable particles.

Fig. 1 shows the results of CORSIKA simulations for differential momenta of muons from various directions at sea-level. As can be noticed, the simulations are in good agreement with the majority of measurements. This result has only partial value, because a too low pion/muon production could be compensated by a higher primary flux. Only the comparison of measurements in different depths of the atmosphere may overcome this difficulty.

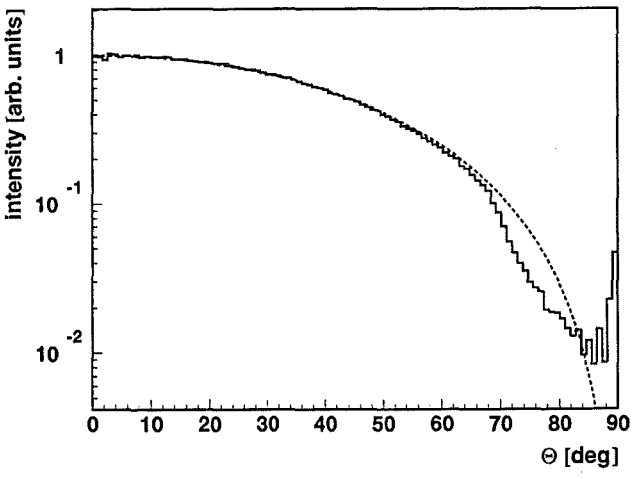

Figure 2: Directional intensity of muons simulated with CORSIKA (plane atmosphere model) compared with a $cos^{2.02}(\theta)$-distribution (dashed line) (Wentz 1995).

Fig. 2 shows the behaviour on the zenith angle. It can be noticed that actual CORSIKA with its plane atmosphere model can be used up to 70° zenith angle. For calculations in more horizontal direction the effect of the curvature of the Earth becomes important. A "curved" version of CORSIKA, which approximates the curvature step by step with a rotated local plane atmosphere is in work and will allow calculations up to the horizontal direction (Heck 1999).

The simulation of the important charge ratio of muons turns out to be more complicated. Tests with GHEISHA at fixed energy show, that there are serious problems in charge conservation. Fig. 3 displays the charge and nucleon number of the remaining nucleus, in E_{lab} = 80 GeV p + ^{14}N reactions. Because GHEISHA does not give the remnant of the target nucleus directly, the values are calculated by charge and baryon number conservation. It can be seen that these conservation laws are not fulfilled by GHEISHA; even if the main number of reactions leads to a possible number of protons and neutrons, the existence of negative charges and baryon numbers for the target rest shows that GHEISHA involves no physical model for the charge exchange from the target to the ejectiles. This results from the simple parametrisations used for the particle generation in the final channel, giving only global conservation of charge, but no conservation in the single reaction.

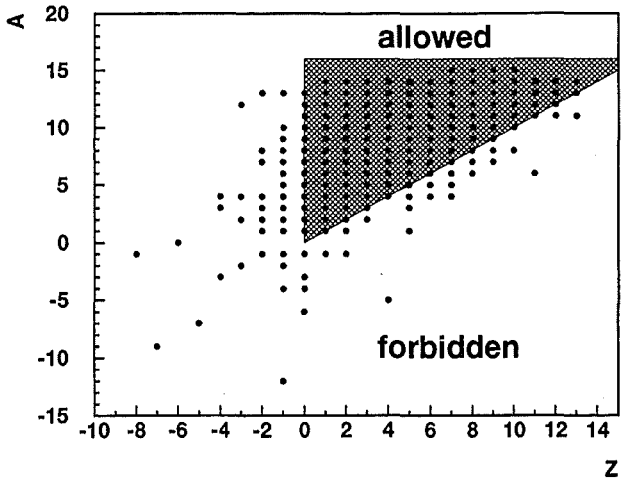

Figure 3: Distribution of the nucleon number A over the charge Z of the remaining nucleus in E_{lab} = 80 GeV p + ^{14}N reactions calculated with GHEISHA, considering charge and nucleon number conservation. The hatched area shows the allowed region between the extremes of a "nucleus" consisting only of protons and a "nucleus" consisting only of neutrons.

3 Simulation of the Charge Ratio at High Energies:

For hadronic interactions with E_{lab} > 80 GeV/u, there are different reaction models implemented in CORSIKA. Fig. 4 shows the ratio of π^+ to π^- vs. momentum of the ejectiles. The results of QGSJET (Kalmykov and Ostapchenko 1993), SIBYLL (Vers. 1.6) (Fletcher 1994) and VENUS (Vers. 4.12) (Werner 1993) are compared. All the three models agree in the general tendency, that the π^+ to π^--ratio increases with the energy. This behaviour is understandable because for the highest energy pions the multiplicity in production is very low and therefore the charge excess highest. At low energies, i.e. in high multiplicity reactions there is an equilibrium of charges and the ratio approaches 1.

But there are also considerable differences between the models. QGSJET shows the lowest excess of positive charge at all pion energies. While VENUS shows a continuous increase towards higher energies, the charge ratio of pions from the SIBYLL is smallest at lowest energies, but supersedes all models at highest pion energies.

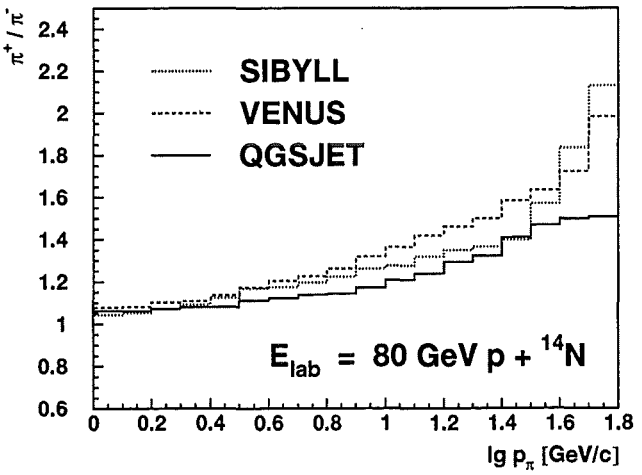

Figure 4: Differential spectra of the charge ratio of pions produced by different high energy hadronic interaction models.

Fig. 5 shows how the difference in the pion production between the models affects the charge ratio of muons on ground-level. The simulations for all three models are based on a primary $E^{-2.7}$-spectrum between 80 - 10^6 GeV. It can be noticed that the SIBYLL-model results in the highest charge ratio of muons, where the QGSJET-model give the lowest. This means, that especially the high charge excess at high ejectile energies propagates in air shower development. The intermediate and constant results of the VENUS model seems to agree best with experimental results.

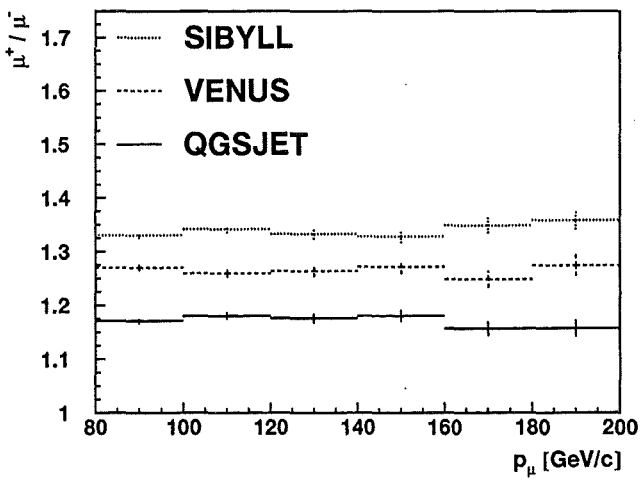

Figure 5: Differential spectra of the charge ratio of vertical muons at sea-level, simulated by CORSIKA with different high energy hadronic interaction models.

4 Conclusions:

The feasibility of calculating the fluxes of atmospheric muons with the air shower simulation program CORSIKA is investigated. The results show that CORSIKA is able to reproduce the differential fluxes and directional intensities very well. But the included hadronic interaction model GHEISHA, responsible for all interactions with $E_{lab} < 80$ GeV/u, producing most of the muons relevant for the atmospheric neutrino anomaly, is not conserving charge in individual reactions. Further it is not based on a fundamental model for describing the flux of charge from the target to the fast moving ejectiles. The code GHEISHA has to be improved or replaced by more sophisticated approaches. The high energy model VENUS seems to be the best choice for reactions with $E_{lab} > 80$ GeV/u. In conclusion it can be stated, that the simulation of atmospheric neutrino fluxes is possible with CORSIKA.

5 Acknowledgement:

One of the authors (J.W.) is grateful to the Deutsche Forschungsgemeinschaft for enabling this work by the grant WE 2426/1-1. The work was partially supported by the grant FZK I/72-709 from the Volkswagen-Stiftung. The authors would like to thank I.M. Brancus and H. Rebel for the guidance and fruitful discussions.

References

Allkofer, O.C. and Andresen, R.D., 1967, Nouvo Cimento 51, 329
Allkofer, O.C. and Clausen K., 1969, Proc. 11^{th} ICRC (Budapest) 44, 689
CERN, 1993, CERN Program Library Long Writeups W5013
Fesefeldt, H., 1985, PITHA-Report 85/02, Physikalisches Institut der Technischen Hochschule Aachen
Fletcher, R.S. et al., 1994, Phys. Rev. D50, 5710
Fukuda, Y. et al., 1998, Phys. Lett. B436, 33
Fukuda, Y. et al., 1998, Phys. Rev. Lett. 81, 1562
Heck, D. et al., 1998, FZKA-Report 6019, Forschungszentrum Karlsruhe
Heck, D. et al., 1999, Proc. 26^{th} ICRC (Salt Lake City) HE 2.5.28
Kalmykov, N.N. and Ostapchenko, S.S., 1993, Yad. Fiz. 56, 105
Vulpescu, B. et al., 1998, Nucl. Inst. Meth. A414, 205
Wentz, J., 1995, FZKA-Report 5500, Forschungszentrum Karlsruhe
Werner, K., 1993, Phys. Rep. 232, 87

HE 6.1.11

Concept and layout of the EAS muon arrival time distribution measurements on Mt. Aragats Observatory

H.-J. Mathes[1†], A.F. Badea[2],H. Bozdog[2], A.V. Daryan[3], I.M. Brancus[2], A.A. Chilingarian[3], G. Hovsepian[3], R. Martirosov[3], M. Petcu[2], H. Rebel[1], M.Z. Zazyan[3]

[1]*Institute for Nuclear Physics, Forschungszentrum Karlsruhe, Germany*

[2]*National Institute of Nuclear Physics and Engineering, Bucharest, Romania*

[3]*Cosmic Ray Division, Yerevan Physics Institute, Armenia*

Abstract

The lateral and longitudinal profiles of the EAS development show specific features depending on the primary mass due to various particle interaction parameters influencing the development of the particle cascade in the atmosphere. The large muon detector of the ANI Cosmic Ray Observatory on Mt. Aragats gives a good opportunity to measure muon arrival times. In view of a possible extension of the muon underground installation EAS simulations have been performed. They consider various detector configurations with respect to the EAS core position. The observed muon time dispersion show specific trends with increasing radial distance and primary mass. Particularly, simulations based on the GEANT package had been done to study the faked detector signals due to secondaries generated in the surrounding material. A design for upgrading the muon detector array is presented which implies additional fast timing photomultipliers attached to the existing scintillation detectors.

1 Introduction:

The temporal structure of the Extended Air Shower (EAS) muon component maps rather directly the longitudinal shower development. The observed time dispersion of the EAS particles arises mainly from two sources: (1) Different transverse momenta of the secondaries produced in the hadronic cascade together with multiple scattering during transport in the atmosphere produce a transversal dispersion. (2) Differences in the velocities and in the path lengths. These dispersions are reflected by the variation of the arrival times of particular particles at a fixed radial distance. In sufficient large distances from the shower core arrival time quantities related to these effects become experimentally accessible, thus providing useful information for the identification of different primaries.

Proton and iron induced particle cascades behave differently in the atmosphere. On average, due to the smaller interaction length of iron primaries, their cascades will develop earlier at higher altitudes in the atmosphere. This feature together with the lower longitudinal momentum of the resulting secondaries as compared with proton induced showers of the same primary energy, lead to a higher probability for muons with longer path lengths. Due to different fluctuations, on observation level muons originating from proton primaries show broader arrival time distributions relative to the arrival time of the core as compared to iron induced showers and additionally they are shifted to slightly higher average values with respect to the shower front (Rebel et al., 1995). Such investigations had been carried out for example in the Haverah Park experiment (Ambrosio et al., 1997 and Agnetta et al., 1997). Most recently the KASCADE experiment studied various aspects of particle arrival times distributions (Haeusler et al., 1999, Badea et al., 1999 and Antoni et al., 1999).

2 The ANI cosmic ray observatory:

The ANI cosmic ray observatory is located at 3200 m a.s.l. on Mt. Aragats, Armenia. Presently it consists of two independently running EAS experiments (Fig. 1). The MAKET ANI experiment is instrumented with scintillation detectors for electron-photon detection and a calorimeter presently out of operation. The second experiment (GAMMA) consists of a surface e/γ detector array and an underground detector array equipped

†corresponding author; e-mail: mathes@ik3.fzk.de

with scintillation detectors for muon detection. The threshold for muon detection has been determined to be between 2 and 5 GeV, independently by detector simulations (Zazyan & Haungs, 1998) as well as by flux measurements. The variation of the threshold energy values is due to the varying thickness of the material on top of the muon detectors location. This requires very detailed detector simulations to obtain precise results.

The detectors used for the muon underground detectors are built into pyramid-shaped housings as shown in Fig. 2. The dimension of the scintillator plate is $100 \cdot 100 \cdot 5$ cm^3. Currently the signal readout is done via Russian FEU-49 photomultipliers with a rise time of about 30 ns. The attached readout electronics is basically designed for the purpose of pulse height measurements. With a specially optimized readout electronics as it is used for timing requirements of the surface detectors (determination of shower arrival direction) an overall timing resolution of approx. 4 ns could be achieved. The presently obtainable timing resolution could be expressed as the Gaussian sum of the effects from the scintillator, the geometrical shape of the detector and of the electronic together with the currently used TDC (laboratory made) modules which have 5 ns digitalization steps (Erlykin et al., 1989).

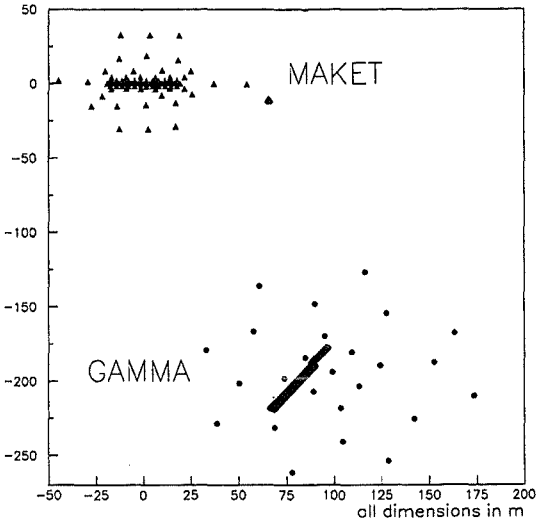

Figure 1: Schematic site map showing the two cosmic ray experiments of the ANI cosmic ray observatory located on Mt. Aragats, Armenia.

3 Monte Carlo simulations:

In view of a possible extension of the present detector setup to study muon arrival times a large number of MC studies were carried out. These studies mainly concentrate on the structure of the expected events under different external conditions. In the frame of these simulations the time resolution and the arrangement of the detectors are modeled. For the time resolution a hypothetical value of 2 ns is assumed. It is supposed that the muon underground detector array with its 150 detectors with $1m^2$ each, is fully instrumented to measure muon arrival times. Furthermore, it is worth to stress that due to the large area of the muon detection system it is possible to subdivide the whole system in 3 subsystems with sufficient number of detectors. This allows us also to investigate correlated features of the observed arrival times (Badea et al., 1998). As possible trigger sources for an imaginary readout system the surface arrays of MAKET and GAMMA are considered, i.e. only showers are evaluated which have their core inside the detection area of these experiments and show up at least 2 muons in any of muon detector subarrays.

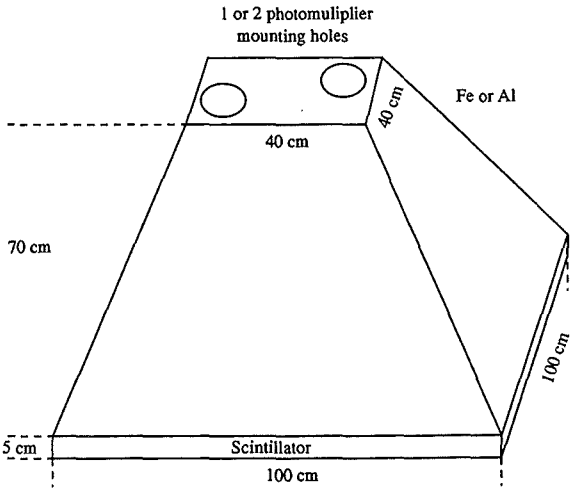

Figure 2: Sketch of the detector housing used for the ANI muon underground installation.

The particle output data delivered from the air shower simulation program CORSIKA (Capdevielle et al., 1992 and Heck et al., 1998) (version 4.60 with NKG, GHEISHA and VENUS option selected) with proton and iron primaries at fixed energies between $1 \cdot 10^{15}$ eV and $1 \cdot 10^{16}$ eV are used to feed the simulation program containing the described model. The choice of the experimental conditions leads to a range of possible core distances of 100 ... 120 m for showers triggered from the GAMMA installation (assuming not the full

instrumentation of the GAMMA surface array) and of 190 ... 230 m for the MAKET installation respectively. The detectors register the arrival time of the first muon (τ_μ^i) at each detector position. On an event-by-event basis mean and median of the arrival times of all hit detectors are calculated. Finally τ_1, τ_{mean} and τ_{med} distributions are obtained and kept for further analysis for different primaries, energies and core distances.

4 The proposed timing experiment:

A realistic first phase of such an timing device installation is a prototype setup with the readout of 32 channels. In order to have a sufficiently large core distance such an installation has to be done with detectors at the end of the muon tunnel. Fig. 3 shows a block diagram of the proposed starting and testing phase of the timing experiment. The two running experiments at the ANI site use already the Camac readout system. So we decided to use also Camac based readout hardware. Other parts of the system could be implemented in any other appropriate standard or adapted for the specific needs.

We have chosen to use the model 3377 Camac TDC (LeCroy Research Systems) for the readout of the timing signals. However the choice implies the use of level translators to adapt the discriminators output signals to the ECL inputs of the TDC as it is only provided with ECL inputs for working in complex and fast readout setups. This TDC has 32 independent channels with a full scale range between 8 ns and 32 μs and with an programmable resolution between 0.5 ns and 4 ns. The full scale range has to be chosen according to the expected size of muon arrival times and dead time considerations. As this TDC is in addition multi-hit capable a new degree of freedom is introduced in this timing experiment. Up to now this is not considered by our simulation calculations.

The experiment plans to use constant fraction discriminators (CFD) to obtain the best timing resolution, though this is not the cheapest solution. It is planned to install these CFDs directly at the photomultipliers site. Eventually an additional fast pre-amplifier is needed in this setup. Tests must show if this can be avoided. The design of these CFDs is already done and a few test exemplars are available.

As the pulse height readout of the detectors is also necessary to estimate the muon number, the detectors have to be equipped with two different photomultipliers each one suited for a specific purpose. For some of the detector boxes this is feasible by the fact that they have two mounting holes for the photo-tube holders. For the remaining detector boxes another solution has to be found.

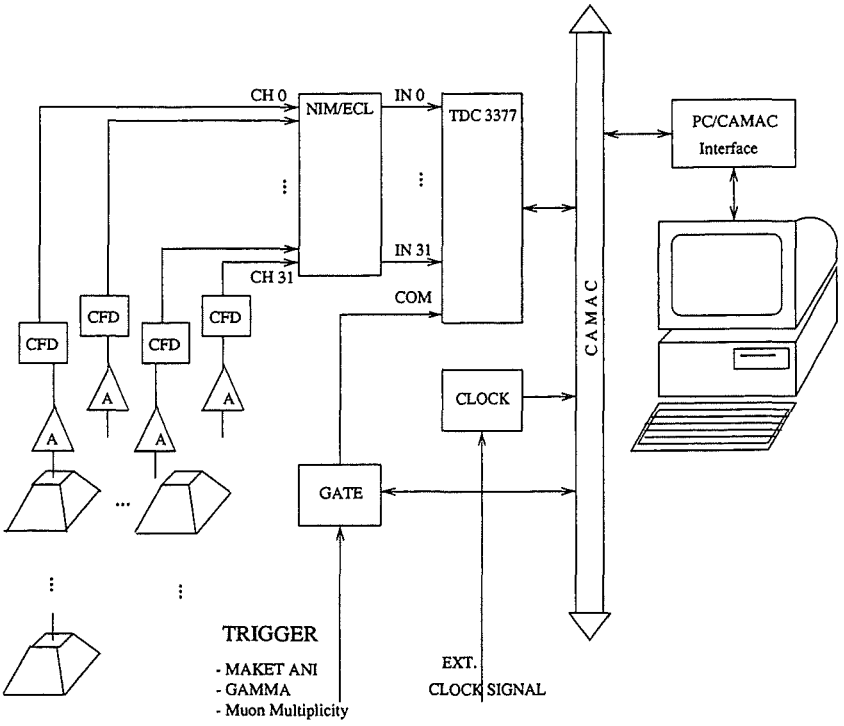

Figure 3: A block diagram of the electronics needed for a possible first phase (32 detectors instrumented) of the proposed timing experiment.

The MC simulations regarded both ANI e/γ-arrays as possible trigger source. Of course the use of the MAKET experiment for the trigger of the device will give us larger spreads of the arrival times which can be measured in an easier way. On the other side, due to the larger core distance the rate of events will be lower.

To simplify the setup in the first phase only the GAMMA experiment will be used as trigger source.

Any further online coupling with the GAMMA experiment is not planned in this phase. This would introduce additional complications for the time critical online software of the GAMMA experiment. Modifications may have some impacts on the actual data taking period. In the near future it is planned to use the coupling between MAKET and GAMMA. Then the merging of event data from the two experiments will become easier. But at the moment the low trigger rate allows us to use the PC's clock for event tagging.

The timing accuracy of the setup is an important aspect of the measurements and depends mainly on the detector properties. These effects have recently been studied more detailed with TDCs of higher resolution. In a setup with a $30 \cdot 30$ cm^2 scintillator a few photomultiplier types are investigated with respect to their timing resolution. The obtained resolutions are $\sigma_{\mathrm{opt}} = 1.7$ ns for FEU-30 and FEU-130 phototubes and $\sigma_{\mathrm{opt}} = 1.5$ ns for EMI 9902 phototubes. The influence of the final detector geometry could not be measured. So this is the subject of tests presently carried out at the Yerevan physics institute. Considerations, based on simple MC simulations, show that the influence coming from the detectors geometry could be estimated to be about $\sigma_D = 0.4$ ns. So a timing resolution of about 2 ns or better seems to be achievable with the present setup just replacing photomultiplier and the discriminating electronics.

In Fig. 3 the schemes of additional electronics needed for the monitoring of the detectors and of the slow control system are missing. To guarantee a proper functioning of the timing detectors and of the CFD threshold settings they have to be monitored continuously. Assigning the timing data with the signal height information readout by the GAMMA experiment allows us to determine the actual thresholds without spending further ADC channels for the new experiment. After this a continuous monitoring of the rates will be done in order to check permanently the adjustments made.

5 Status and Conclusions:

The temporal structure of the EAS muon component reflects the features of the longitudinal shower development. For a proposed extension of the muon underground detectors of the ANI cosmic ray experiment a number of MC simulations were carried out in order to study these effects for this setup. The achieved timing accuracy of such a system turns out to be the crucial factor. For the ANI muon detectors the timing resolution has to be improved to reach this goals.

Presently detector tests are performed to obtain the actual detector performance and compare it with the expected values. When the experiment site will become accessible the installation of a few timing channels will be started.

References

Ambrosio M. et al., Astrop. Phys. 6 (1997) 301
Agnetta G. et al., Astrop. Phys. 7 (1997) 329
Antoni T. et al., subm. to Elsevier Preprint
Badea A.F. et al., Proc. ANI workshop, Report FZKA 6215 (1998) 77
Badea A.F. et al., Proc. 26th ICRC (Salt Lake City,1999) HE 2.5.29
Capdevielle J.N. at al., Report KfK 4998 (1992) and Heck D. et al., Report FZKA 6019 (1998)
Erlykin A.D. et al., Voprosi Atomnoj Nauki i Tekhniki, ser. techn. fiz. exp. V 4(4), Yerevan (1989) 4
Haeusler R. et al., Proc. 26th ICRC (Salt Lake City, 1999), HE 2.2.38
Rebel H. et al., JPhys. G: Nucl. Part. Phys. 21 (1995) 451
Zazyan M.Z., Haungs A., Proc. ANI workshop, Report FZKA 6215 (1998) 37